Large-scale Processing and Synthesis Techniques to Address Challenges for Nanoparticle Commercialization

A Thesis
Presented to the Faculty of the Graduate School
Of Cornell University
In Partial Fulfillment of the Requirements for the Degree of
Master of Science

by
Joseph McNab Caron
August 2015

ABSTRACT

Today several challenges exist which inhibit the transition of nanoparticles (NPs) from laboratory curiosity to achieve their acclaimed large-scale commercial potential. Scaling up synthesis and processing techniques to meet demands for emerging applications presents interesting scientific and engineering challenges. Commercial forces dictate these issues be addressed before NPs can displace incumbent materials in applications such as energy storage and lighting, where they can significantly increase the efficiency of such devices. Herein, I address these issues using novel approaches to scalable NP synthesis and processing pioneered by the Robinson Lab at Cornell University, and contextualize them within today's university IP landscape; that is, I not only develop such techniques, but understand what commercial steps must be taken to see them implemented in real commercial devices.

This work demonstrates a general lithium-ion battery electrode fabrication method for colloidal nanoparticles using electrophoretic deposition (EPD). EPD is a fast, robust, and scalable method for creating NP films with high conductivity, and do so without the use of additives traditionally used in electrode fabrication. After EPD, we show two post-processing treatments ($(NH_4)_2S$ and inert atmosphere heating) to effectively remove surfactant ligands and create a linked network of particles. The NP films fabricated by this simple process exhibit excellent electrochemical performance as lithium-ion battery electrodes. Additive-free $Cu_{2-x}S$ and MnS NP films each show a well-defined plateaus at ~1.7 V, demonstrating potential for use as cathode electrodes. We go on to perform a size-dependent investigation of $Cu_{2-x}S$ NPs and demonstrate that there is no significant relationship between size and capacity when comparing small (3.8

nm), medium (22 nm), and large (75 nm) diameter $Cu_{2-x}S$ NPs up to 50 cycles; however, the 75 nm NPs show higher coulombic efficiency. Ex-situ TEM analysis suggests that $Cu_{2-x}S$ NPs eventually break into smaller particles (< 10 nm), explaining a weak correlation between the size and performance. We also report for the first time on additive-free Ge NP films, which show stable capacities for up to 50 cycles at 500 mAh/g.

This work also includes a preliminary exploration of the challenges involved in creating high-efficiency copper indium sulfide ($CuInS_2$) quantum dots (QDs) for use as down-converters in solid-state lighting applications. We find that the primary challenges include balancing the relative reactivity of the Copper (I) (Cu^+) and Indium (III) (In^{3+}) cations towards the sulfur source of choice, elemental sulfur, as well as controlling the phase of the product, which can take either the tetragonal chalcopyrite or hexagonal wurtzite phases. Our work suggests that $CuInS_2$ formation begins with the formation $Cu_{2-x}S$ particles, into which In diffuses, and that higher heating temperatures and longer growth times facilitate this process. Overall we suggest there are optimal temperature and time parameters between 100 and 200 °C and 5 – 20 minutes for $CuInS_2$ QD growth. With regard to controlling phase, we find the choice of precursor salt anion is the chief factor in determining the phase of the final product. If chloride (Cl^-) is the only anion present in the reaction, wurtzite was produced. If both Cl^- and acetate are present, the chalcopyrite phase is produced. Finally, we explore the role of shelling $CuInS_2$ cores with a layer of ZnS to improve efficiency. We find that the results are highly dependent on the choice of ligand for both the core and the core-shell material. The best result occurred when oleylamine was chosen in both cases.

Biographical Sketch

Joseph Caron was born to Angela and Christopher Caron on the 7th of February, 1991 in Virginia Beach, VA. When Joseph was 3 years old his father took active leave of the United States Navy, and settled down with his family in Monroe, CT, where Joseph lived throughout his childhood. Joseph attended Choate Rosemary Hall in Wallingford Connecticut.

Joseph did his undergraduate work at Johns Hopkins University, double majoring in philosophy and chemistry and graduating with honors in chemistry in May 2013. While at Johns Hopkins he founded and ran JHU GED Prep, a club that helped local adults earn high school equivalency degrees, and enjoyed participating in the school Chinese Lion Dance Club. He worked for over two years in Tyrel McQueen's solid-state chemistry research laboratory where he authored two papers on superconductivity. He also received several distinctions, including honorable mention for the NSF GRFP, the Johns Hopkins Kilpatrick Family Prize in Chemistry, and a Maryland ACS Student Award.

Joseph pursued graduate work in materials science and engineering in Richard Robinson's Laboratory at Cornell University. There he worked on nanomaterials research for high-efficiency batteries and low-energy lighting. While at Cornell Joseph founded a project team on biofuels for Engineers for a Sustainable World and co-founded a startup based on his graduate work. This startup raised over $50,000 and won the Cleantech Open's Rising Star Award. On August 7th, 2015 Joseph will be married to his girlfriend and fiancée of 9 years in Old Lyme, CT.

This work is dedicated to my mother who has been my model and my inspiration, to my family for supporting me throughout my life, and to my fiancée for keeping me grounded and focused on the important things in life.

I would also like to thank Curtis Williamson and Doug Nevers for being patient, insightful, and hardworking co-worker and friends, as well as Richard Robinson for making me the researcher I am today.

Acknowledgements

This work made use of the Cornell Center for Materials Research Shared Facilities, which are supported through the NSF MRSEC program (DMR-1120296). The work was supported in part by the National Science Foundation under Award Number CHE-1152922 and CMMI-1344562. I acknowledge Alberto Purwada for his tireless efforts in developing PureQuantum's 2015 business plan (Appendix A). Thank you, also, to Jeffery Albert, Thomas Cupo, Andrew DiPasquale, Anirudha Kinhal, William Graves, Garin Murphy, J. Luke Finch, and Dean Bell of the Syracuse Technology Commercialization Law program for their work on the PureQuantum Research Report, which made large portions of Chapter 2 possible. I would also like to acknowledge the NEXUS-NY and Cleantech Open accelerators for supporting my research for clean energy applications.

Table of Contents

ABSTRACT iii

Biographical Sketch v

Acknowledgements vii

Chapter 1: Introduction 1
- **1.1 Nanoparticles in the Modern Era** 1
- **1.2 Nanoparticles, Definition** 2
- **1.3 Synthesis** 3
- **1.4 Quantum Dots** 8
- **1.5 Quantum Yield** 10
- **1.6 Applications** 11
  - 1.6.1 Electronic Applications 11
  - 1.6.2 Display and Lighting Applications 11
  - 1.6.3 Photovoltaic Applications 12
  - 1.6.4 Biomedical Applications 13
- **1.7 Current Challenges** 13
- **1.8 Statement of Purpose** 16

Chapter 2: Business Meets Science 17
- **2.1 Introduction** 17
- **2.2 Intellectual Property** 18
- **2.3 Using Intellectual Property** 20
- **2.4 The Business Model Canvas** 22
  - 2.4.1 Customer Segments 23
  - 2.4.2 Value Proposition 24
  - 2.4.3 Partners, Key Activities, and Key Resources 24
  - 2.4.4 Revenue and Cost Structure 25
- **2.5 The Business Plan** 26
- **2.6 The Intersection of Business and Academia** 28
- **2.7 Networking and Customer Discovery** 31

Chapter 3: A General Method for High-Performance Li-ion Battery Electrodes from Colloidal Nanoparticles without the Introduction of Binders or Conductive-Carbon Additives: The Cases of MnS, $Cu_{2-x}S$, and Ge 33
- **1.1 Abstract** 33
- **1.2 Introduction** 34
- **1.3 Experimental** 38
- **1.4 Results and Discussion** 40
  - 1.4.1 Metal Sulfides 43
  - 1.4.2 Germanium 45
  - 1.4.3 Size dependent performance 46
- **1.5 Conclusion** 50
- **1.6 Acknowledgments** 53
- **1.7 References** 54

Supporting Information **57**
Supplementary Figures **66**
Supporting InformationReferences **75**

Chapter 4: Challenges for $CuInS_2$ NP Synthesis: Understanding Phase and Growth Mechanisms through Heat Control and Reagent Choice **76**
4.1 Abstract **76**
4.2 Introduction **77**
4.3 Experimental **83**
4.5 Conclusion **96**
4.6 Supplemental Part 1: Extended Reaction Results **98**
4.7 Supplemental Part 2: Supernatant Analysis **105**

Chapter 5: Conclusions and Future Outlook **109**
5.1 Summary **109**
5.2 Next Steps for PureQuantum **109**
5.3 Future Work for Additive-free Nanoparticle Electrodes Processed by EPD **110**
5.4 Future Work for Large-scale Copper Indium Sulfide Synthesis **111**

Appendix A: PureQuantum Business Plan **112**
Executive Summary **114**
Market Opportunity and Size **115**
Macroeconomic Trends **117**
Competition **118**
Company and Products **120**
Development Plan **123**
Manufacturing Plan **125**
Sales and Marketing Plan **126**

Chapter 1: Introduction

1.1 Nanoparticles in the Modern Era

Though the use nanomaterials dates back as early as the 4th century when the Romans used their unique optical properties to create novel visual effects[1], nanomaterials have only recently have begun to find use in the modern era. The first scientific analysis of the unique properties of materials with dimensions on the nanoscale is credited to Michael Faraday, who in 1857 found that thin films of gold undergoes a variety of optical transformations when subjected to different stimuli, such as heat and pressure.[2] It is interesting then, that though researchers have been aware of the unique properties of nanomaterials for over a century and a half, they have only recently begun to impact the world in meaningful ways. In fact, many challenges yet remain before these unique materials find wider adoption in applications such as low-energy displays, high-efficiency lighting, quantum computing, and photovoltaics. It is the aim of this thesis to discuss and address many of these challenges, with the hope that the work contained will contribute to the transition of (NPs) from lab curiosity to commercial product. Specifically I address challenges related to the large-scale synthesis of useful fluorescent nanomaterials known as quantum dots (QDs) and processing challenges related to large area NP electrode fabrication.

[1] I. Freestone, N. Meeks, M. Sax, and C. Higgitt, *Gold Bulletin*, 2007, 4, 270-277
[2] M. Faraday, *Phil. Trans. Roy. Soc. London,* 1857, 147, 145–181

1.2 Nanoparticles, Definition

The National Nanotechnology Initiative defines nanomaterials as materials with one of more dimension on the scale of 1 – 100 nm.[3] This puts the size of the material near the scale of individual atoms, and as a result many of the bulk material properties undergo a radical change. These changes include physical properties, such as melting point, optical properties, such as absorption and emission, and electronic properties, such as ion diffusion length. These changes may be related to the change in surface-to-volume ratio, energetic structure of the material, how light is scattered, and many other causes. Furthermore, the ability to tune the dimension of the material within the nano-regime affords a unique element of control over the property related to size. For example, the photoluminecent (PL) emission frequency of semiconductor nanoparticles, QDs, is related to the size of the material. By creating QDs of various diameters, researchers can engineer a variety of emission wavelengths.[4] The diameter is often a function of the synthetic conditions employed. By deepening our understanding of how to achieve specific dimensions of nanomaterials, they can be optimized for various applications and will find further penetration into the commercial sphere. Due to their unique optical and optoelectronic properties within the visable spectrum, the most widely studied NP is cadmium selenide, as well as cadmium sulfide and cadmium telluride for similar reasons. Cadmium selenide, for instance, can already be found in several consumer devices, such as the Kindle Fire 7, HD.

[3] www.nano.gov. Accessed April 2, 2014
[4] C.B. Murray, C.R. Kagan, and M.G. Bawendi, *Annu. Rev. Mater. Sci*, 200, 30, 545-610

1.3 Synthesis

Nanoparticles may be synthesized through a variety of means, such as sol-gel, ball-milling, hydrothermal, and pyrolysis, to name but a few.[5] The work described here focuses on the colloidal method of nanoparticle growth. This method has been shown to reliably produce monodisperse, well-stabilized, and surface passivated NPs. Growing mondisperse particles is of critical importance, as NP size must be carefully controlled in order to take full advantage of the novel properties associated with the nanoscale regime.

Colloidal synthesis refers the growth of the material in a two phase suspension: a non-polar solvent, polar particles, and organic surfactant ligands bridging the gap. The NPs are growth within a coordinating solvent at a particular temperature for a short amount of time before rapidly cooling to prevent further growth. The growth of the particles is commonly understood according to the Le Mer model, developed by Le Mer and Dinegar.[6] This model posits that monodisperse (that is, of a narrow size distribution commonly understood as $\sigma < 10\%$) may be grown by first rapidly introducing reagents into a coordinating solvent. If the reagent concentration exceeds the supersaturation limit of the system, a "nucleation burst" occurs, whereby the super saturation is relieved by a discrete nucleation event. After this initial relief of the system, no further nucleation occur. The nuclei then grow upon the reagent that did not participate in the nucleation burst. By rapidly cooling the solution, further growth is prevented. Controlling size is then a function of the relative speeds of nuclei formation and growth, as well as the amount of time they are allowed to grow.

---

[5] Id.

[6] V.K. La Mer, R.H. Dinegar, *J. Am. Chem. Soc.,* 1950, 72, 4847-4854

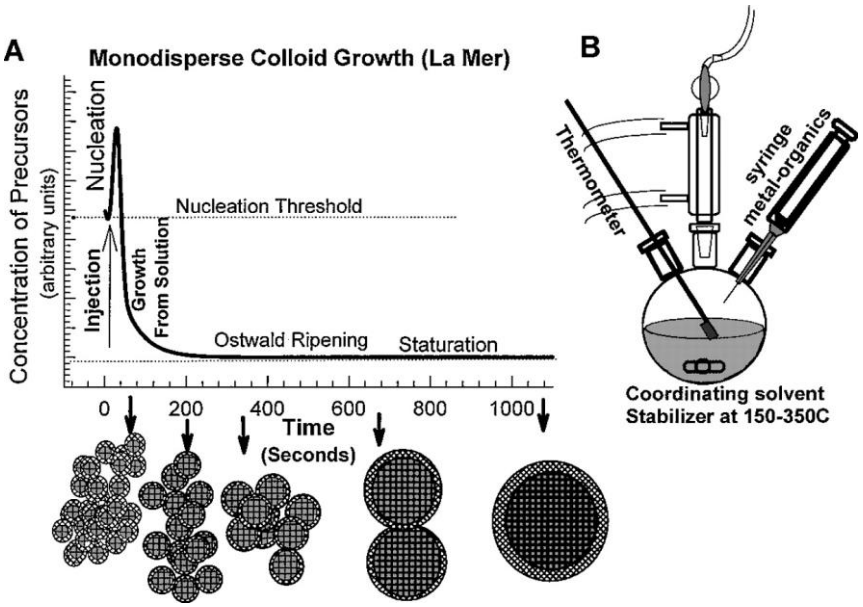

Figure 1. A) shows the La Mer model. This model for particle growth in colloidal systems is commonly used to understand the growth of monodisperse NPs. In the hot injection method, the burst of precursor concentration introduced by the injection exceeds the nucleation threshold. This leads to the formation of a discrete amount of NP nuclei that go on to grow from the remaining precursor. B) shows the traditional hot inject set-up. *(Both) C.B. Murray, C.R. Kagan, and M.G. Bawendi, Annu. Rev. Mater. Sci., 200, 30, 545-610*

The typical method of nanoparticle growth according to this model is known as the hot injection method.[7] In this method, the reaction solvent is first heated to the desired growth temperature, typically 200 – 300 °C. Precursor dissolved in a suitable solvent is then rapidly injected into the system. The precursor material exceeds the saturation threshold and overcomes the activation energy for nuclei formation at the reaction temperature, rapidly generating nuclei. The precursor concentration quickly drops below the nucleation threshold, and nuclei production is halted while the existing nuclei continue to grow. Usually within 5 minutes the desired size is achieved and the flask is cooled externally by a water bath.

[7] X. Peng, J. Wickham, and A.P. Alivisatos, *J. Am. Chem. Soc.,* 1998, 120, 5343 - 5344

Though the hot injection method is simple and quick, it has some important shortcomings. Due to the quick timescales of nuclei formation and growth, nanoparticle growth is highly sensitive. Two important factors which influence formation in growth are temperature and concentration. If nuclei and particles are exposed to different heat and concentration profiles polydisperse growth may occur. The hot injection method executes the heating and mixing steps together, which introduces a level of delicacy to the process, as the injection and the mixing must happen quickly in order for the concentration and heat to become suitably uniform throughout. This problem is exacerbated at larger scales, where the larger reaction volume is much more difficult to mix and heat, and the uniformity of concentration and temperature are therefore much harder to maintain. This is why nanoparticle syntheses are typically done in volumes of 5 – 10 mL.

A second method, known as the heat up method, attempts to solve this shortcoming of the hot injection method. Taeghwan Hyeon of Seoul National University is credited with pioneering this approach. In his paper "Ultra-large-scale Syntheses of Monodisperse Nanocrystals," Hyeon showed that hot injection is not the only robust method for creating dots.[8] Instead, through the so-called heat up method, he was able to combine his reagents at room temperature and heat the solution to the reaction temperature. This method decouples of the heating and mixing steps, allowing for unprecedented control over particle growth. Taking advantage of this, Hyeon created a 40 g batch of iron oxide nanoparticles, far exceeding the typical sub-gram batch.

[8] J. Park, K. An, Y. Hwang, J.-G. Park, H.-J. Noh, J.-Y. Kim, J.-H. Park, N.-M. Hwang, and T. Hyeon, *Nat. Mater.,* 2004, 3, 981-895

In order to improve the optical properties of a QD, it is common to employ a core-shell structure. A core-shell structure is a QD which has had a shell layer grown on the surface. Due to their wide band gap, shell layers act as a potential-well barrier for the wavefunction of the carriers, confining them to the interior of the particle. Therefore, the carriers cannot access the surface defects of the particle, which act as traps for non-radiative recombination. The lattice of the shell material should closely match that of the core, in order to prevent introducing defects at the interface. Because of their wide bandgap and good lattice match with cadmium selenide, the most widely studied quantum doc, zinc sulfide and cadmium sulfide are commonly chosen as shell materials.[9, 10]

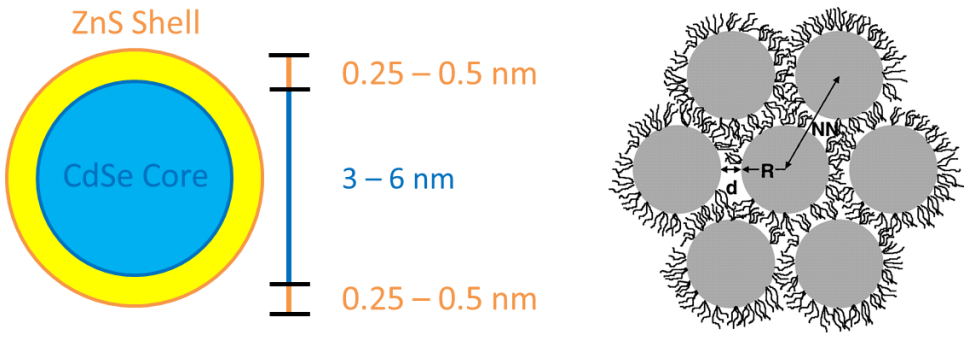

Figure 2. (Left) A model of the core-shell nanoparticle structure. Typically a photoluminecesnt core is coated in a high bandgap material to help prevent the carriers from reaching surface defects. (Right) A simplification of ligands coordinated to NP surfaces. *(Right) C.B. Murray, C.R. Kagan, and M.G. Bawendi, Annu. Rev. Mater. Sci, 200, 30, 545-610*

Finally, it is important to discuss surface passivation through ligand coverage. Ligands are coordinating organic molecules that passivate the surface of the particles during and after

[9] D.V. Talapin, I. Mekis, S. Gotzinger, A. Kornowski, O. Benson, H. Weller, *J. Phys. Chem. B,* 2004, 108 (49), 18826-18831

[10] B.O. Dabbousi, J. Rodriguez-Viejo, F.V. Mikulec, J.R. Heine, H. Mattoussi, R. Ober, K.F. Jensen, and M.G. Bawendi, *J. Phys. Chem. B,* 1997, 101 (46), 9463-9475

growth. This passivation is considered critical to the growth of nanoparticles, as they prevent the aggregation of the particles, allow them to be easily precipitated, and in some cases functionalize the surface. In some reactions, they are also believed to be necessary for intermediate steps in the growth reaction.[11] In others they are necessary to dissolve and activate the precursor. However it must be noted the exact role of the ligand in NP growth is not well understood. The ligand may also be chosen to provide certain functionalities to the NPs, such as targeting particular cells in the body[12], or to control interparticle spacing, as in battery electrode fabrication.[13]

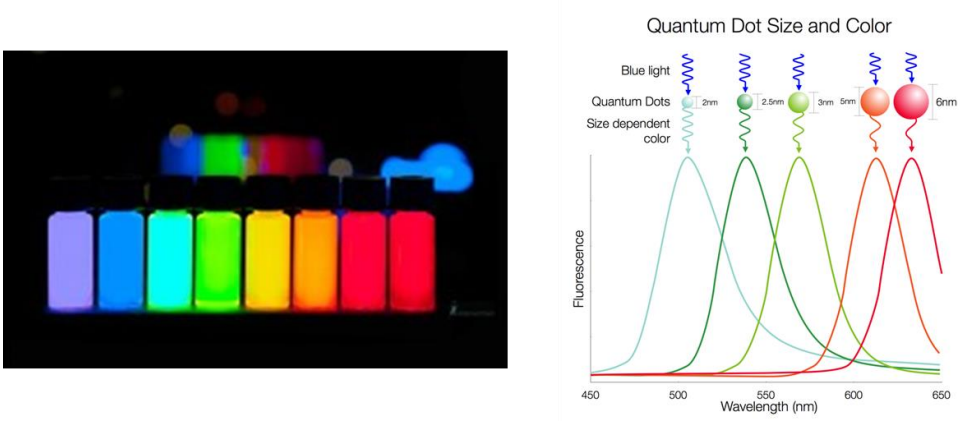

Figure 3. (Left) Quantum dots as advertised by PlasmaChem. What's notable here is that the material in each vial is CdSe of a different sizes. (Right) This figure from the quantum dot manufacturer Nanosys shows how the emission from CdSe QDs varies with size. *(Left) Nanosys Inc., nanosysinc.com/what-we-do/quantum-dots/ (accessed April 3rd, 2015). (Right) PlasmaChem GmbH, www.plasmachem.com/shop/en/226-zncdses-alloyed-quantum-dots (accessed April 3rd, 2015)*

[11] K. Nose, Y. Soma, T. Omata, and S. Otsuka-Yao-Matsuo, *Chem. Mater.,* 2009, 21, 2607-2613
[12] J.E. Fuller, G.T. Zugates, L.S. Ferreira, H.S. Ow, N.N. Nguyen, U.B. Wiesner, R.S. Langer, *Biomaterials,* 2008, 29, 1526-1532
[13] D.-H. Ha, L.M. Moreau, S. Honrao, R.G. Henning, and R.D. Robinson, *J. Phys. Chem. C*, 2013, 117, 14303-14312

1.4 Quantum Dots

Quantum dots are a class of nanoparticles composed of semiconducting material. Once the diameter of the particle is below the Bohr radius, these materials exhibit unique, size-related electronic states. At and below the Bohr radius, the NP size is on the order of the wavefunctions of the carriers and therefore "feel" the physical limits of the system. The system may be treated much like the classic particle on a box, that is, as an electron or hole in a spherical potential well bound by the nanoparticle surface.[14]

As shown in **Fig. 5** the effective mass theory of electronic states approximates a Gaussian-like relationship between the conduction and valence energies and the wave vector, k. According to the particle-in-a-box understanding, the smaller the particle, the larger the k-space necessary to contain the particle inside the potential well. At non-zero k-spaces the conduction band is effectively driven up and the valence band is driven down as the particle diameter shrinks. Therefore, at smaller quantum dot sizes, the effective band gap of the material is increased.[15]

[14] C.B. Murray, C.R. Kagan, and M.G. Bawendi, *Annu. Rev. Mater. Sci*, 200, 30, 545-610.
[15] Id.

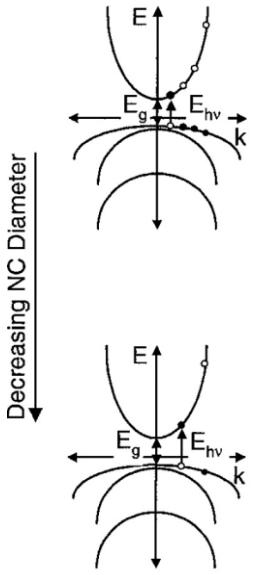

Figure 4. An idealized band structure based upon effective theory exemplify how the bandgap of QDs vary with size. Confinement of the exciton to smaller areas requires a larger region of k-space, moving the lowest energetic transition out to higher bandgaps. *C.B. Murray, C.R. Kagan, and M.G. Bawendi, Annu. Rev. Mater. Sci, 200, 30, 545-610*

In his 1986 paper, Brüs formulated an equation which describes the size-bandgap relationship.[16] Assuming Bloch wavefunction, electron-hole in a shielded coulumbic interaction, and the assumption described above, Brüs devises the following equation. It may be physically understood as the band gap of the material corrected for the effective mass of the exiton and columbic interactions.

$$E^* \cong E_g + \frac{\hbar^2 \pi^2}{2R^2}\left[\frac{1}{m_e} + \frac{1}{m_h}\right] - \frac{1.8e^2}{\epsilon R}$$

[16] L. Brus, *J. Phys. Chem.,* 1987, 90, 2555-2560.

E* is the new bandgap energy, E_g is the bandgap of the bulk material, R is the radius of the particle at or below the Bohr radius, m_e and m_h are the effective masses of the electrons and holes respectively of the bulk material, and ϵ is the dielectric constant of the crystallite.

1.5 Quantum Yield

Central to the discussion of quantum dots is the figure of merit for any material florescent material, quantum yield. Quantum yield is a measurement of efficiency of such materials, and figures strongly into any conversation on the quality of quantum dots. Simply put, quantum efficiency is the rate constant of radiative processes within the material divided by the sum of all possible relaxation pathways from a photonically excited state, both radiative and non-radiative (e.g. internal conversion, trap states, phonons, etc.).[17,18] It is a way to quantify the efficiency of how absorbed photons are converted into emitted photons. Though it is possible to measure this number directly, the process requires a highly precise set up and specialized equipment. In literature the ubiquitous approach is to find the relative quantum yield. That is, devise the quantum yield by comparing the emission against a standard of known quantum yield. The equation below describes the relationship between the quantum yield of an unknown material and a standard.[19]

$$\Phi_f^i = \frac{F^i f_s n_i^2}{F^s f_i n_s^2} \Phi_f^s$$

[17] Jobin Yvon, Horiba, A Guide to Fluorescence Quantum Yields, www.horiba.com.
[18] A.M. Brouwer, *Pure Appl. Chem.,* 2011, 83 (12), 2213-2228.
[19] Id.

F^i and F^s are the integrated emission intensities of the emissive sample and standard, respectively. f_x is the absorption factor (the fraction of light absorbed, $1 - 10^{-Ax}$, where A = absorbance). n_x is the refractive index of the solvent of the sample and standard (if different).

1.6 Applications

1.6.1 Electronic Applications

Nanoparticles find use in a variety of electronic applications. In Li-ion batteries, for instance, their short diffusion length for ionic transport and capability to accommodate strain through cycles can greatly increase battery performance.[20] Nanoparticles are also being investigated for their use in catalysis. Development of more efficient oxygen reduction and oxygen evolution catalysts is of critical importance for fuel cell efficiency.[21] The incumbent platinum material suffers from scarcity and high cost. Other materials, such as Co_3O_4, have been shown to exhibit faster kinetics and lower over potentials when fabricated on the nano-scale and may very well be the key to devising non-platinum oxygen reduction and oxygen evolution catalysts.

1.6.2 Display and Lighting Applications

There is currently much development around using quantum dots to make and/or augment light-emitting diodes for more efficient displays and light sources. Quantum dots are valued for displays because of the narrow full width half maximum of their emission. This can result in a displays and lighting that more accurately render the colors that the human eye can

[20] D.-H. Ha, M. A. Islam and R. D. Robinson, *Nano Lett.*, 2012, 12, 5122-5130.
[21] M. Fayette, A. Nelson, and R.D. Robinson, *J. Mater. Chem. A,* 2015, 3, 4274-4283.

perceive. This in turn makes them more efficient, since more of the light produced is used effectively. The range of colors possible for a quantum dot enhanced display is 30 % greater than in CRT displays. The Kindle Fire HDX 7, for example, takes advantage of quantum dots fabricated by the company Nanosys to create more vibrant displays.[22] This product is one of Amazon's best-selling tablets, winning critical acclaim for its vibrant display. Quantum dots are also well known as efficient down converters. Down converters absorb one wavelength of light and emit another. They are a critical element of solid-state lighting devices, a low-energy source of light. In such a device, light from a blue LED is absorbed by a down converter and converted into the desired energy of light.[23]

1.6.3 Photovoltaic Applications

Quantum dots may be able to increase the efficiency and reduce the cost of today's typical silicon photovoltaic cells. Multi-junction solar cells made from colloidal QDs have been able to achieve around 9% conversion efficiency in the lab with a theoretical conversion efficiency limit is 45%.[24] This is possible because when a single photon is absorbed by a quantum dot can produce more than one exciton, increasing normal conversion efficiency numbers seen in single-junction silicon cells.[25]

---

[22] Nanosys, nanosysinc.com/in-the-news/2013/12/12/gizmodo-kindle-fire-hdx-7-incredibly-innovative-first-tablet-display-to-use-super-high-tech-quantum-dots, accessed April 27th, 2015.
[23] U.S. Department of Energy, Manufacturing Roadmap: Solid-State Lighting Research and Development, August 2014. Prepared by Bardsley Consulting, Navigant Consulting, SB Consulting, and SSLS, Inc.
[24] C.-H. M. Chuang, P.R. Brown, V. Bulović, and M.G. Bawendi, *Nature Materials,* 2014, 13, 796-801.
[25] Id.

1.6.4 Biomedical Applications

Currently, various kinds of organic dyes are used in modern biomedical analysis. However, quantum dots are approximately 20 times brighter and 100 times more stable than traditional fluorescent reporters. While the irregular blinking of quantum dots is a drawback, their usage for highly sensitive cellular imaging has seen major advances over the past decade.[26] The improved photostability of quantum dots, for example, allows the acquisition of many consecutive focal-plane images that can be reconstructed into a high-resolution three-dimensional image.[27] Furthermore, by controlling the surface functionalization the QDs can deliver antibodies, streptavidin, peptides, DNA, and nucleic acid aptamers to specific proteins on cells.[28]

1.7 Current Challenges

Currently there are several shortcomings to the state-of-the-art NP synthesis techniques preventing their more widespread adoption in the applications listed above. As mentioned before, such reactions are highly sensitive. In particular the ubiquitous hot-injection method of NP synthesis is not inherently scalable, due to the fact mixing and heating are necessarily coupled. This leads to three interrelated problems: the products of traditional nanoparticle syntheses are expensive, difficult to scale, and hard to reproduce. In order to address these issues literature nanoparticle syntheses are typically made in sub gram batches. There are some examples of large scale reactions, such as Hyeon's "Ultra-large-scale" batch.[29] However such

[26] M.A. Walling, J.A. Novak, J.R.E. Shepard, *Int. J. Mol. Sci*, 2009, 10 (2), 441-491.
[27] F. Tokumasu, R.M. Fairhurst, G.R. Ostera, N.J. Brittain, J. Hwang, T.E. Wellems, J.A. Dvorak, *J. Cell Sci.,* 2005, 1 118 (Pt5), 1091-1098.
[28] B. Ballou, B.C. Lagerholm, L.A. Ernst, M.P. Bruchez, A.S. Waggoner, *Bioconjug. Chem.,* 2004, 15 (1), 79-86.
[29] J. Park, K. An, Y. Hwang, J.-G. Park, H.-J. Noh, J.-Y. Kim, J.-H. Park, N.-M. Hwang, and T. Hyeon, *Nat. Mater.,* 2004, 3, 981-895

batch are still too small for commercial purposes, the produce is more organic surfactant ligand than NP, and it is unclear how widely applicable this approach is. Commercial producers of quantum dots have also kilogram batches of quantum dots[30], but the engineering problems associated with reaching such batches comes at a price. Nanoco serves as one of the few public examples of large scale quantum dot sale, when they sold a single kilogram of cadmium selenide quantum dots to Samsung for $2 MM.[31] This problem is exacerbated by the difficultly reproducing high quality dots. Due to many open questions as to the exact mechanism by which nanoparticle growth occurs, the relative influence of controls such as heat and concentration, and the types of reagents used, it is difficult for researches to reliably reproduce the results of other labs. A more robust, scalable, and low-cost approach to making these materials is required.

[30] Nanoco Group, PLC. (2014), *From Patents to Products: 2014 Annual Report and Accounts.* http://www.nanocotechnologies.com/system/files/uploads/financialdocs/2014-Annual-Report.PDF. Accessed April 27th, 2015.
[31] Id.

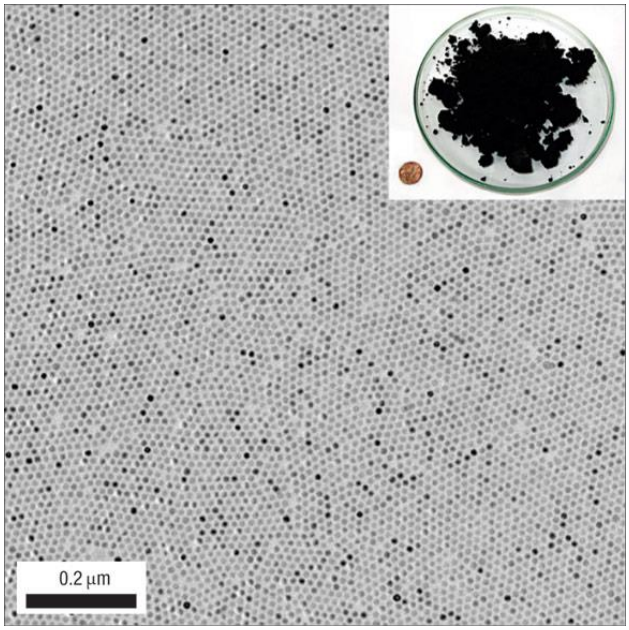

Figure 5. The lauded 40 g "ultra large-scale" batch of Fe_3O_4 nanoparticles from Hyeon *et al.* made by the heat-up method in their 2004 paper. *J. Park, K. An, Y. Hwang, J.-G. Park, H.-J. Noh, J.-Y. Kim, J.-H. Park, N.-M. Hwang, and T. Hyeon, Nat. Mater., 2004, 3, 981-895*

There are also many challenges surrounding the large-scale processing of nanomaterials for applications such as photovoltaics, LEDs, and batteries. In the LED industry, for example, the method for creating thin films of active material is well understood and strongly entrenched in industry. In order for nanomaterials to replace the incumbent materials in applications such as these, simply making them at commercial scale is not enough. New processing methods must be developed that can effectively and efficiently handle large volumes of nanoparticles. There is high potential for quantum dots in this area, as they are amenable to a variety of such techniques, such as doctor blading, spin casting, and, as I will cover in detail here, electrophoretic deposition.

The final challenge is environmental. Commonly quantum dots are made with unsustainable materials. For example, the most popular and efficient quantum dot material for commercial applications is cadmium selenide. The televisions and kindle fires mentioned earlier,

for example, make use of this material. However cadmium is toxic, known to cause cancer, kidney problems, and bone softening. In fact is it currently one of six substances banned in the European Union by Directive 2011/65/EU for consumer products.[32] Indium phosphide is another material under development for commercial applications. However this synthesis makes use of Tris(trimethylsilyl)phosphine, a highly pyrophoric and environmentally dangerous material.[33] If quantum dots are going to find long term commercial success, techniques and materials must be developed that are efficient yet environmentally benign.

1.8 Statement of Purpose

The challenges outlined are commercial in nature, but their solutions lie squarely in the domain of materials research. The purpose of this thesis is to summarize my efforts to address these challenges in my graduate work, but frame them within the context of the business forces driving them. It will be in part summation of my progress in this area, but will also serve as a guide to researchers hoping to follow in my example of informing research work with commercial interests. Much of my work was dedicated not only to developing this research, but also seeing it tangibly implemented through the development of my own business. Therefore, some of this work will go beyond that lab to explore the intersection of business and research, and to explain how intellectual property developed within a research institution becomes part of a business to help to improve lives.

[32] Dir. 2011/65/EU of the European Parliament and of the Council, 8 June.
[33] R. Xie, M. Rrutherford, X. Peng, *J. Am. Chem. Soc.,* 2009 131, 5691-5697.

Chapter 2: Business Meets Science

2.1 Introduction

Now more than ever the realms of academic research, manufacturing, and business are overlapping, particularly in energy and biomedicine. This is because the challenges facing the world around global warming, natural resource depletion, and health loom large. A concerted effort must be made to not only push the boundaries of academic knowledge in meaningful directions, but also to use that work in meaningful ways that solve tangible problems. This means continuing to strengthen the relationships between business and academia. From the establishment of Harvard's Innovation Lab, to the fact that in 2014 twenty-five startup were launched based on MIT technology, there is evidence to suggest that this relationship is already growing strong.[34,35] However for most researchers, the idea of starting a business, and indeed business in general, is a confusing and often times frightening notion. This chapter will serve first and foremost to demystify the business sector for researchers. It will focus first upon IP, and specifically how an IP goes from a lab setting and into the world. Second, I will discuss on a high level how a business operates, in order to dissect how IP fits into the overall strategy of a business.

My experience starting a business based on my work will serve as a useful reference throughout this chapter. PureQuantum is a startup, quantum dot (QD) manufacturer based on the nanoparticle (NP) scale-up work being done in Richard Robinson's Lab at Cornell University.

[34] i-lab.harvard.edu
[35] tlo.mit.edu/about/statistics

Made up of researchers in the Robinson group, PureQuantum plans to develop the technology at Cornell before going on to either manufacture QDs or sub-license the process.

2.2 Intellectual Property

The way in which most researchers intersect with the business world is with respect to intellectual property (IP). The World Intellectual Property Organization defines IP as "any creation of the mind, such as inventions; literary and artistic works; designs; and symbols, names, and images used in commerce." It goes on to say "IP is protected in law by, for example, patents, copyright, and trademarks, which enable people to earn recognition or financial benefit from what they invent or create."[36] In a university setting, the primary mode by which IP is protected is a patent. Patents are legal documents that protect the IP of an inventor or patent holder from competition. It is important to note that a patent does not give one the right to execute up an IP, but rather grants "the right to *exclude others* from making, using, offering for sale or selling the invention."[37] There are three types of patent: a utility patent, which covers a useful process, machine, article of manufacture, composition of matter or improvement thereof; a design patent, which covers design for an article of manufacture; and a plant patent, which protects new species of plants. Trademarks and copyrights are two other common ways to protect IP, though they will not be covered here.[38]

When a researcher is developing a technology that may have commercial use, it is imperative he or she contact the university tech transfer office, which handles university IP, in

[36] wipo.int
[37] Id.
[38] uspto.gov

order to protect their invention. The tech transfer office will first assess the novelty of the IP through a preliminary due diligence search. If deemed interesting and novel, the tech transfer office will file a provisional application. The provisional application is a brief summary of the actual patent, and it establishes a filing date for the patent. It is not a patent itself. Instead it establishes a "priority date" for the invention in case of a future dispute. If a formal patent is not filed within a year the provisional application will expire. As the provisional application costs a mere $260[39], a tech transfer office is usually quick to file it for an interesting IP.

The next step is to file the patent application. The tech transfer office first conducts a more thorough investigation of the IP novelty. If the executive board decides to execute upon the IP, they will contract a third party to produce a patent application, which is a lengthy, technical, and exhaustive description of the IP. This step costs $5,000 - $10,000. Once filed, the patent is usually reviewed within 6 month and if accepted, is granted within an amount of time proportional to the paperwork required, typically another 6 months.[40] Filing costs can exceed $1,000.[41] The tech transfer office will also file for protection under the Patent Cooperation Treaty.[42] According to the Patent Cooperation Treaty, a patent filed within a participating nation is establishes a priority date for up to 18 months in other participating nations, which typically costs over $10,000. If a patent is not filed in a nation outside the US within this time, the priority date is nullified. Filing patents in other nations is expensive, must be done individually by nation, and usually makes up the bulk of the cost around university IP. Each patent can cost anywhere

[39] uspto.gov/learning-and-resources/fees-and-payment/uspto-fee-schedule#Patent Fees, accessed May 23rd, 2015
[40] uspto.gov/patents-getting-started/general-information-concerning-patents#heading-22, accessed May 23rd, 2015
[41] Id.
[42] wipo.int/pct/en/

between $10,000 and $30,000 per nation. Therefore the nations one selects for protection must be considered carefully.

2.3 Using Intellectual Property

Once a patent is established, there are three ways the patent holder can make use of it: assignment, licensing, and manufacture.

Assignment is the outright sale of the patent protection as a piece of property. "Applications for patent, patents, or any interest therein" can be assigned to another party by contract. Once assigned the IP becomes the sole property of the assignee, including the right to then assign or license the patent to someone else, and the technology developer has no further claim of right to the IP. Assignment is a quick and easy way to monetize a technology, and is a useful method for quickly recovering the cost of research and development.[43]

License of IP is much like a lease, and once the license expires the rights return to the licensor. Use of the licensed IP can be exclusive, nonexclusive, and/or limited exclusive. Exclusive use means that the licensee will be the only entity that can use the technology, while a nonexclusive agreement defines no such limits. Limited exclusive use licenses allow the licensor to license to a specified number of licensees. A license may also define a specific right of use, for example the right to *use the method* described in the patent. Furthermore, territories of use may be defined, which are geographic boundaries within which the licensee can use the IP, for example in the United States or other countries. Revenue in a licensing agreement is generated

[43] 35 U.S.C.A. § 261 (2013).

through fixed payments, such an annual fee; royalties, such a percentage of revenue; and/or an upfront payment.[44]

A patent holder can of course execute upon his or her right to make commercial use of an IP through manufacture. This allows the holder to exercise the most control over the IP, as well as the opportunity to gain knowledge, experience, and more intellectual property. There are many startup costs associated with this method, such as manufacture space and human resources, as well as a number regulatory requirements. Furthermore, once a patent is published, it can be incredibly difficult to know whether another company is infringing upon it, particularly for a process patent. Such a problem makes this expensive use of IP even more perilous.[45]

A university is the sole owner of any IP developed by its laboratories. In the case of Cornell University, the tech transfer office has full authority to make use of the patent however it wishes. It is subject, however, to any government stipulations associated with the federal grant that funded the work, including, usually, a right to the IP for government use. Cornell Tech transfer office does not engage in assignment or manufacture, but rather monetizes IP through licensing agreements. The inventors are also compensated.

Cornell often includes a clause that holds the licensee accountable for certain milestones, such a revenue goals, and gives Cornell the right to terminate the agreement if these milestone are not met. Any person or entity looking to make use of Cornell owned IP must license the

[44] Harold J. Evans, Introduction to Technology Licensing, 35 Arkansas Lawyer (2000).
[45] Paul Flignor & David Orozco, Intangible Asset & Property Valuation: A Multidisciplinary Perspective, World Intellectual Property Organization, available at: http://www.wipo.int/sme/en/documents/ip_valuation_fulltext.html.

technology, whether the interested party is associated with the university or not. This includes the inventor(s).[46]

2.4 The Business Model Canvas

Commercialization is traditionally the most prolific way for an idea to make it out into the world in a meaningful way. Any researcher interested in seeing their work succeed in this way should know the core elements of how a business operates. A business will (usually) only make use of an idea if it "adds value" to the company. That is, does help the company make more revenue. The way an IP adds value to a company, however, is not always clear. Here I will try to simplify how a business operates in order to explain in what ways an IP can add value to a company.

The simplest understanding of the business model currently in vogue is the so-called business model canvas. The canvas presented here was developed by business theorist Alexander Osterwalder as a way to dissect and model the core elements of how a business spends and makes money.[47] The elements of this model serve as an excellent introduction to what makes a business tick, and I will leverage it here to explain the ways in which IP developed in a university can add value to a company.

Finding and executing on IP is critical to how a business creates value, and the better academia and industry communicate, the more seamlessly academically generated IP can be

[46] ctl.cornell.edu/industry/forms/Invention-License-Web.pdf
[47] Osterwalder, Alexander, Yves Pigneur, and Tim Clark. Business Model Generation: A Handbook for Visionaries, Game Changers, and Challengers. Hoboken: John Wiley and Sons, 2010. Print.

integrated into a business. For this reason I urge all researchers to find and cultivate industry contact and become literate in the language of business.

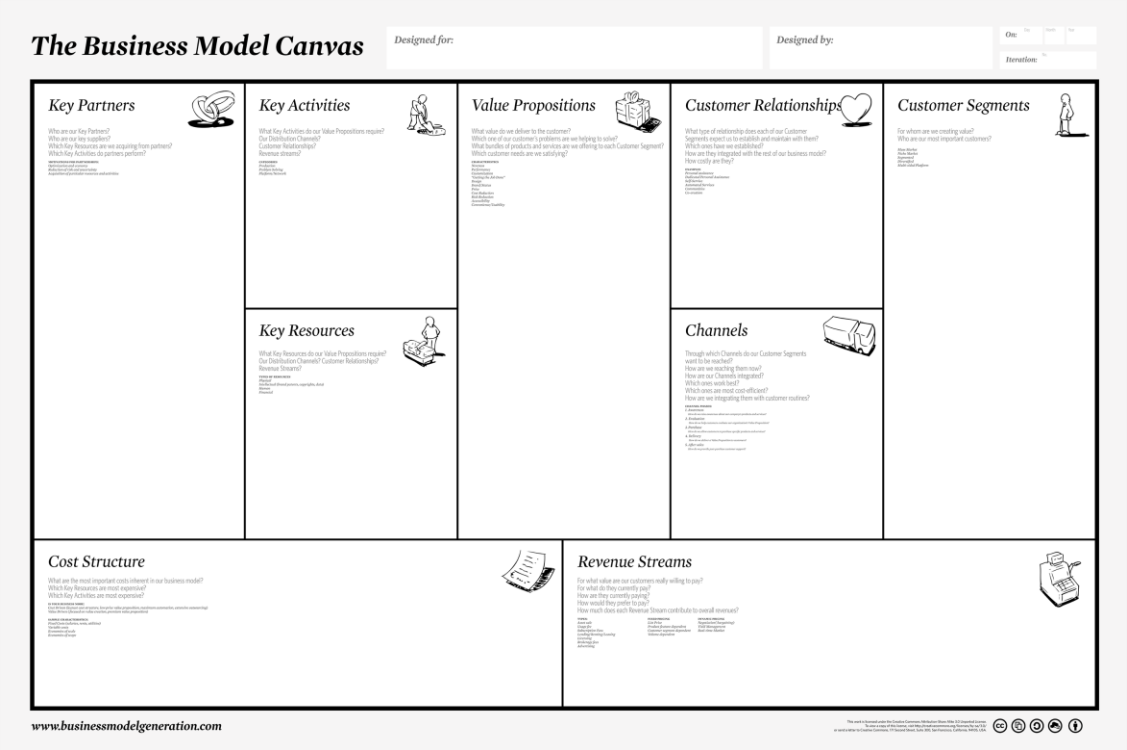

Figure 1. The business model canvas. A brainstorming tool that allows entrepreneurs to simplify and understand the core elements of a business. Key partners, activities, and resources make up the "backend" of the business, while the value proposition, customer relationships, channels, and customer segments make up the "frontend." The backend is made up of the elements which the company actively engages in, while the frontend includes those with which the customer engages as well. Cost structure and revenue stream make up a business's financials.

2.4.1 Customer Segments

The first element worth exploring in detail is customer segments. That is, who does the company aims to reach and serve? Companies often serve many different types of customers, each with their own resources, needs, and preferred mode of interaction. There are many types of customer segments, such as the mass market or a niche segment. If one's IP can expand a company's portfolio to reach new markets, capture more of an existing market, or offer

something new to an existing market, it is the quickest and easiest way to attract attention from the commercial sector.[48]

2.4.2 Value Proposition

The next element, and likely most difficult to grasp, is the value proposition. It describes what goods and services a company offers, and, more specifically, what it is about those goods and services a customer finds valuable. Is it the first of its kind? Does it perform better, have a strong brand, reduce cost, or look better? These are a few of many possible ways a product has value for a customer.[49] A value proposition defines a company. For example, the company PureQuantum, if it were to pursue a manufacturing plan, would offer a process for creating QDs at *large-volume* and *high-quality* at a *highly competitive price*.

Even if PureQuantum did not have the best channels established (how one physically makes and deliver a value proposition) nor customer relationships (marketing and customer outreach), we hope that the strength of our value proposition will compensate for such short comings to our customers, chemical and lighting device manufactures. Together, this is an example of how the front-end of a company (customers, value proposition, channels, and customer relationships) might fit together.

2.4.3 Partners, Key Activities, and Key Resources

As far as the researcher is concerned, discussion of the backend of a company (partners, key activities, and key resources) needs little baring out. Key resources describes the assets

[48] Id.
[49] Id.

required by a company to make everything it does possible. This includes physical resources, like facilities, software, and distribution networks; and financial resources, such as credit; and human resources. Importantly it also includes intellectual resources, such as brands, copyrights, partnerships, and patents.[50]

Key activities describe what a company actually does to make everything work, such as production and problem solving. Particularly in industries where margins are small, such as the battery industry, any IP which can drive down the cost of production or speed up logistics will have great benefit for the company. This includes understanding the current industrial processes, how much each step costs, and quantitatively how much money a newer, better, and faster approach saves.

2.4.4 Revenue and Cost Structure

The final elements of the canvas are revenue streams and cost structure. Revenue streams are how a company makes money from the served customer segment, e.g. sales, usage fee, subscription, licensing, advertising etc. For instance as a manufacturer, PureQuantum would buy the relevant Cornell patents and make a profit by the physical sale of quantum dots. Alternatively, PureQuantum could sub-license the IP rights and earn money through fees and royalties. Both structures are detailed in **Fig 2**. Cost structure describes all of the costs associated with running a business. It is either a value-driven structure, where cost is minimized wherever possible; or value-driven, where companies focusing more on creating a high value product and

[50] Id.

are less concerned with high costs.[51] An example of PureQuantum's financials are presented in Appendix A.

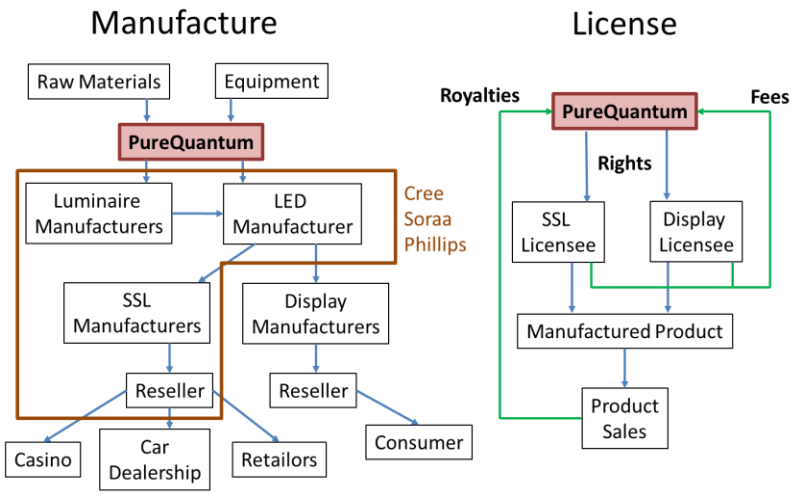

Figure 2. The flow charts above detail two possible business approaches for the startup PureQuantum. The first suggests how PureQuantum could manufacture QDs and sell them for lighting and display applications, while the second details how PureQuantum would profit by licensing the IP to lighting and display manufacturers.

2.5 The Business Plan

In reality the business model canvas is a highly simplified version of a true business plan. It is worth exploring in more detail some of the elements present in a business plan as it is a critical tool for raising capital, and it is worth knowing what potential investors find most important in a startup when deciding to invest.

In a business plan, a thorough examination of the addressed market is required. This touches on elements of the business canvas's customer segment portion, discussed above. However, while the customer segment is a very broad strokes examination of the type of person

[51] Id.

a business wishes to serve, the market analysis in the business plan is a hard numbers look at exactly how large the market it. For instance if it is a billion dollar market, a business owner must consider the inevitable competition, and how much the market he or she can reasonably expect to capture. In a thousand dollar market, the business owner must consider if it is even a big enough market to become profitable. Essentially the business plan answers the question, "is the market large enough for us and competitors to exist?" This is typically done by a "total addressable markets" analysis. An example is included in **Fig. 3**.

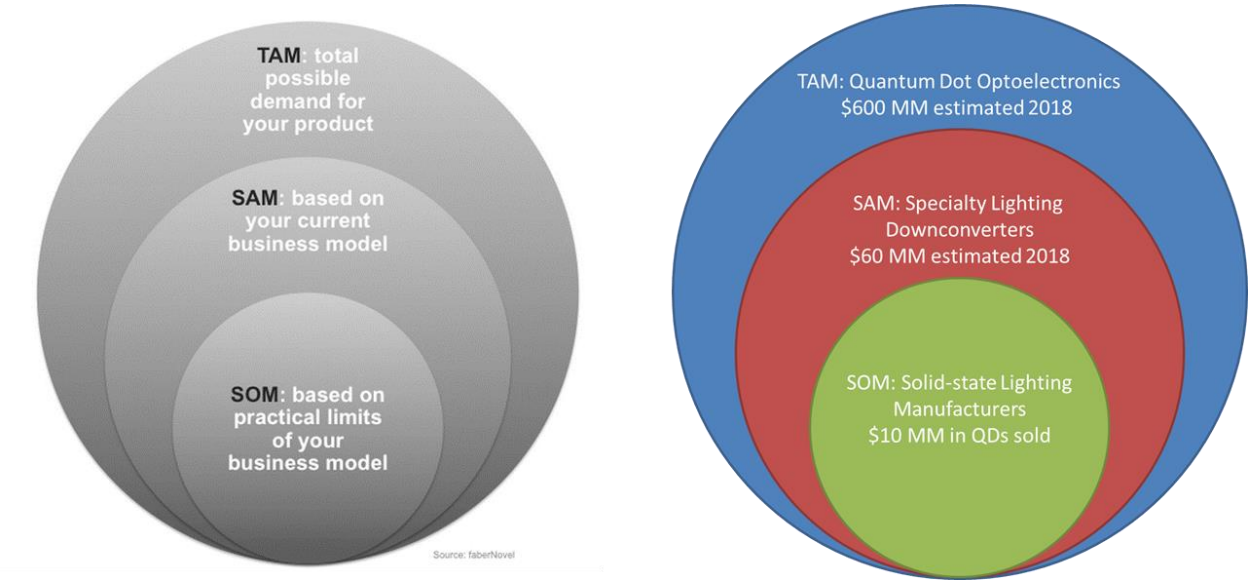

Figure 3. The left figure explains the total addressable market analysis, while the right figure gives an example based on PureQuantum. The total addressable market (TAM) is the entire market of customers who could make use of one's product. The segmented addressable market (SAM) is the specific portion of the TAM the business is targeting with its offerings. The share of the market (SOM) is the fraction of the SAM which the business can realistically serve. Such diagrams serve as a quick and easy way to show investors and other businesspeople the size of a commercial opportunity. (Left) *Bplans, http://articles.bplans.com/tam-sam-and-som-huh/ (accessed April 4th, 2015)*

An IP discussion also makes up a critical part of the business plan. Indeed, questions surrounding IP are sure to come up in any conversation with a potential investor. It is key that a

business be able to demonstrate that it has the rights to the necessary IP, that the IP is novel, and the protection is strong enough to prevent infringement.

An analysis of the competition along with a list of competitive advantages often follows. Competition is not a bad thing. It is a sign of a healthy market, and indicates to investors that there is a profit to be made. However the business plan must indicate an understanding of the capabilities of the competitor and how the businesses compare. At the heart of this is value proposition. What value will one's company offer that a competitor cannot? Cost? Convenience? Design? A business savvy researcher would be wise to understand the value propositions of the key commercial players in his or her field of interest. This will help shape the research in meaningful ways not only for commercial purposes, but for acquiring funding as well.

An underrated element of the plan is the team. The business must demonstrate a strong team is leading the company. This element too may seem of little use to the researcher, and so its importance is worth highlighting here. It is difficult to overstate the importance of strong leadership. One might be tempted to weight things like IP and competitive advantage more when valuing a company, but investors realize that a strong team is critical to a business's success. The team must have the skills, passion, and commitment to put in the hours, raise the money, the charisma to realize the vision of the business.

2.6 The Intersection of Business and Academia

The reader should now have a strong understanding of IP and business basics. The discussion has been kept general enough as to be useful for a researcher looking to intersect with business in a variety of ways, including representing a university to business or starting one's own

business. In closing off this section, it is worth highlighting a few key points and drawing some important conclusions.

The bottom line for a company is that it must add value for its customers. This means must develop its value proposition and select customer segments with extreme care. A researcher looking to do work for the purposes of commercial applications would do well to remember that their IP is be judged solely on what value it can add for the company. This can be achieved by offering tangible advantages over the competition, by opening up new customer segments, reducing costs, or creating a new industry entirely. If one's project does none of these things, it likely does not have use for industry.

There is one important way that researchers can understand if their work can add value to a commercial entity, and that is to cultivate industry contacts. This means calling, meeting in person, and going to gatherings of those involved in the industry of interest. This is the only way that one can truly understand the specific problems that industry is facing, and become literate in the language of business and manufacturing. Oftentimes researchers are complacent with their handful of contacts at large companies and local startups, however this is not sufficient to achieve the insight into the market necessary to understand where the real problems can be solved. Researchers can benefit immensely from taking a page out of the businessperson's book, and cultivating a large network of many kinds of people. Anecdotally, this is the only way to truly understand the state of the industry. Indeed, in this author's experience, the archetype of the academic and the business person are overlapping more than ever, and those who succeed at existing in the nexus will find great success in both fields.

The conventional wisdom for a businessperson trying to understand the market is to treat every conversation with analysts, entrepreneurs, industry engineers, and CEOs like an experiment to test one's business assumptions, complete with genuine hypothesis.[52] For example, PureQuantum originally intended to use our process for creating large scale monodisperse nanoparticles battery anodes. Our hypothesis was that our process would add value for battery manufactures by lowering production costs of nanoparticles and creating higher quality materials. We tested this assumption in over a dozen conversations with experts in business owners in the field, and we concluded that the current method for creating nanoparticle battery anodes is already very inexpensive, and further, that the higher quality nanoparticles we designed would not significantly improve performance over the competition. Our IP did not add enough value to the battery industry, and caused us to explore other possible customers.

After many more conversations we recognized our value proposition matched well the needs solid-state lighting device manufactures. We adjusted our research accordingly, and are confident that our work is directed towards applications with more environmental, societal, and business impact. Beyond this, our conversations lead us to make many meaningful contacts across many industries, many of whom expressed willingness to support our work in grant applications. In return, they got a meaningful take on cutting edge research related to their industry. This serves as a concrete example of how meaningful conversations between academia and business can lead both parties in more fruitful directions.

[52] Blank, Steven G., and Bob Dorf. The Startup Owner's Manual: The Step-by-step Guide for Building a Great Company. Pescadero, CA: K&S Ranch, 2012. Print.

2.7 Networking and Customer Discovery

In closing this section, I believe it will be useful for certain readers to discuss the "nitty-gritty" of customer discovery and how it lead us to quantum dots and solid-state lighting as the most promising application of our process. First of all, this process is not for the faint of heart, but rather requires fortitude, grit, patience, and social tact in equal measures. The first step is research (though not the academic kind). Do research on the customer segment or industry of interest. Understand who the key players are, how they do business, who they deal with, how they earn money, and which events they attend.

Next, one must figure out what value, if any, his or her product can offer such customers. In practice, this means discovering their "pain points." That is, what is it that causes one's customer the most worry, the most time, or the most money? And remember, the most efficient way of doing this is to let the customer spend 90% of the time talking. In customer discovery one is NOT trying to push the product. Instead, he or she is trying to see things from the customer's point of view, and understand what "pain points" can be addressed. Addressing pain points is equivalent to adding value to a company. Develop a list of hypotheses around this, e.g. "nanostructured battery electrode made from monodisperse particles will increase capacity of commercial batteries." Customer discovery conversation are all about answering questions such as these in order to really understand a customer's main pain points.

Of course one must eventually make initial contact. This means making use of any and all contacts, cold calling, and attending events. For PureQuantum, attending industry conferences proved the most useful in building our network. Meet in person whenever possible and always staying focused on testing one's hypotheses. At the end of the conversation, it is critical to ask who else might be interested in talking about the project in order to grow one's network. Be sure to ask for an introduction.. After the conversation, one must think about the hypotheses, what he or she learned, and reevaluate the approach

often. Focus on what customers don't say, as well as what they say, and keep an eye out for trends among their responses between customers.

For example, after many conversations with battery manufactures, we heard many times that monodisperse particles would not offer enough electrochemical performance boost to merit overhauling a manufactures approach to making devices. We continued to push however. Enough of our contacts (after 25 or so conversations) told us that when it comes to nanoparticles, the up and coming applications are optoelectronic, especially in displays and solid-state lighting. We went back to our hypothesis, tweaked them, learned about the solid-state lighting market, and started our process anew. This time we found success, validating our hypotheses in the solid-state lighting market. Our approach did have something important to offer customers looking to take advantage if highly-quality, monodisperse quantum dots for optical and optoelectronic applications.

Chapter 3: A General Method for High-Performance Li-ion Battery Electrodes from Colloidal Nanoparticles without the Introduction of Binders or Conductive-Carbon Additives: The Cases of MnS, $Cu_{2-x}S$, and Ge

*Don-Hyung Ha†, Tiffany Ly†, Joseph M. Caron, Haitao Zhang, Kevin E. Fritz, and Richard D. Robinson**
Department of Materials Science and Engineering, Cornell University, Ithaca, NY 14853

† Authors contributed equally to this work
* To whom correspondence should be addressed. E-mail: rdr82@cornell.edu.

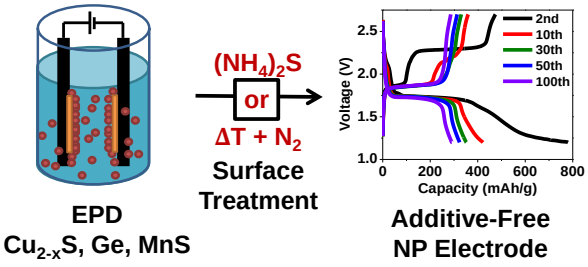

NOTE ON REFERENCES: In order to authentically reproduce this submitted work, references of this section, Chapter 3, are presented at the end of the work.

1.1 Abstract

In this work, we demonstrate a general lithium-ion battery electrode fabrication method for colloidal nanoparticles (NPs) using electrophoretic deposition (EPD). Our process is capable of forming robust electrodes from copper sulfide, manganese sulfide, and germanium NPs without the use of additives such as polymeric binders and conductive agents. After EPD, we show two post-processing treatments ($(NH_4)_2S$ and inert atmosphere heating) to effectively remove surfactant ligands and create a linked network of particles. The NP films fabricated by this simple process exhibit excellent electrochemical performance as lithium-ion battery electrodes.

Additive-free $Cu_{2-x}S$ and MnS NP films show well-defined plateaus at ~1.7 V, demonstrating potential for use as cathode electrodes. Due to the absence of additives in the NP film, this additive-free NP film is an ideal template for ex-situ analyses of the particles to track particle morphology changes and deterioration as a result of Li ion cycling. To this end, we perform a size-dependent investigation of $Cu_{2-x}S$ NPs and demonstrate that there is no significant relationship between size and capacity when comparing small (3.8 nm), medium (22 nm), and large (75 nm) diameter $Cu_{2-x}S$ NPs up to 50 cycles; however, the 75 nm NPs show higher coulombic efficiency. Ex-situ TEM analysis suggests that $Cu_{2-x}S$ NPs eventually break into smaller particles (< 10 nm), explaining a weak correlation between the size and performance. We also report for the first time on additive-free Ge NP films, which show stable capacities for up to 50 cycles at 500 mAh/g.

Keywords: Additive-free, Copper sulfide, Manganese sulfide, Germanium, Size dependent, Colloidal Nanoparticle, Electrophoretic deposition, Ammonium sulfide

1.2 Introduction

Nanomaterials have strong promise for use in lithium-ion battery (LIB) electrodes due to their greatly reduced diffusion length for ionic transport and capability to accommodate strain through cycles.[1-2] In particular, colloidal nanoparticles (NPs) are emerging as ideal building blocks for creating and designing LIB electrodes with enhanced electrochemical performance.[3-6] The solution processability of colloidal NPs is a great advantage for the fabrication of complicated devices and for mass production methods, such as roll-to-roll manufacturing. Furthermore,

colloidal NPs syntheses can both tailor the NPs' properties through a wide selection of materials and exercise fine control of size and shape.[7-13] Traditionally, NP LIB electrodes require polymeric and carbon-based additives to bind NPs to the electrodes, support mechanical integrity, and increase their conductivity. These additives, which do not participate in the electrochemical reaction, generally make up 10 – 40 wt% of the electrode,[3, 14-16] greatly decreasing their value for portable energy storage. In addition, additives can influence the battery performance significantly, confounding our understanding of the interactions between of Li ions, electrons, and the active materials.[17-18] Our group has demonstrated that electrophoretic deposition (EPD) is a viable technique to assemble NPs onto an electrode without the use of additives.[3] The NP assemblies are mechanically and chemically robust, possess strong inter-particle coupling, have good electrical properties[3, 19-20], and increase the gravimetric and volumetric capacities of LIBs.[3]

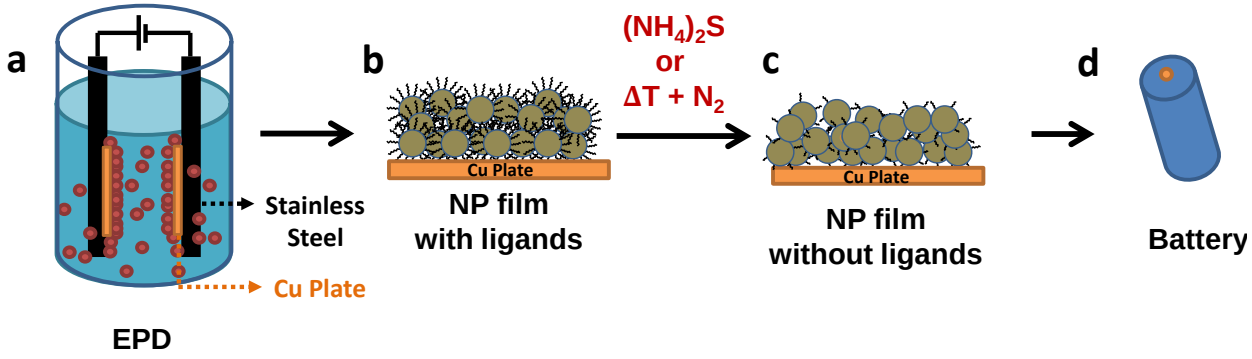

Figure 1. Schematic of process for fabrication of additive-free battery electrodes for colloidal nanoparticles. (a) EPD is used to form NP films from colloidal NPs. (b) NP films are formed on Cu plates. (c) $(NH_4)_2S$ treatment or heat treatment removes organic ligands from the NPs. (d) NP films are used as electrodes for Li-ion batteries.

In the EPD process, two metal plates with an electric potential between them are immersed in a liquid solution of colloidal NPs.[21-23] The potential drives the NPs to the EPD electrodes, to which they adhere. This fabrication method has proven that it is applicable for

large area processes[24-25] and useful for other applications, such as light-emitting devices[26], electrocatalysts[20, 27], and solar cells.[28] Previously, we have shown that EPD can create arrays of NPs with high mobilities and conductivities an order of magnitude higher than traditional spin-cast films, ideal for printable electronics.[19] This enhanced carrier-transport performance was shown to be due to better inter-particle coupling created from the EPD processing.[19] We have also shown EPD-formed cobalt metal NP assemblies can be transformed into a robust cobalt oxide for NP LIB electrodes[3] and high-performance oxygen reduction/oxygen evolution catalysts.[20]

For this work we demonstrate the versatility of EPD to make additive-free battery electrodes by applying EPD to both metal-sulfide NPs and the less commonly investigated metal NPs. Copper sulfide is an emerging material for battery electrodes due to its relatively high working voltage and high capacity.[29-31] Previously considered an attractive positive electrode material in primary lithium batteries[29], copper sulfide has emerged as a promising reversible secondary battery electrode due to advances in electrolyte performance that help prevent polysulfide shuttling in nanosized electrode materials.[32] Manganese sulfide nanomaterials have also recently demonstrated their promise as high-performance battery electrode materials due to their high capacity and excellent cyclability.[33-34] Germanium is considered a potential next-generation material for lithium-ion battery electrodes due to its high capacity, 1,600 mAh/g.[35-38] Ge is structurally similar to Si, and although Si has a higher theoretical capacity, Ge undergoes an isotropic expansion during lithiation that reduces strain and pulverization. Furthermore, Ge has 10^4 times the electrical conductivity and 400 times the lithium-ion diffusivity when compared to Si.[35-37]

Our general method to form robust, additive-free LIB electrodes from both semiconductor NPs and metal NPs combines EPD with processes to remove surfactant ligands by either chemical treatment or inert atmosphere heating. The chemical treatment process we pioneer is simple, fast, and scalable, while the heating technique may be employed to preserve the chemical composition of the electrode. Our new technique eliminates the need for additives in batteries, and can increase their specific capacity drastically (~30%) due to the absence of additives, which are universally considered essential for battery electrodes from nanoparticles. The promise of our technique is evident by the high capacity (>70% of theoretical value) and coulombic efficiency (~95%) of the MnS system, as well the stable capacities achieved by the Ge system, which is also the first reported additive-free Ge NP electrode system. Furthermore, the additive-free process allows us to rigorously explore the effect of NP size on the robustness of LIB electrodes. Surprisingly, 3.8, 22, and 75 nm diameter copper sulfide NPs produce high-quality LIBs with nearly identical capacities. Equally surprising is that large NP electrodes have higher coulombic efficiency than the smaller NPs electrodes.

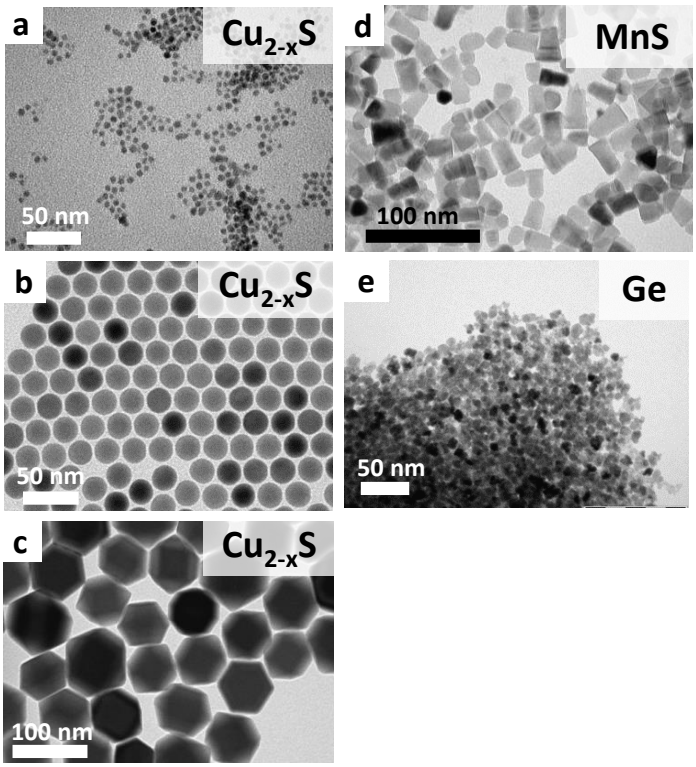

Figure 2. TEM images of copper sulfide, MnS, and Ge NPs. Copper sulfide NPs show a wide range of NP sizes from 3.8 nm (**a**), and 22 nm (**b**), to ~75 nm (**c**). MnS NPs (**d**) display ~ 15 nm size. Ge NPs (**e**) are ~14 nm in size.

1.3 Experimental

EPD has been utilized as a powerful tool to fabricate NP films with excellent mechanical properties.[3, 39] It creates NP films that are 10× more electrically conductive than those assembled through conventional solution-processing methods, such as a spin-coating.[19] **Fig. 1** shows a schematic of the fabrication process for additive-free NP films for lithium-ion battery electrodes. First, colloidal NPs are suspended in a nonpolar solvent, such as hexanes, at a concentration of ~0.1-0.5 g/L. Then copper plates, which serve as the NP film substrates, are attached onto larger stainless steel plates. The plates are submerged in the solvent and a voltage (300-600 V) is applied between two parallel steel plates. This potential causes colloidal NPs to bind to both the

steel plates and the copper plates (**Fig. 1a**). The brown color of the initial NP solution approaches transparency after a few minutes, indicating most of the NPs are removed from the solvent and assembled on the plates under the high voltage. The NP-coated copper plates are then removed from the steel, subject to a surface ligand removal treatment, and tested in half-cell batteries. The thickness of the film can be controlled from a few hundreds of nm to 2 μm. We target 1 μm for the purposes of this study, having been previously determined to be the optimal thickness for good conductivity between the current collector and counter electrode.[3] This provides an average active material loading of 0.13 mg/cm^2. When a film is greater than ~1.15 μm, the assembled half-cell typically shows no open circuit voltage or poor performance, evidence of poor conductivity.

We have found two potent means to eliminate the native organic species on the NP surfaces of the EPD NP films: an ammonium sulfide ($(NH_4)_2S$) treatment[40] and an inert-atmosphere heating treatment. The ammonium sulfide treatment chemically removes the organic surfactant ligands bound to the NPs' surface, leaving behind metal-sulfur bonded surfaces.[40] The treatment is performed by dipping a NP film into a 0.02 M $(NH_4)_2S$ methanol solution for 30 seconds and then into pure methanol to clean off unreacted ammonium sulfide and any free organics. Alternatively, heating the NP films at 300 °C for 1-3 hours in an inert atmosphere eliminates ~85% of the organic species, as shown by thermogravimetric analysis (**Fig. S1**).

The ammonium sulfide-treated or heat-treated NP film on a Cu plate (current collector) is used as a lithium-ion battery electrode without the addition of any additive materials, such as polymeric binders and carbon black. The electrochemical battery cells are assembled in air-free

conditions and use a lithium foil counter electrode. Because no additives are added, ex-situ TEM experiments can be carried out for further characterization of size-dependent battery cycling performance of copper sulfide NPs. After the battery is cycled, the NP film is removed from the testing cell and rinsed with ethanol and hexanes in order to remove electrolyte residues. The NP samples for TEM imaging are then scraped off from the NP film and placed on a TEM grid.

1.4 Results and Discussion

The colloidal $Cu_{2-x}S$ NPs are synthesized with three different diameters – 3.8 nm (**Fig. 2a**), 22 nm (**Fig. 2b**), and 75 nm (**Fig. 2c**) – to examine size-dependent cycling performance. TEM images show the MnS and Ge NPs to be ~15 nm and ~14 nm in size, respectively. (**Fig. 2d,e**). XRD results show that the 3.8 nm $Cu_{2-x}S$ NPs are djurleite phase (**Fig. 3a**, blue bars, JCPDS 23-0959, structural information in **Fig. S2**), and the 22 nm and 75 nm $Cu_{2-x}S$ NPs are roxbyite phase (**Fig. 3a**, black bars, JCPDS 23-0958, structural information in **Fig. S2**). MnS NPs show faceted shapes with a size of ~15 nm (**Fig. 2d**). The XRD pattern confirms the NPs are MnS cubic zinc blende phase (**Fig. 3b**, red bars, JCPDS 40-1288) with a small contribution of MnS rock-salt phase (denoted by * in **Fig. 3b**). Ge NPs exhibit a ~14 nm size (**Fig. 2e**) and are well matched with diamond cubic Ge (**Fig. 3c**, red bars, JCPDS 4-0545). Our previous study showed that the $(NH_4)_2S$ treatment does not induce any phase transformations to the copper sulfide NPs.[19] MnS and Ge NP samples also show no phase change after the $(NH_4)_2S$ treatment (**Fig. S3**).

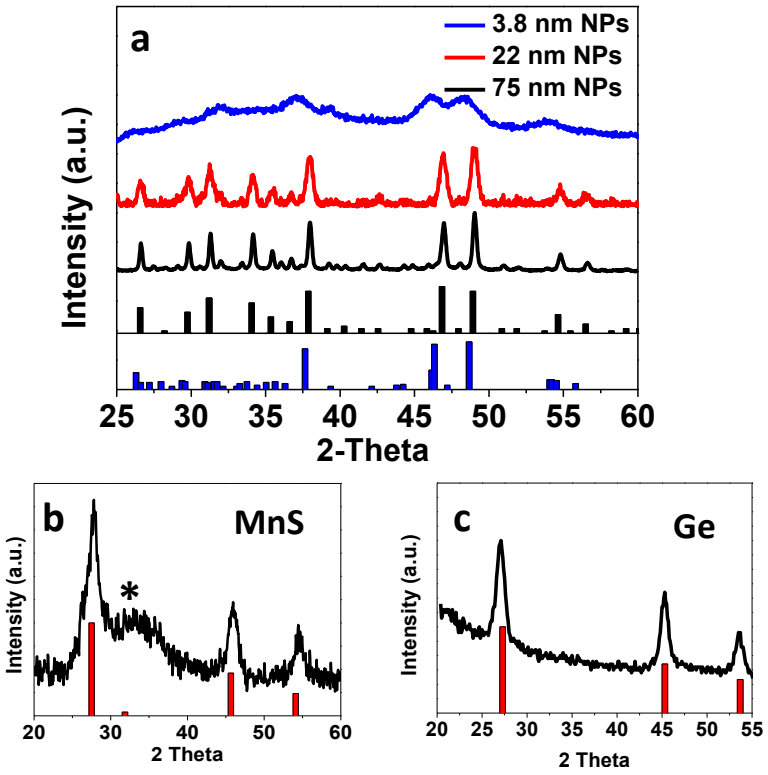

Figure 3. XRD patterns of copper sulfide, MnS, and Ge NPs. (a) XRD results show that 3.8 nm copper sulfide NPs are djurleite phase (blue bars, JCPDS 23-0959) and 22 nm and 75 nm copper sulfide NPs are roxbyite phase (black bars, JCPDS 23-0958). (c) XRD result confirms that MnS sample is cubic zinc blende phase (red bars, JCPDS 40-1288). In (b), the broad peak at approximately 34° marked by * corresponds to a small contribution from rock-salt α-MnS phase. XRD results of Ge NPs (c) show that Ge is pure diamond cubic Ge (red bars, JCPDS 4-0545).

Fig. S4 shows TEM images of the 3.8 nm and 75 nm diameter NPs, respectively, after 1 hr of an inert-atmosphere heating. The smaller-sized NPs show significant sintering and morphology change, while the larger NPs (~75 nm) show little size and morphology change. XRD is used to determine if the heating process causes a phase change in the NPs after heating. In **Fig. S5a,b**, it can be seen that both the 3.8 nm and 22 nm NPs undergo a partial phase change and reduction to Cu, as the XRD pattern is matched to contributions from both copper metal and different copper sulfide phases, including djurleite and chalcocite. Conversely, XRD patterns in

Fig. S6 suggest the 75 nm NPs remain the $Cu_{2-x}S$ phase and are well matched with the djurleite copper sulfide phase. The slight phase change from roxbyite to djurleite should be caused by the phase stability difference (djurleite phase is more stable than roxbyite).[41] Since the inert heating method converts smaller particles to the bulk phase, the heat treatment method is a viable fabrication technique to form LIB NP electrodes from the larger-sized $Cu_{2-x}S$ NPs. The smaller particles are more susceptible to reduction into the copper metal phase because their higher surface-to-volume ratio increases the amount of surfactant ligand, oleylamine, which can act as a reducing agent that converts copper sulfide into copper phase.[42]

1.4.1 Metal Sulfides

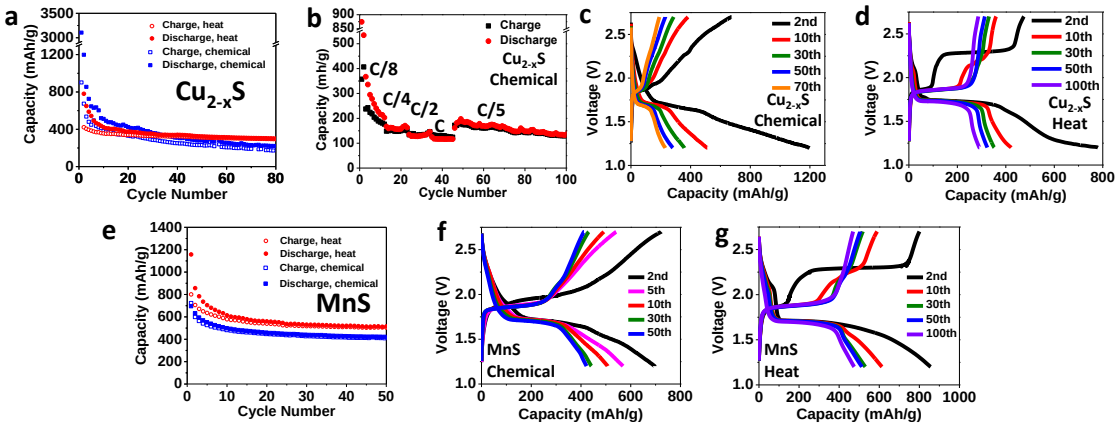

Figure 4. Electrochemical performance of copper sulfide (3.8 nm and 75 nm) and MnS NP films without carbon black and polymeric binder additives. (a) Capacity retention of copper sulfide NP (3.8 nm) film at C/2 rate show the charge (open red circles and open blue squares for heat- (75 nm) and chemically-treated (3.8 nm) sample, respectively) and discharge (solid red circles and solid blue squares for heat- and $(NH_4)_2S$-treated samples, respectively). (b) Cycling performance of $(NH_4)_2S$-treated copper sulfide NP (3.8nm) film at various current rates show discharge (red circles) and charge (black squares) capacities. (c) Galvanostatic charge–discharge curves of $(NH_4)_2S$-treated copper sulfide (3.8 nm) NP film show a voltage plateau at 1.7 V. (d) Galvanostatic charge-discharge curves of inert-atmosphere heat-treated copper sulfide (75 nm) NP film show well-defined voltage plateaus at 1.7 V, which is the same as for $(NH_4)_2S$-treated copper sulfide NP films. (e) Capacity retention of MnS NP film at C/5 rate show the charge (open red circles and open blue squares for heat and chemically treated sample, respectively) and discharge (solid red circles and solid blue squares for heat- and $(NH_4)_2S$-treated samples, respectively). (f) Voltage profiles of chemically-treated MnS NP film show well-defined plateau at 1.7 V. (g) Inert-atmosphere heat-treated MnS NP film also shows ~1.7 V voltage plateau in galvanostatic curves similar to the $(NH_4)_2S$-treated MnS sample.

The additive-free $Cu_{2-x}S$ and MnS films show outstanding battery performance. The $(NH_4)_2S$-treated copper sulfide NP (3.8 nm) films retain capacities greater than 200 mAh/g at C/2 rate even after 50 cycles (**Fig. 4a**). Even copper sulfide NP (75 nm) films cycled at 2C rate still demonstrate good capacity retention (**Fig. S7**). Cycling performances at various other current rates demonstrate excellent capacity recovery after cycles at high current rates (**Fig. 4b**). Galvanostatic charge–discharge curves of copper sulfide (3.8 nm) NP films show a well-defined plateau at ~1.7 V (**Fig. 4c**) indicating that the conversion reaction from $Cu_{2-x}S$ to Cu + Li_2S occurs.[30,

[43] The inert atmosphere heat-treated NP film electrodes are tested under the same conditions as the ammonium sulfide treated electrodes and exhibit better electrochemical performance. **Fig. 4a** shows the high capacity and stable cyclability of the 75 nm $Cu_{2-x}S$ films, capable of retaining capacities greater than 280 mAh/g up to the 100th cycle. The galvanostatic charge-discharge curves shown in **Fig.4d** demonstrate the same well-defined voltage plateau at ~1.7 V.

The $(NH_4)_2S$-treated MnS system shows stable cyclability over 50 cycles with a well-defined voltage plateau also at ~1.7 V (**Fig. 4e,f**). The voltage plateau at 1.7 V of both metal sulfides suggests that they may be useful as cathode materials in LIBs. The MnS NP films show stable capacity at 420 mA/g even after 50 cycles, which is ~70% of the value of its theoretical capacity (616 mAh/g). After heat treatment, the MnS NP films show excellent cyclability and capacity retention of ~470 mAh/g after 100 cycles (**Fig. 4e**) and a voltage plateau at ~1.7 V as well (**Fig. 4f**). This 1.7 V plateau might correspond to the Li^+ ion insertion into the MnS lattice creating a homogeneous phase of Li_xMnS.[33] Overall our additive-free $Cu_{2-x}S$ and MnS results show comparable performance to literature reports that rely on the use of additives.

1.4.2 Germanium

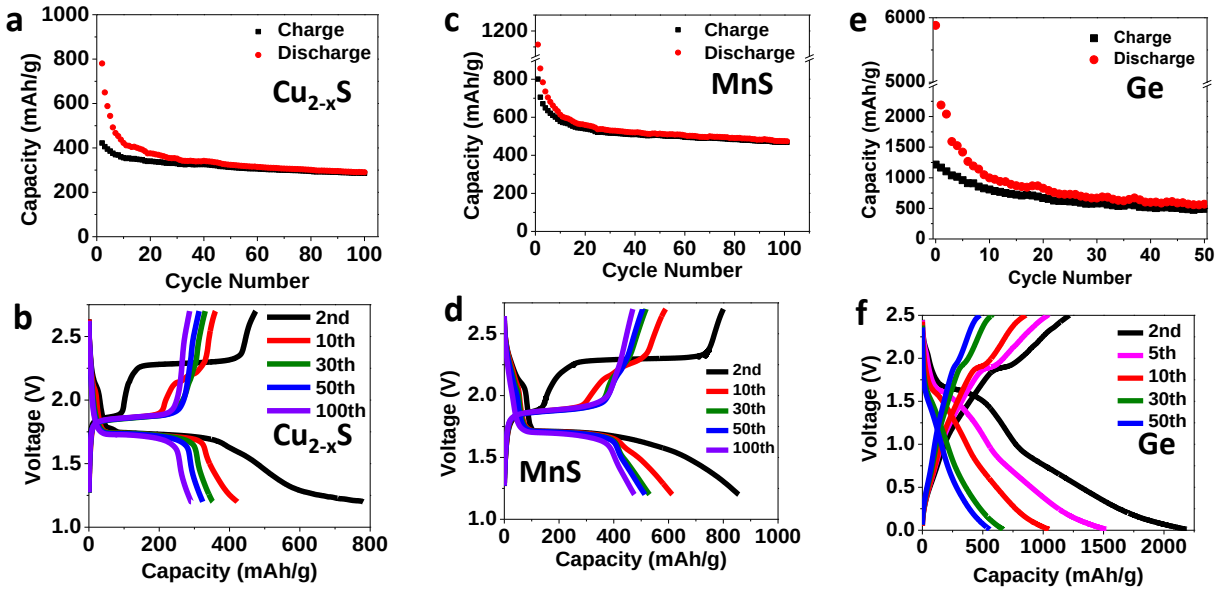

Figure 5. Electrochemical performance of Ge NP films. (a) Capacity retention of Ge NP film at C/2 rate show the charge (open red circles and open blue squares for heat and chemically treated sample, respectively) and discharge (solid red circles and solid blue squares for heat and $(NH_4)_2S$ treated samples, respectively). (b) Galvanostatic curves of $(NH_4)_2S$-treated Ge sample show characteristic charge-discharge curves after the first discharge. (c) Charge-discharge curves at C/5 rate of heat treated Ge sample show cycle stability and capacity at >500 mAh/g even up to 50th cycle.

The $(NH_4)_2S$-treated Ge electrode exhibits capacities over 350 mAh/g after 50 cycles (**Fig. 5a,b**), and the heat-treated Ge electrode shows a stable capacity of over 500 mAh/g after 50 cycles (**Fig. 5a,c**). Both exhibit a voltage plateau at ~1.7 V that gradually diminishes over cycles, which might be due to the formation of SEI layer and the decomposition of native oxide formed on the Ge NP surface.[37] These SEI layer and native oxide may induce the large irreversible capacity in the first few cycles as well.[37] It is interesting to note that this high voltage plateau may make the Ge electrode feasible as a cathode rather than an anode. Further studies will be undertaken to identify and isolate this effect. While other groups report better NP battery results for Ge, our system is the first Ge NP electrode that does not make use of additives, allowing more

scientific studies of only the active materials without the introduction of unknowns from slurry processing (supplemental).

1.4.3 Size dependent performance

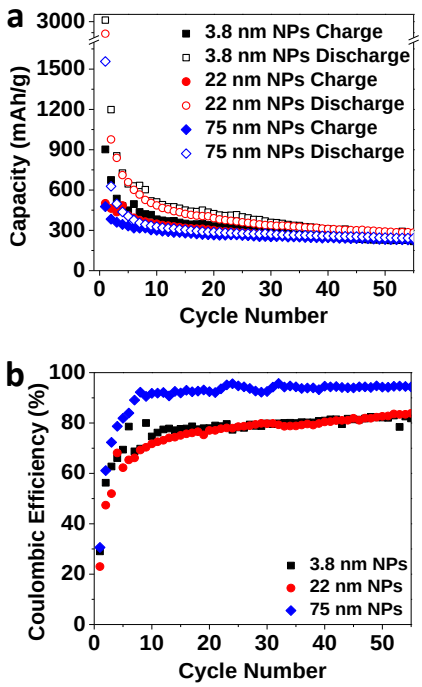

Figure 6. Size dependent cycle performance of copper sulfide NP EPD films with $(NH_4)_2S$ treatment at C/2 rate. Larger particle NP sizes demonstrate higher (**a**) cycle stability and (**b**) coulombic efficiency.

The coulombic efficiency of the NP films formed with the ammonium sulfide treatment and heat treatment are compared in **Fig. S8a,b,c**. After a stable capacity has settled in by the 20-25th cycle, no significant difference between treatments can be seen in coulombic efficiency, implying that the lithiation and delithiation mechanism is not significantly affected by the treatments. However, a significant difference can be seen between the coulombic efficiency of

each material system. In both cases—ammonium sulfide treatment (**Fig. S8d**) and heat treatment (**Fig. S8e**)—the MnS system has the highest efficiency (~95%), followed by the $Cu_{2-x}S$ system (~90%), and lastly the Ge system, which has a stable efficiency of ~80%. These results suggest that the coulombic efficiency depends primarily on the materials system and not the post-processing treatments, though we will show later that NP size offers a complication to this trend.

The slight difference in capacity retention and performance between the $(NH_4)_2S$-treated and heat-treated NP film electrodes can be attributed to several factors. In addition to removing surfactant ligands from the NP surfaces, the ammonium sulfide also reacts with the Cu plate substrate to produce a copper sulfide film. This unwanted copper sulfide film formation can decrease electrical conductivity to the NPs through poor contact. After an ammonium sulfide treatment, the mass of an NP film electrode increases an average of ~20%. As ligand removal by $(NH_4)_2S$-treatment can account for a ~10-17% mass decrease in the electrode, the total copper sulfide film formation can be estimated to be ~30 wt% of the electrode (supplemental). Our supplemental work suggests copper created in this way contributes relatively little to the performance of the electrode.

Conversely, the difference in performance may be explained by sintering of the heat treated samples. Heat treatment of the NP films over several hours not only ensures removal of ~85% of organic ligands (**Fig. S1**) but can also increase conductivity through sintering of the NPs. However, it is not a feasible method for small NP sizes due to over-sintering into a bulk phase (**Fig. S5a,b)**. Heat treatment is also a time consuming process that requires time for heating

and cooling, unlike the ammonium sulfide treatment that only requires minutes for successful ligand removal.

Size-dependent battery performance of nanomaterials is a critical topic in battery electrodes. The role of nanosize in a battery system is only studied for a limited number of cases, such as Si,[44] SnO_2,[45] and GeO_2.[46] **Fig. 6** compares the electrochemical performance of batteries assembled with NP film electrodes formed from differently sized copper sulfide NPs and treated with $(NH_4)_2S$. After 50 cycles at C/2 rate, the performances of all three NP film electrodes are comparable and attain similar stable capacities (~300 mAh/g). TEM results (**Fig. 7**) suggest this equalizing of capacities is likely due to the fracturing of the larger NPs into smaller particles (<10nm) after several lithiation-delithiation cycles. Because our electrode films are assembled without any additives, their post-cycling fracture may be easily examined with TEM. **Fig. S9** show the 22 nm $(NH_4)_2S$-treated NPs begin to break into smaller particles after the first lithiation process, analogous to other NP materials for conversion reactions, such as metal fluorides[47] and metal oxides.[48] The addition of the electrolyte to the NP film (i.e., addition of electrolyte without cycling) does not cause any change in NP shape or size; therefore, we suggest it is the lithiation process that breaks down the large particles into smaller particles. These particles are likely composed of Li_2S and Cu, as suggested by the 1.7 V voltage plateau.[43] The number of cycles required to fracture the $(NH_4)_2S$-treated copper sulfide large NPs (~75 nm) through discharge/charge cycling is higher than that of the 22 nm-sized NPs. The large 75 nm NPs retain their overall morphology through the first lithiation, but smaller (3-15 nm) particles appear, likely from the outer shell of these large particles pulverizing (**Fig. 7c**). After further cycling, the large

NPs eventually lose their overall shape and break into smaller particles similar to the 22 nm NPs case, implying that a stable NP size less than 10 nm is indeed reached regardless of initial size.

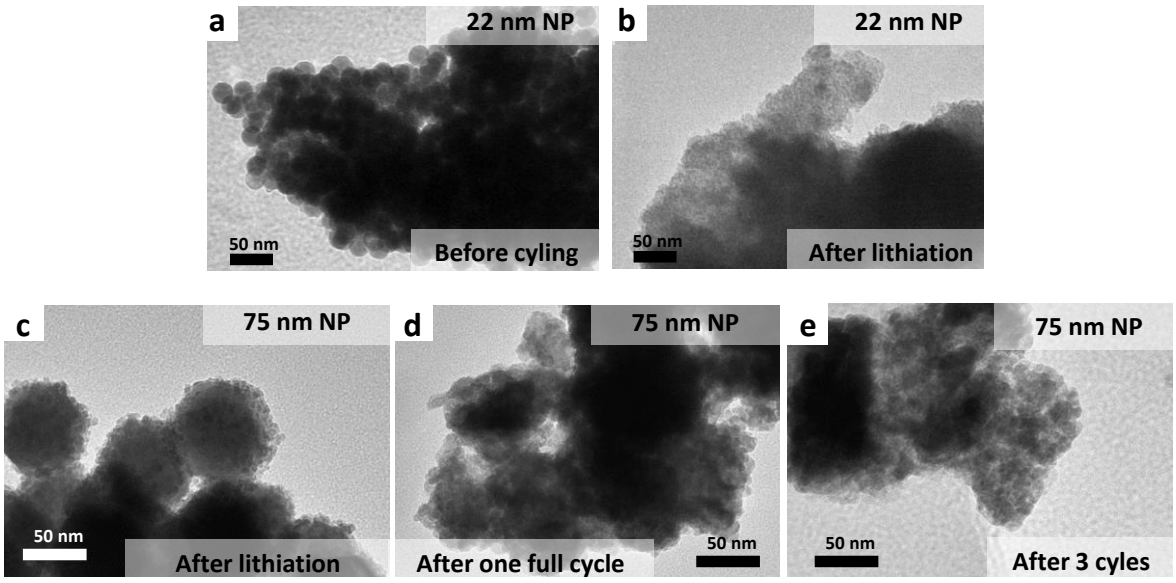

Figure 7. TEM images of copper sulfide NPs through battery cycling process. (a) 22 nm copper sulfide NPs assembled in a battery cell with electrolyte do not show any degradation. (b) After the first lithiation process, 22nm copper sulfide NPs convert to smaller NPs (2-6 nm). (c) Copper sulfide NPs with 75 nm size retain their overall shape after one lithiation process but start to break down to a smaller sized particles (3-10 nm). (d) After one full cycle (lithiation + delithiation), the 75nm NPs start to loose their overall morphology. (e) Three full cycles lead to the aggregation of small NPs (3-15 nm) without evidence of the initial 75 nm size particles.

The cycling performance of the $(NH_4)_2S$ treated $Cu_{2-x}S$ electrodes (**Fig. 6)** shows that coulombic efficiency is related to size. The coulombic efficiency of the 75 nm NPs is significantly greater than the 22 or 3.8 nm NPs, which show similar coulombic efficiencies. This discrepancy may be attributed to the insufficient removal of surfactant ligands from the smaller particles through the ammonium sulfide treatment. Since the surface-to-volume ratio is much larger on the smaller particles, there are many more ligands per unit mass of NPs. Therefore a more concentrated $(NH_4)_2S$ solution or longer exposure to the solution is required to remove all of the

ligands. However, extended exposure times and high concentrations of $(NH_4)_2S$ treatment, the $Cu_{2-x}S$ films begin to delaminate (**Fig. S10,11**). We have empirically shown in a previous work that the parameters of the $(NH_4)_2S$ procedure described here is the most reliably rigorous treatment that can be performed before the material begins to delaminate.[33] The presence of unremoved ligands in the NP film may result in an irreversible process, causing the disparity between the charge and discharge capacities.

1.5 Conclusion

We have demonstrated that EPD is a general, simple, and effective technique for processing NPs for electronic applications that eliminates the need for conductive agents and polymeric binders. Both metal-sulfide and metal NPs were shown to deposit into well-connected and robust assemblies, which remain intact even after ultrasonication, and are capable of forming additive-free battery electrodes of excellent electrochemical performance. This performance is likely attributable to the superior inter-particle coupling and electrical properties such as high electrical conductivity afforded by EPD processing when compared to traditional methods, as we have reported earlier.[19] The performance is best demonstrated by the high capacity retained by the $Cu_{2-x}S$ system through 50 cycles, the stable cyclability of the MnS system for over 50 cycles, and the high capacity achieved by the Ge system of 500 mAh/g. The 1.7 V voltage plateau of the metal sulfides shows the promise of $Cu_{2-x}S$ and MnS as cathode materials for LIBs, and the cyclability of the Ge system suggests its viability as an anode material.

Two different ligand removal treatments of the NP electrodes were explored in detail: the $(NH_4)_2S$ chemical treatment and the inert-atmosphere heating treatment. The $(NH_4)_2S$ treatment was shown to be quick, simple, and effective for all materials and sizes explored in this study. However, this treatment formed additional $Cu_{2-x}S$ via a side-reaction with the Cu substrate. The heat treatment, though slower and less energy efficient, was shown to be a useful technique for all three material systems. Heat treatment can, however, cause sintering and bulk transformation in smaller NP sizes. Therefore, in order to take advantage of the properties of smaller NPs, $(NH_4)_2S$ treatment should be used to treat NP films.

A study was also performed to relate NP size and performance. 3.8, 22, and 75 nm $Cu_{2-x}S$ NPs all exhibited similar performances after a just a few cycles. This result, alongside TEM studies, suggests that NP size does not play a significant role in battery electrode performance in the $Cu_{2-x}S$ system because of fracturing during cycling. Coulombic efficiencies were found to be higher in larger particles, which we attribute to more effective surfactant ligand removal with decreasing surface to volume ratio.

Our reported method is meant to introduce a scientific procedure to isolate and characterize the active materials, rather than engineering the materials and/or structure for a record capacity performance. By isolating the active nanoparticles, we set the stage for future works to use these methods to understand the active system without the interference of the additives. For instance, to understand the effects of nanoparticle size on capacity, an ideal study would remove the unknowns introduced by the additives – such as size effects with mixing and adhesion, or homogeneity of the slurry – and focus solely on the active nanoparticles. Since we

do not need additional supportive material, our system is very close to a pure system, which makes our electrodes ideal for systematic studies.

1.6 Acknowledgments

This work made use of the Cornell Center for Materials Research Shared Facilities which are supported through the NSF MRSEC program (DMR-1120296). The work was supported in part by the National Science Foundation under Award Number CHE-1152922 and CMMI-1344562. D-H.H. and R.D.R. were supported as part of the Energy Materials Center at Cornell (EMC^2), an Energy Frontier Research Center funded by the U.S. Department of Energy, Office of Science, Office of Basic Energy Science under Award Number DE-SC0001086. The authors thank Alexandria Cruz for help with synthesis and NP film fabrication. The authors also thank Doug Nevers for TGA analysis.

Supporting Information

Supporting Information Available: Supporting Information includes materials and methods detailing the synthetic reactions, characterization techniques, and electrochemical measurements, as well as supplemental figures intended to support information presented in the paper. This material is available free of charge via the Internet at http://pubs.acs.org

1.7 References

1. Chan, C. K.; Peng, H. L.; Liu, G.; McIlwrath, K.; Zhang, X. F.; Huggins, R. A.; Cui, Y., High-Performance Lithium Battery Anodes Using Silicon Nanowires. *Nat. Nanotechnol.* **2008,** *3* (1), 31-35.
2. Poizot, P.; Laruelle, S.; Grugeon, S.; Dupont, L.; Tarascon, J. M., Nano-Sized Transition-Metaloxides as Negative-Electrode Materials for Lithium-Ion Batteries. *Nature* **2000,** *407* (6803), 496-499.
3. Ha, D.-H.; Islam, M. A.; Robinson, R. D., Binder-Free and Carbon-Free Nanoparticle Batteries: A Method for Nanoparticle Electrodes without Polymeric Binders or Carbon Black. *Nano Lett.* **2012,** *12* (10), 5122-5130.
4. Bodnarchuk, M. I.; Kravchyk, K. V.; Krumeich, F.; Wang, S.; Kovalenko, M. V., Colloidal Tin–Germanium Nanorods and Their Li-Ion Storage Properties. *ACS Nano* **2014,** *8* (3), 2360-2368.
5. Koo, B.; Xiong, H.; Slater, M. D.; Prakapenka, V. B.; Balasubramanian, M.; Podsiadlo, P.; Johnson, C. S.; Rajh, T.; Shevchenko, E. V., Hollow Iron Oxide Nanoparticles for Application in Lithium Ion Batteries. *Nano Lett.* **2012,** *12* (5), 2429-2435.
6. Kravchyk, K.; Protesescu, L.; Bodnarchuk, M. I.; Krumeich, F.; Yarema, M.; Walter, M.; Guntlin, C.; Kovalenko, M. V., Monodisperse and Inorganically Capped Sn and Sn/Sno2 Nanocrystals for High-Performance Li-Ion Battery Anodes. *J. Am. Chem. Soc.* **2013,** *135* (11), 4199-4202.
7. Yin, Y. D.; Rioux, R. M.; Erdonmez, C. K.; Hughes, S.; Somorjai, G. A.; Alivisatos, A. P., Formation of Hollow Nanocrystals through the Nanoscale Kirkendall Effect. *Science* **2004,** *304* (5671), 711-714.
8. Milliron, D. J.; Hughes, S. M.; Cui, Y.; Manna, L.; Li, J.; Wang, L.-W.; Paul Alivisatos, A., Colloidal Nanocrystal Heterostructures with Linear and Branched Topology. *Nature* **2004,** *430* (6996), 190-195.
9. Murray, C. B.; Kagan, C. R.; Bawendi, M. G., Synthesis and Characterization of Monodisperse Nanocrystals and Close-Packed Nanocrystal Assemblies. *Annu. Rev. Mater. Sci.* **2000,** *30* (1), 545-610.
10. Yin, Y.; Alivisatos, A. P., Colloidal Nanocrystal Synthesis and the Organic-Inorganic Interface. *Nature* **2005,** *437* (7059), 664-670.
11. Ibáñez, M.; Zamani, R.; Gorsse, S.; Fan, J.; Ortega, S.; Cadavid, D.; Morante, J. R.; Arbiol, J.; Cabot, A., Core–Shell Nanoparticles as Building Blocks for the Bottom-up Production of Functional Nanocomposites: Pbte–Pbs Thermoelectric Properties. *ACS Nano* **2013,** *7* (3), 2573-2586.
12. Wang, C.; Lin, C.; Zhang, L.; Quan, Z.; Sun, K.; Zhao, B.; Wang, F.; Porter, N.; Wang, Y.; Fang, J., Pt3co Concave Nanocubes: Synthesis, Formation Understanding, and Enhanced Catalytic Activity toward Hydrogenation of Styrene. *Chem. Eur. J.* **2014,** *20* (6), 1753-1759.
13. Tienes, B. M.; Perkins, R. J.; Shoemaker, R. K.; Dukovic, G., Layered Phosphonates in Colloidal Synthesis of Anisotropic Zno Nanocrystals. *Chem. Mater.* **2013,** *25* (21), 4321-4329.
14. Lou, X. W.; Deng, D.; Lee, J. Y.; Feng, J.; Archer, L. A., Self-Supported Formation of Needlelike Co3o4 Nanotubes and Their Application as Lithium-Ion Battery Electrodes. *Adv. Mater.* **2008,** *20* (2), 258-262.
15. Kang, B.; Ceder, G., Battery Materials for Ultrafast Charging and Discharging. *Nature* **2009,** *458* (7235), 190-193.
16. Wang, D.; Yu, Y.; He, H.; Wang, J.; Zhou, W.; Abruña, H. D., Template-Free Synthesis of Hollow-Structured Co3o4 Nanoparticles as High-Performance Anodes for Lithium-Ion Batteries. *ACS Nano* **2015,** *9* (2), 1775-1781.
17. Wu, M.; Xiao, X.; Vukmirovic, N.; Xun, S.; Das, P. K.; Song, X.; Olalde-Velasco, P.; Wang, D.; Weber, A. Z.; Wang, L.-W.; Battaglia, V. S.; Yang, W.; Liu, G., Toward an Ideal Polymer Binder Design for High-Capacity Battery Anodes. *J. Am. Chem. Soc.* **2013,** *135* (32), 12048-12056.
18. Chou, S.-L.; Wang, J.-Z.; Liu, H.-K.; Dou, S.-X., Rapid Synthesis of Li4ti5o12 Microspheres as Anode Materials and Its Binder Effect for Lithium-Ion Battery. *J. Phys. Chem. C* **2011,** *115* (32), 16220-16227.

19. Otelaja, O. O.; Ha, D.-H.; Ly, T.; Zhang, H.; Robinson, R. D., Highly Conductive Cu2–Xs Nanoparticle Films through Room-Temperature Processing and an Order of Magnitude Enhancement of Conductivity Via Electrophoretic Deposition. *ACS Appl. Mater. Interfaces* **2014,** *6* (21), 18911-18920.
20. Fayette, M.; Nelson, A.; Robinson, R. D., Electrophoretic Deposition Improves Catalytic Performance of Co3o4 Nanoparticles for Oxygen Reduction/Oxygen Evolution Reactions. *J. Mater. Chem. A* **2015,** *3* (8), 4274-4283.
21. Islam, M. A.; Xia, Y.; Steigerwald, M. L.; Yin, M.; Liu, Z.; O'Brien, S.; Levicky, R.; Herman, I. P., Addition, Suppression, and Inhibition in the Electrophoretic Deposition of Nanocrystal Mixture Films for Cdse Nanocrystals with Γ-Fe2o3 and Au Nanocrystals. *Nano Lett.* **2003,** *3* (11), 1603-1606.
22. Islam, M. A.; Xia, Y.; Telesca, D. A.; Steigerwald, M. L.; Herman, I. P., Controlled Electrophoretic Deposition of Smooth and Robust Films of Cdse Nanocrystals. *Chem. Mater.* **2003,** *16* (1), 49-54.
23. Dickerson, J. H.; Boccaccini, A. R., *Electrophoretic Deposition of Nanomaterials*. Springer: **2012**; p 376.
24. Ahmed, S.; Ryan, K. M., Centimetre Scale Assembly of Vertically Aligned and Close Packed Semiconductor Nanorods from Solution. *Chem. Commun.* **2009,** (42), 6421-6423.
25. Gonzalo-Juan, I.; Krejci, A. J.; Rodriguez, M. A.; Zhou, Y.; Fichthorn, K. A.; Dickerson, J. H., Dipole Moment-Tuned Packing of Tio2 Nanocrystals into Monolayer Films by Electrophoretic Deposition. *Appl. Phys. Lett.* **2014,** *105* (11), 113108.
26. Song, K. W.; Costi, R.; Bulović, V., Electrophoretic Deposition of Cdse/Zns Quantum Dots for Light-Emitting Devices. *Adv. Mater.* **2013,** *25* (10), 1420-1423.
27. Tanakit, R.; Luc, W.; Talbot, J. B., Electrophoretic Deposition of Cobalt Ferrite and Platinum Cobalt Nanoparticles as Electrocatalysts. *ECS Trans.* **2014,** *58* (42), 1-9.
28. Xue, Z.; Zhang, W.; Yin, X.; Cheng, Y.; Wang, L.; Liu, B., Enhanced Conversion Efficiency of Flexible Dye-Sensitized Solar Cells by Optimization of the Nanoparticle Size with an Electrophoretic Deposition Technique. *RSC Adv.* **2012,** *2* (18), 7074-7080.
29. Cabana, J.; Monconduit, L.; Larcher, D.; Palacín, M. R., Beyond Intercalation-Based Li-Ion Batteries: The State of the Art and Challenges of Electrode Materials Reacting through Conversion Reactions. *Adv. Mater.* **2010,** *22* (35), E170-E192.
30. Débart, A.; Dupont, L.; Patrice, R.; Tarascon, J. M., Reactivity of Transition Metal (Co, Ni, Cu) Sulphides Versus Lithium: The Intriguing Case of the Copper Sulphide. *Solid State Sci.* **2006,** *8* (6), 640-651.
31. Lai, C.-H.; Huang, K.-W.; Cheng, J.-H.; Lee, C.-Y.; Hwang, B.-J.; Chen, L.-J., Direct Growth of High-Rate Capability and High Capacity Copper Sulfide Nanowire Array Cathodes for Lithium-Ion Batteries. *J. Mater. Chem.* **2010,** *20* (32), 6638-6645.
32. Jache, B.; Mogwitz, B.; Klein, F.; Adelhelm, P., Copper Sulfides for Rechargeable Lithium Batteries: Linking Cycling Stability to Electrolyte Composition. *J. Power Sources* **2014,** *247* (0), 703-711.
33. Liu, Y.; Qiao, Y.; Zhang, W.-X.; Li, Z.; Hu, X.-L.; Yuan, L.-X.; Huang, Y.-H., Coral-Like [Small Alpha]-Mns Composites with N-Doped Carbon as Anode Materials for High-Performance Lithium-Ion Batteries. *J. Mater. Chem.* **2012,** *22* (45), 24026-24033.
34. Beltran-Huarac, J.; Resto, O.; Carpena-Nuñez, J.; Jadwisienczak, W. M.; Fonseca, L. F.; Weiner, B. R.; Morell, G., Single-Crystal Γ-Mns Nanowires Conformally Coated with Carbon. *ACS Appl. Mater. Interfaces* **2014,** *6* (2), 1180-1186.
35. Hwang, I.-S.; Kim, J.-C.; Seo, S.-D.; Lee, S.; Lee, J.-H.; Kim, D.-W., A Binder-Free Ge-Nanoparticle Anode Assembled on Multiwalled Carbon Nanotube Networks for Li-Ion Batteries. *Chem. Commun.* **2012,** *48* (56), 7061-7063.
36. Kennedy, T.; Mullane, E.; Geaney, H.; Osiak, M.; O'Dwyer, C.; Ryan, K. M., High-Performance Germanium Nanowire-Based Lithium-Ion Battery Anodes Extending over 1000 Cycles through in Situ Formation of a Continuous Porous Network. *Nano Lett.* **2014,** *14* (2), 716-723.

37. Chan, C. K.; Zhang, X. F.; Cui, Y., High Capacity Li Ion Battery Anodes Using Ge Nanowires. *Nano Lett.* **2007,** *8* (1), 307-309.
38. Seng, K. H.; Park, M.-H.; Guo, Z. P.; Liu, H. K.; Cho, J., Self-Assembled Germanium/Carbon Nanostructures as High-Power Anode Material for the Lithium-Ion Battery. *Angew. Chem. Int. Ed.* **2012,** *51* (23), 5657-5661.
39. Hasan, S. A.; Kavich, D. W.; Dickerson, J. H., Sacrificial Layer Electrophoretic Deposition of Free-Standing Multilayered Nanoparticle Films. *Chem. Commun.* **2009,** (25), 3723-3725.
40. Zhang, H.; Hu, B.; Sun, L.; Hovden, R.; Wise, F. W.; Muller, D. A.; Robinson, R. D., Surfactant Ligand Removal and Rational Fabrication of Inorganically Connected Quantum Dots. *Nano Lett.* **2011,** *11* (12), 5356-5361.
41. Ha, D.-H.; Caldwell, A. H.; Ward, M. J.; Honrao, S.; Mathew, K.; Hovden, R.; Koker, M. K. A.; Muller, D. A.; Hennig, R. G.; Robinson, R. D., Solid–Solid Phase Transformations Induced through Cation Exchange and Strain in 2d Heterostructured Copper Sulfide Nanocrystals. *Nano Lett.* **2014,** *14* (12), 7090-7099.
42. Xu, Z.; Shen, C.; Hou, Y.; Gao, H.; Sun, S., Oleylamine as Both Reducing Agent and Stabilizer in a Facile Synthesis of Magnetite Nanoparticles. *Chem. Mater.* **2009,** *21* (9), 1778-1780.
43. Chen, Y.; Davoisne, C.; Tarascon, J.-M.; Guery, C., Growth of Single-Crystal Copper Sulfide Thin Films Via Electrodeposition in Ionic Liquid Media for Lithium Ion Batteries. *J. Mater. Chem.* **2012,** *22* (12), 5295-5299.
44. Kim, H.; Seo, M.; Park, M.-H.; Cho, J., A Critical Size of Silicon Nano-Anodes for Lithium Rechargeable Batteries. *Angew. Chem. Int. Ed.* **2010,** *49* (12), 2146-2149.
45. Kim, C.; Noh, M.; Choi, M.; Cho, J.; Park, B., Critical Size of a Nano Sno2 Electrode for Li-Secondary Battery. *Chem. Mater.* **2005,** *17* (12), 3297-3301.
46. Son, Y.; Park, M.; Son, Y.; Lee, J.-S.; Jang, J.-H.; Kim, Y.; Cho, J., Quantum Confinement and Its Related Effects on the Critical Size of Geo2 Nanoparticles Anodes for Lithium Batteries. *Nano Lett.* **2014,** *14* (2), 1005-1010.
47. Wang, F.; Robert, R.; Chernova, N. A.; Pereira, N.; Omenya, F.; Badway, F.; Hua, X.; Ruotolo, M.; Zhang, R.; Wu, L.; Volkov, V.; Su, D.; Key, B.; Whittingham, M. S.; Grey, C. P.; Amatucci, G. G.; Zhu, Y.; Graetz, J., Conversion Reaction Mechanisms in Lithium Ion Batteries: Study of the Binary Metal Fluoride Electrodes. *J. Am. Chem. Soc.* **2011,** *133* (46), 18828-18836.
48. Luo, L.; Wu, J.; Xu, J.; Dravid, V. P., Atomic Resolution Study of Reversible Conversion Reaction in Metal Oxide Electrodes for Lithium-Ion Battery. *ACS Nano* **2014**.

Supporting Information

A General Method for High-Performance Li-ion Battery Electrodes from Colloidal Nanoparticles without the Introduction of Binders or Conductive-Carbon Additives: The Cases of MnS, $Cu_{2-x}S$, and Ge

*Don-Hyung Ha†, Tiffany Ly†, Joseph M. Caron, Haitao Zhang, Kevin E. Fritz, and Richard D. Robinson**

Department of Materials Science and Engineering, Cornell University, Ithaca, NY 14853

† Authors contributed equally to this work

* To whom correspondence should be addressed. E-mail: rdr82@cornell.edu.

Synthesis

Chemicals

All synthesis was carried out in a dry, oxygen-free, nitrogen gas atmosphere by employing standard Schlenk line and glove box techniques. Acetone (≥ 99.5%), hexanes (≥ 98.5%), ethanol (≥ 99.5%), oleylamine (70%), oleic acid (90%), tri-*n*-octylphosphine (TOP, 97%), hexamethydisilazane (> 99%), copper(I) chloride (99.995%), ammonium sulfide (40-48 wt% solution in water), di-tert-butyl disulfide (97%), germanium (IV) iodide (99.99%), and manganese (II) chloride (99.999%) were purchased from Sigma-Aldrich. $CuCl_2 \cdot 2H_2O$ (99.999%) was purchased from Alfa Aesar. Molecular sieves (UOP type 3 Å) were purchased from Sigma-Aldrich and activated at 300 °C under dynamic vacuum for 3 hours before use.

3.8 nm copper sulfide NP synthesis

3.8 nm copper sulfide nanoparticles (NPs) were synthesized according to the literature.[1] A mixture of 1 g copper (I) chloride and 10 mL oleylamine was heated at 80 °C until the solution became clear. Temperature was then lowered to ~50 °C (lowest temperature to maintain a clear copper (I) chloride oleylamine solution) and molecular sieve-dried $(NH_4)_2S$ oleylamine solution (0.5 mmol/mL, 10 mL) was added. The reaction kept for 5 minutes and the reaction flask was then immersed into a 180 °C oil bath. The reaction was allowed to proceed for 40 mins and cooled down by removing the oil bath. Ethanol was added to the solution to precipitate out NPs, separated by centrifugation, and washed one more time with hexanes/ethanol. The purified NPs were dissolved in hexanes.

22 nm copper sulfide NP synthesis

The synthesis of 22 nm copper sulfide NPs is slightly modified from the standard procedure.[2] A mixture of $CuCl_2 \cdot 2H_2O$ (340.8 mg) and oleylamine (59 mL) was vacuumed for 30 minutes at room temperature and another 30 minutes at 100 °C to remove water and impurities. The solution was then heated to 200 °C under a nitrogen flow. The solution was maintained at 200 °C for one hour after it became a transparent yellow color. The di-tert-butyl disulfide solution (8 mL) was injected into the solution at 180 °C and the reaction was allowed to proceed for 40 minutes. The solution was quenched with a water bath. The NPs were collected by centrifugation and then washed twice with hexane/acetone. The 22 nm copper sulfide NPs were kept in hexane.

75 nm copper sulfide NP synthesis

The synthesis of 75 nm copper sulfide NPs is slightly modified from the standard procedure.[2] A mixture of $CuCl_2 \cdot 2H_2O$ (1.363 g) and oleylamine (15 mL) was vacuumed for 30 minutes at room temperature and another 3 hours at 100 °C to remove water and impurities. The solution was then heated to 200 °C under a nitrogen flow. The solution was maintained at 200 °C for one hour after it became a transparent yellow color. The di-tert-butyl disulfide solution (2 mL) was injected into the solution at 200 °C and the reaction was allowed to proceed for 60 minutes. The solution was quenched with a water bath. The NPs were collected by centrifugation and then washed twice with hexane/acetone. The 75 nm copper sulfide NPs were kept in hexane.

MnS NP synthesis

The synthesis of ~ 14 nm manganese sulfide NPs is slightly modified from a previously reported method.[1] A mixture of $MnCl_2$ (0.11 g), oleylamine (16 mL), and oleic acid (mL) was vacuumed for 30 minutes at room temperature and another 3 hours at 100 °C to remove water and impurities. The solution was then heated to 250 °C under nitrogen flow, at which point the reagents had dissolved and the solution appeared a faint, clear, yellow. A molecular sieve-dried $(NH_4)_2S$ oleylamine solution (0.5 mmol/mL, 3.6 mL) was injected, turning the solution light peach in color. After 5 minutes the solution was quenched with a water bath. The NPs were precipitated in ethanol, collected by centrifugation, and washed twice with hexane/ethanol. The NPs were kept in hexane.

Ge NP synthesis

~ 15 nm germanium NPs were synthesized according to a slightly modified literature procedure.[3] GeI_4 (60 mg) was combined with oleylamine (10 mL) and oleic acid (0.75) in a scintillation vial and sealed. This solution was sonicated until clear, usually 5 minutes. It was then transferred to a reaction vessel and vacuumed for 30 minutes at room temperature and another 30 minutes at 100 °C to remove water and impurities. Hexamethyldisilazane (1 mL) was added before heating (~ 2 °C/min) to 272 °C. At this temperature the solution turns a dark brown-red. The solution was quenched in a water bath after 30 min. The NPs were precipitated in ethanol, collected by centrifugation, and washed twice with hexane/ethanol. The NPs were kept in hexane.

Transmission Electron Microscopy

TEM images of the nanoparticle samples were obtained using a FEI Tecnai F12 microscope operating at 120 keV. At least 100 particles were analyzed per sample to obtain a representative size distribution.

X-ray Diffraction

XRD (X-ray diffraction) spectra were collected using a Scintag theta-theta x-ray diffractometer (Cu Kα radiation).

EPD Notes

For $Cu_{2-x}S$ and MnS NPs, the film deposited on a positive electrode is generally much thicker (~ 2 times) than that deposited on a negative electrode, indicating that negatively charged NPs are the dominant product for the metal sulfide NPs. This tendency to form a thicker film on the positive electrode is similar to the behavior of other materials, such as cobalt NPs.[4] To create even thicknesses of NP films on both the positive and negative plates, the EPD polarity of each electrode is flipped every minute during the deposition. For Ge, the amount deposited on the negative electrode is below instrument sensitivity.

Electrolyte for Battery Assembly

The metal sulfide batteries use 1 M lithium bis(trifluoromethanesulfonyl)imide (LiTFSI) in DOL(1,3-dioxolane)/DME(Dimethoxy ethane), a common electrolyte for the sulfur system.[5-6] The germanium system uses 1 M lithium hexafluorophosphate ($LiPF_6$) in EC (ethylene carbonate)/DC

(diethyl carbonate) with 3 wt% vinylene carbonate, which has been shown to improve the performance of Ge electrodes.[7]

Electrochemical Measurement

All the electrochemical performances were tested by using the nanoparticle (NP) films as a working electrode in a Swagelok-type electrochemical cells. The cells used counter electrode (Li foil), an electrolyte (see above), and a polypropylene separator (Celgard 2400) that had a 43 nm pore size with 25 μm thickness. The assembling of the cell was carried out in a glove-box with oxygen and water free conditions (<2ppm). Galvanostatic electrochemical charge-discharge measurements were carried out using Biologic VMP3.

Estimates of Ligand Removal

The ammonium sulfide treatment causes the electrode to undergo a mass change attributed to three factors: surfactant ligand removal, formation of a metal sulfide atomic layer, and copper sulfide film formation on the substrate. The ligand removal causes a mass decrease, and the metal-sulfide bond and additional copper sulfide formation causes a mass increase. Because of the mass disparity between the ligand and metal-sulfide bond formation, the formation of the atomic layer of metal sulfide that replaces the metal-ligand surface is considered negligible in this estimation of ligand removal.

The mass change due to ammonium sulfide treatment can be seen in **Fig. S10a,b**, where standard electrodes with 75 nm nanoparticle (NP) films are treated at a constant ammonium sulfide concentration for different lengths of time and at different concentrations for the same

length of time. A standard electrode refers to substrate with ~0.13 mg/cm^2 area density of active material deposited through electrophoretic deposition (EPD). When forming the NP film electrodes, each copper plate substrate is weighed before and after deposition. This quantifies the amount of active material placed on the electrode. Each electrode is also weighed after the ammonium sulfide treatment to estimate the resulting mass increase. On average, the ammonium sulfide treatment results in a mass increase of ~20% for NP film electrodes formed under standard treatment conditions of a 0.02 M $(NH_4)_2S$ methanol solution for 30 seconds. More specifically, for the 3.8 nm NPs, the average mass increase is ~20%; 22 nm, ~18%; 75 nm, ~21%.

More aggressive ammonium sulfide treatments are performed to estimate the amount of ligand removal and side product formation. An experiment is conducted to treat NPs at the standard concentration for longer times. The samples used in this control experiment are NP films drop casted onto glass slides, which do not react with the ammonium sulfide to produce any side product. The percent mass change for each sample can be seen in **Fig S10**. The percent mass change also experiences a plateau between the times of 20 and 30 minutes of ammonium sulfide treatment before decreasing further. The additional decrease may be attributed to delamination of the NP film from the substrate. After 5 minutes of treatment, the 3.8 nm NP sample decreases in mass by ~10%, while the 75 nm sample decreases in mass by ~17%. These samples required longer treatment times than the EPD NP film electrodes because drop casting produces a much thicker film.

By estimating that complete surfactant ligand removal corresponds to an average 13% decrease in mass and $Cu_{2-x}S$ formation causes a 20% increase in mass from the initial electrode,

about 30 wt% of the total electrode is attributed to copper sulfide film formation during ammonium sulfide treatment.

The heat treatment method for removing surfactant ligands from the NPs does not produce any side product and serves as an additional control experiment for estimating the mass change attributed to the ligand removal. The average percent mass decrease of the NP film electrodes is ~35% for the 3.8 nm NPs and ~26% for the 75 nm NPs. Thermogravimetric analysis is used to confirm surfactant ligand removal from the NPs by heat treatment. **Fig S1** shows that after being heated to 300 °C for several hours, the 3.8 nm NPs decrease in mass by ~20% and the 75 nm NPs decrease by ~7%. A control sample of 70% oleylamine shows a mass decrease of ~85%.

Ammonium Sulfide Treatment - Effect of Copper Sulfide Film Formation

Electrochemical tests are performed on bare copper plates treated ammonium sulfide under standard conditions to estimate how much the copper sulfide film side product may influence or contribute to battery performance. Constant current cycling tests are used at a C/2 rate assuming 0.10 mg of $Cu_{2-x}S$ active material to normalize testing conditions. Electrodes formed with these treated Cu plates have inconsistent and generally poor performance. In most cases, batteries assembled with these electrodes either suffer poor electrical conductivity and cannot be cycled. If cycled, the electrodes suffer quick capacity loss due to pulverization of the copper sulfide film material. On occasion, the electrodes do attain a stable capacity up to 100 cycles between 50-150 mAh/g (**Fig. S12**). This specific capacity is calculated assuming 0.10 mg of active material.

However, for NP coated copper plates, most of the copper sulfide film side product is formed on the backside of the copper plate, where there is no NP film to react with the ammonium sulfide. This side is not in contact with the separator or lithium foil counter electrode. Coupled with the inconsistent performance during cycling from the ammonium sulfide treated bare copper plates, the capacity contribution is considered negligible.

Supplementary Figures

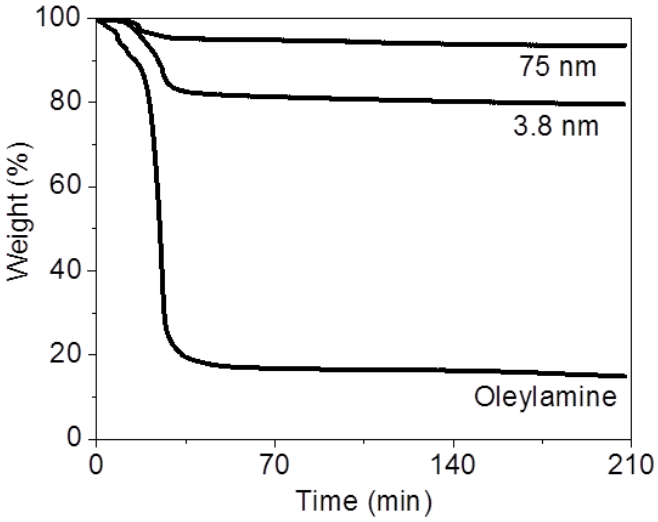

Figure S1. Thermogravimetric analysis results for 70% oleylamine, 3.8 nm NPs, and 75 nm NPs heated to 300 °C for 3.5 hrs.

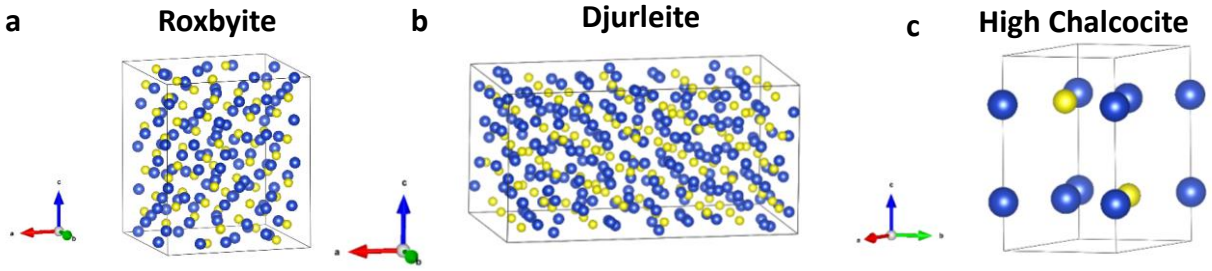

Figure S2. Crystal structures of copper sulfide phases. Blue and yellow spheres represent copper and sulfur atoms, respectively. (a) Roxbyite phase is triclinic with space group P $\bar{1}$. (b) Djurleite is monoclinic with space group P 1 2/n1. (c) High chalcocite is hexagonal with space group $P6_3/mmc$.

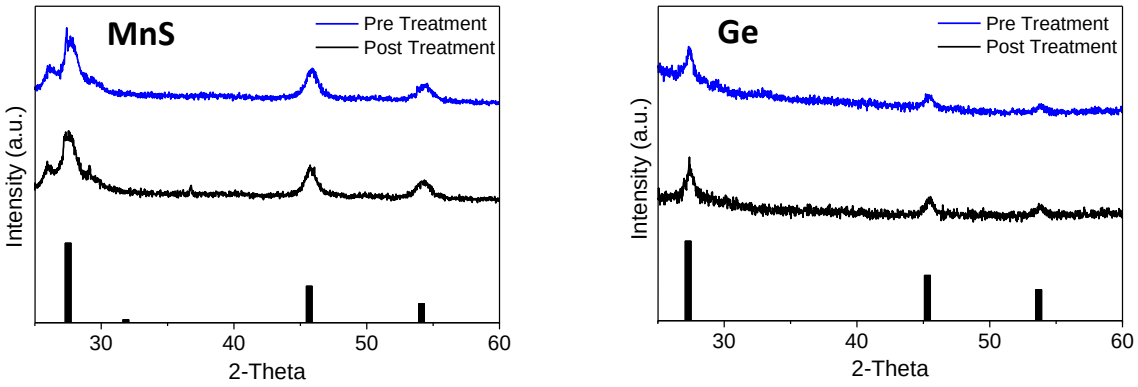

Figure S3. XRD patterns of MnS and Ge NP samples before and after the $(NH_4)_2S$ treatment show no phase changes.

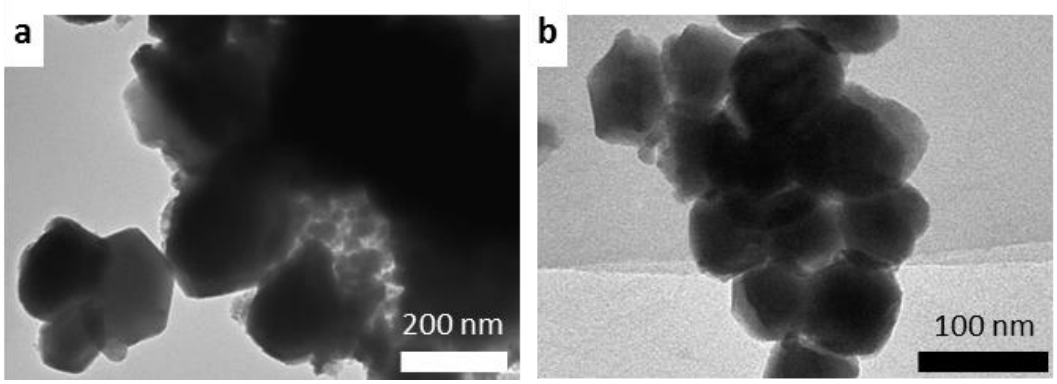

Figure S4. TEM image of $Cu_{2-x}S$ NPs after heating. (**a**) 3.8 nm $Cu_{2-x}S$ NPs after show significant sintering after heat treatment while (**b**) 75 nm NPs retain their shape after heating.

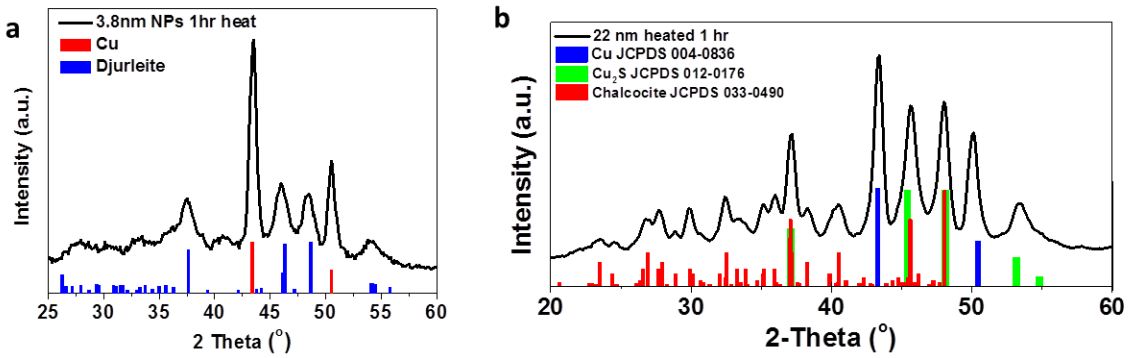

Figure S5. XRD of $Cu_{2-x}S$ NPs after 1 hr of heating at 300 °C in inert atmosphere. (a) The peaks for 3.8 nm NPs are well matched with the djurleite phase, and there is a strong contribution from the Cu phase. (b) The peaks for 22 nm NPs also show a strong contribution from the Cu phase and are well matched with the chalcocite phase.

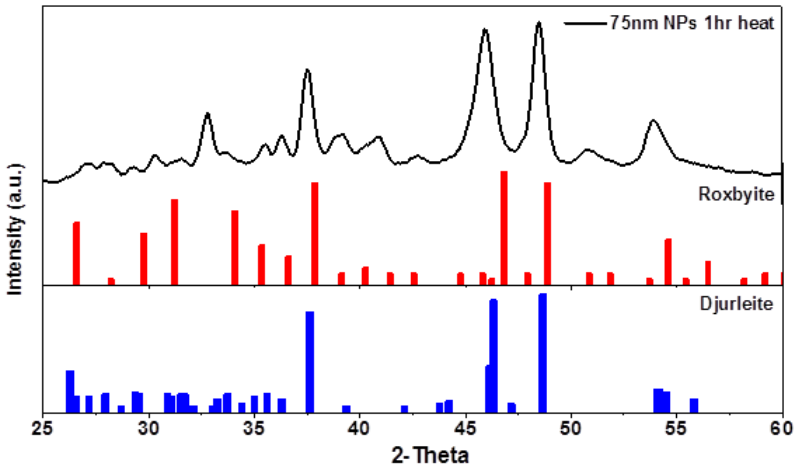

Figure S6. XRD of 75 nm $Cu_{2-x}S$ NPs after 1 hr of heating at 300 °C in inert atmosphere. The peaks are well matched with the djurleite and roxbyite phases.

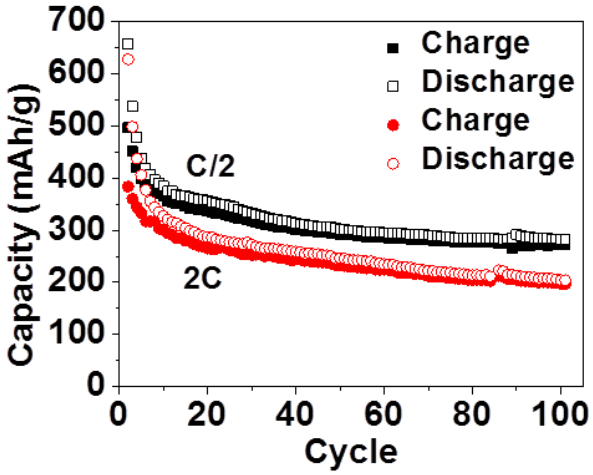

Figure S7. Cycling performance of 75 nm $Cu_{2-x}S$ roxbyite nanoparticles at C/2 and 2C rates. Capacity retention after 100 cycles is ~ 280 mAh/g at C/2 and ~ 200 mAh/g at 2C.

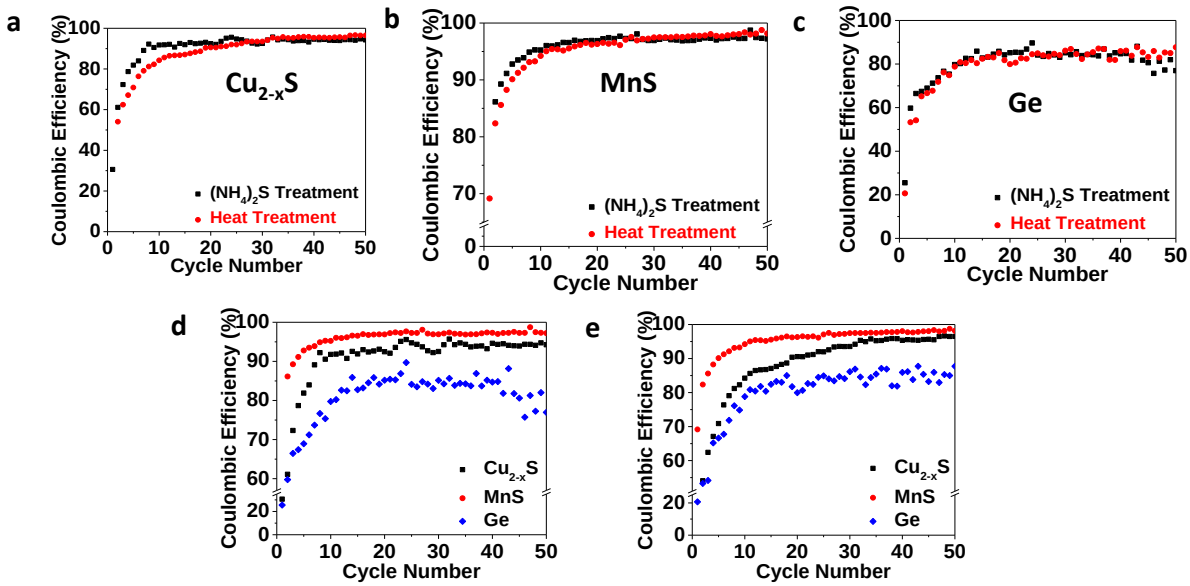

Figure S8. Coulombic efficiency comparison of $(NH_4)_2S$ to heat treatment for (a) $Cu_{2-x}S$, (b) MnS, and (c) Ge. Coulombic efficiency comparison of each NP system for (d) $(NH_4)_2S$ treatment and (e) heat treatment.

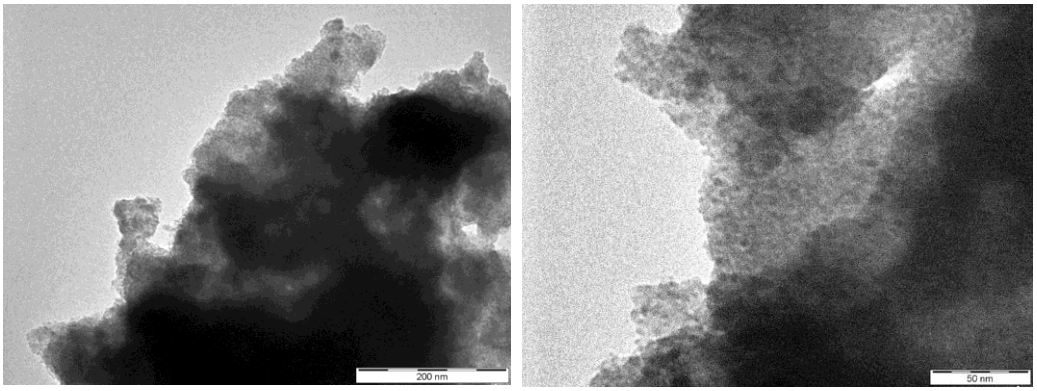

Figure S9. TEM images of 22 nm copper sulfide NPs after the first lithiation process.

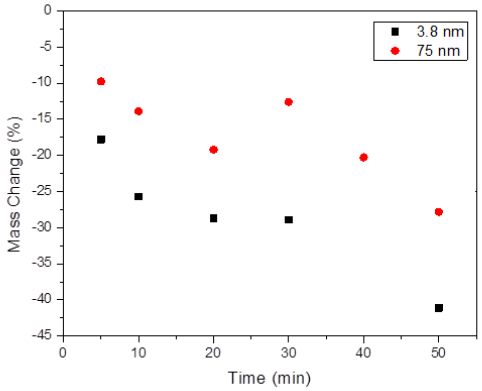

Figure S10. Percent mass change for $Cu_{2-x}S$ NP films drop casted on glass slides treated with 0.02 M $(NH_4)_2S$ methanol solution for different lengths of time. The additional loss of mass after a brief plateau between 2-30 min is due to delamination of the NP film from the substrate. These samples required longer treatment times than the EPD NP film electrodes because drop casting produces a much thicker film.

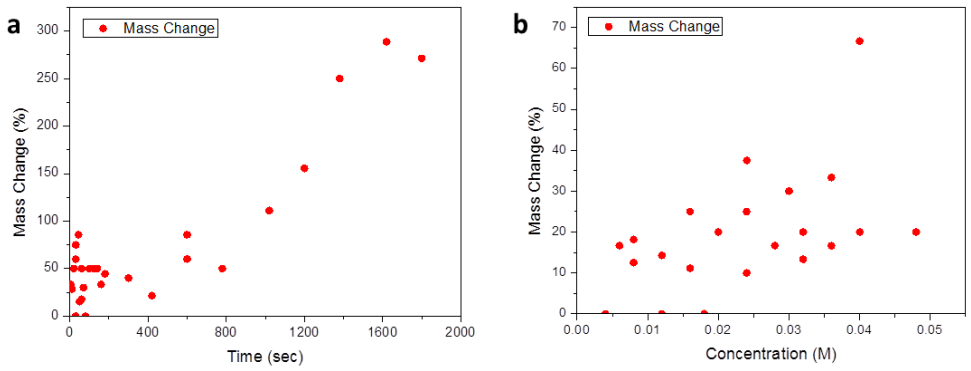

Figure S11. Percent mass change of 3.8 nm $Cu_{2-x}S$ NP film electrodes treated in (a) 0.02 M $(NH_4)_2S$ methanol solution for different lengths of time and (b) different concentrations of $(NH_4)_2S$ methanol solution for 30 seconds.

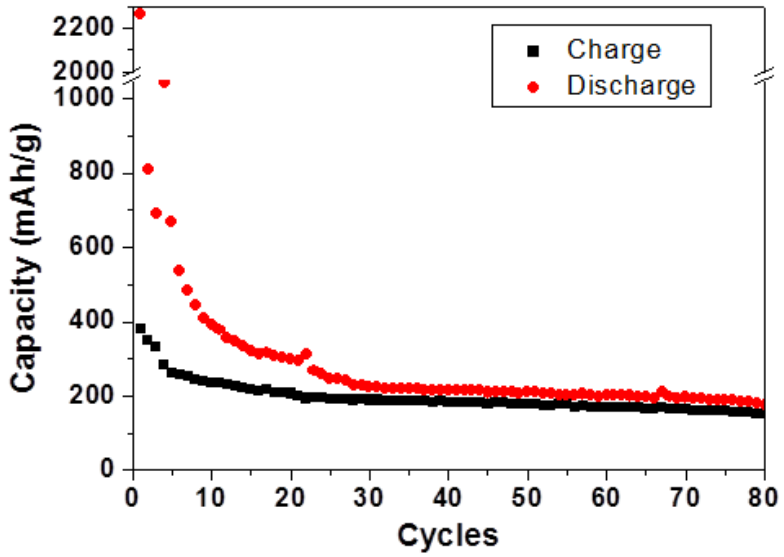

Figure S12. Bare Cu plates treated with $(NH_4)_2S$ shows the negligible effect of the $Cu_{2-x}S$ side product.

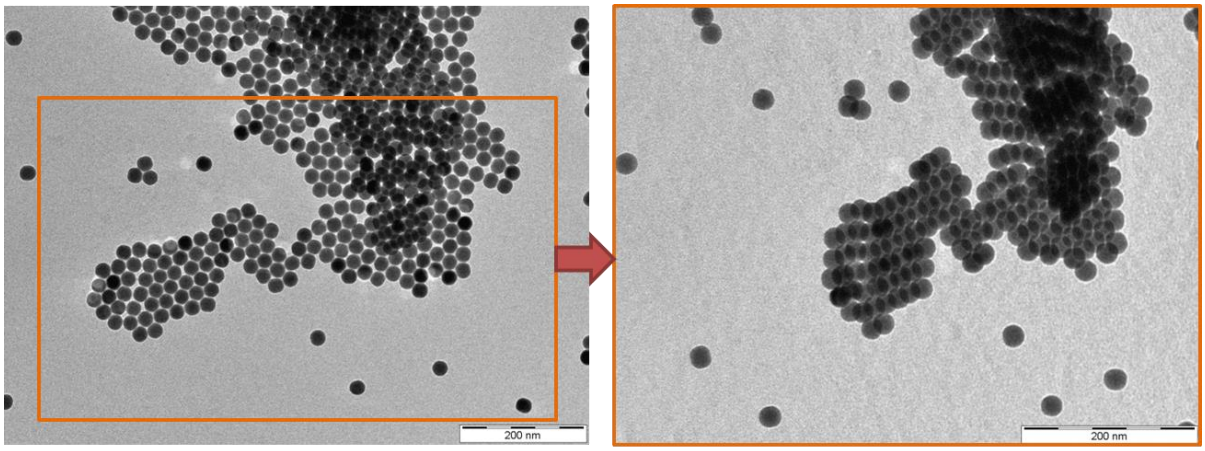

Figure S13. Figures compare the 22 nm $Cu_{2-x}S$ NPs before and after a TEM stage tilting experiment. 60° tilted TEM image (right) confirms that the 22 nm $Cu_{2-x}S$ NPs are spherical.

Table S1. Comparison of battery performance for nanostructured $Cu_{2-x}S$

Sample	Synthesis method	Number of cycle (n)	Current density (mA/g)	Additives	Capacity reported (mAh/g)	Capacity Including additives (mAh/g)	Ref.
$Cu_{2-x}S$ NPs through EPD with $(NH_4)_2S$ treatment	Colloidal	50	167 (0.5 C)	None	230	230	This work
$Cu_{2-x}S$ NPs through EPD with heat treatment	Colloidal	100	167 (0.5 C)	None	286	286	This work
Cu_2S nanowire	Growth on Cu substrate	100	673.8 (2C)	None	230	230	8
Cu_2S/tubular mesoporous carbon composite	charge–discharge processes of S/tubular mesoporous carbon	300	67.4 (0.2 C)	10 wt% C + 10 wt% PVDF	270	240	9

Table S2. Comparison of battery performance for nanostructured MnS

Sample	Synthesis method	Number of cycle (n)	Current density (mA/g)	Additives	Capacity reported (mAh/g)	Capacity Including additives(mAh/g)	Ref.
MnS NPs through EPD with $(NH_4)_2S$ treatment	Colloidal	50	123.2 (0.2 C)	None	420	420	This work
MnS NPs through EPD with heat treatment	Colloidal	100	308 (0.5 C)	None	470	470	This work
Coral-like a-MnS nitrogen-doped carbon composites	hydrothermal	400	500	10 % C 10 % PVDF +Carbon composite	699	560 (not clear - carbon composite)	10
γ-MnS Nanowires with C coating	CVD Growth on substrate	60	1000	8 % PVDF + Carbon coating	321	295.3 (not clear - carbon composite	11

Table S3. Comparison of battery performance for nanostructured Ge

Sample	Synthesis method	Number of cycle (n)	Current density (mA/g)	Additives	Capacity reported (mAh/g)	Capacity Including additives (mAh/g)	Ref.
Ge NPs through EPD with $(NH_4)_2S$ treatment	Colloidal	50	320 (0.2 C)	None	350	500	This work
Ge NPs through EPD with heat treatment	Colloidal	50	320 (0.2 C)	None	500	500	This work
Ge NPs With CNT		200	1600 (1C)	CNT	1,143 (70% wt)	800	12
Germanium /Carbon Nanostructures	Acetylene gas C coating GeO, hydrogen reduction	120	1600 (1 C)	Carbon coating (binderless)	unclear	896	13
Germanium Carbon Nanocomposite	Pyrolysis of tetraallylgermane	50	150	Carbon Coating (binderless)	2,250 (42% wt)	900	14
High-Germanium-Nanoparticle-Loading Graphere Nanocomposites	Solution Grown	75	320 (0.2 C)	Graphene	1,730 (80% wt)	1,384	15
Ge@C Core-Shell Nanoparticle w/ graphene networks	Solution Method Based	50	50	Carbon and reduced graphene oxide	1516 mAh/g (62% wt)	940	16
Porous Ge nanowire network	In situ growth and network formation	1,100	800 (0.5 C)	None	900	900	7

Supporting InformationReferences

1. Zhang, H.; Hyun, B.-R.; Wise, F. W.; Robinson, R. D., A Generic Method for Rational Scalable Synthesis of Monodisperse Metal Sulfide Nanocrystals. *Nano Lett.* **2012,** *12* (11), 5856-5860.
2. Li, W.; Shavel, A.; Guzman, R.; Rubio-Garcia, J.; Flox, C.; Fan, J.; Cadavid, D.; Ibanez, M.; Arbiol, J.; Morante, J. R.; Cabot, A., Morphology Evolution of Cu2-Xs Nanoparticles: From Spheres to Dodecahedrons. *Chem. Commun.* **2011,** *47* (37), 10332-10334.
3. Vaughn, D. D.; Bondi, J. F.; Schaak, R. E., Colloidal Synthesis of Air-Stable Crystalline Germanium Nanoparticles with Tunable Sizes and Shapes. *Chem. Mater.* **2010,** *22* (22), 6103-6108.
4. Ha, D.-H.; Islam, M. A.; Robinson, R. D., Binder-Free and Carbon-Free Nanoparticle Batteries: A Method for Nanoparticle Electrodes without Polymeric Binders or Carbon Black. *Nano Lett.* **2012,** *12* (10), 5122-5130.
5. Chen, S.; Dai, F.; Gordin, M. L.; Wang, D., Exceptional Electrochemical Performance of Rechargeable Li-S Batteries with a Polysulfide-Containing Electrolyte. *RSC Adv.* **2013,** *3* (11), 3540-3543.
6. Jache, B.; Mogwitz, B.; Klein, F.; Adelhelm, P., Copper Sulfides for Rechargeable Lithium Batteries: Linking Cycling Stability to Electrolyte Composition. *J. Power Sources* **2014,** *247* (0), 703-711.
7. Kennedy, T.; Mullane, E.; Geaney, H.; Osiak, M.; O'Dwyer, C.; Ryan, K. M., High-Performance Germanium Nanowire-Based Lithium-Ion Battery Anodes Extending over 1000 Cycles through in Situ Formation of a Continuous Porous Network. *Nano Lett.* **2014,** *14* (2), 716-723.
8. Lai, C.-H.; Huang, K.-W.; Cheng, J.-H.; Lee, C.-Y.; Hwang, B.-J.; Chen, L.-J., Direct Growth of High-Rate Capability and High Capacity Copper Sulfide Nanowire Array Cathodes for Lithium-Ion Batteries. *J. Mater. Chem.* **2010,** *20* (32), 6638-6645.
9. Han, F.; Li, W.-C.; Li, D.; Lu, A.-H., In Situ Electrochemical Generation of Mesostructured Cu2s/C Composite for Enhanced Lithium Storage: Mechanism and Material Properties. *ChemElectroChem* **2014,** *1* (4), 733-740.
10. Liu, Y.; Qiao, Y.; Zhang, W.-X.; Li, Z.; Hu, X.-L.; Yuan, L.-X.; Huang, Y.-H., Coral-Like [Small Alpha]-Mns Composites with N-Doped Carbon as Anode Materials for High-Performance Lithium-Ion Batteries. *J. Mater. Chem.* **2012,** *22* (45), 24026-24033.
11. Beltran-Huarac, J.; Resto, O.; Carpena-Nuñez, J.; Jadwisienczak, W. M.; Fonseca, L. F.; Weiner, B. R.; Morell, G., Single-Crystal Γ-Mns Nanowires Conformally Coated with Carbon. *ACS Appl. Mater. Interfaces* **2014,** *6* (2), 1180-1186.
12. Hwang, I.-S.; Kim, J.-C.; Seo, S.-D.; Lee, S.; Lee, J.-H.; Kim, D.-W., A Binder-Free Ge-Nanoparticle Anode Assembled on Multiwalled Carbon Nanotube Networks for Li-Ion Batteries. *Chem. Commun.* **2012,** *48* (56), 7061-7063.
13. Seng, K. H.; Park, M.-H.; Guo, Z. P.; Liu, H. K.; Cho, J., Self-Assembled Germanium/Carbon Nanostructures as High-Power Anode Material for the Lithium-Ion Battery. *Angew. Chem. Int. Ed.* **2012,** *51* (23), 5657-5661.
14. Cui, G.; Gu, L.; Zhi, L.; Kaskhedikar, N.; van Aken, P. A.; Müllen, K.; Maier, J., A Germanium–Carbon Nanocomposite Material for Lithium Batteries. *Adv. Mater.* **2008,** *20* (16), 3079-3083.
15. Yuan, F.-W.; Tuan, H.-Y., Scalable Solution-Grown High-Germanium-Nanoparticle-Loading Graphene Nanocomposites as High-Performance Lithium-Ion Battery Electrodes: An Example of a Graphene-Based Platform toward Practical Full-Cell Applications. *Chem. Mater.* **2014,** *26* (6), 2172-2179.
16. Xue, D.-J.; Xin, S.; Yan, Y.; Jiang, K.-C.; Yin, Y.-X.; Guo, Y.-G.; Wan, L.-J., Improving the Electrode Performance of Ge through Ge@C Core–Shell Nanoparticles and Graphene Networks. *J. Am. Chem. Soc.* **2012,** *134* (5), 2512-2515.

Chapter 4: Challenges for $CuInS_2$ NP Synthesis: Understanding Phase and Growth Mechanisms through Heat Control and Reagent Choice

4.1 Abstract

This work represents a preliminary exploration of the challenges involved in creating high-efficiency copper indium sulfide ($CuInS_2$) quantum dots (QDs) for use as down-converters in solid-state lighting applications. We find that the primary challenges include balancing the relative reactivity of the Copper (I) (Cu^+) and Indium (III) (In^{3+}) cations towards the sulfur source of choice, elemental sulfur, as well as controlling the phase of the product, which can take either the tetragon chalcopyrite or hexagon wurtzite phases. We first explore the role of longer aging times and higher growth problems as a way to mitigate this problem of high Cu^+ reactivity relative to In^{3+}. Our work suggests that $CuInS_2$ formation begins with the formation $Cu_{2-x}S$ particles, into which In diffuses, and that higher heating temperatures and longer growth times facilitate this process. Overall we believe there are optimal temperature and time parameters between 100 and 200 °C and 5 – 20 minutes for $CuInS_2$ QD growth. With regard to controlling phase, we find the choice of precursor salt anion is the chief factor in determining the phase of the final product. If chloride (Cl^-) is the only anion present in the reaction, wurtzite was produced. If both Cl^- and acetate are present, the chalcopyrite phase is produced. We attribute this to the influence of these particles over the thermodynamics and kinetics of the system. Finally, we explore the role of results of shelling $CuInS_2$ cores with a layer of ZnS in order to improve efficiency. The results are highly dependent on the choice of ligand for both the core and the core-shell material. The best result occurred when oleylamine was chosen in both cases.

4.2 Introduction

Copper Indium Sulfide ($CuInS_s$) quantum dots (QDs) are currently considered a prime candidate as a next generation material for a variety of optical and optoelectronic applications, such as photovoltaics, biological labels, and light emitting diodes, due to a set of unusual and desirable optical properties.[53,54] This direct bandgap semiconducting material has a narrow bandgap (1.5 eV) that falls in the infrared region light as well as a Bohr radius (4.1 nm).[55] Furthermore, much work has shown that the emission can also be controlled by changing the bandgap directly through alloying with such materials as zinc and gallium.[56,57] Controlling emission without changing size is important for applications that take advantage of the low-light scattering in these emitters. The absorption and emissive characteristics of $CuInS_2$ are very different than other QD emitters. Unlike cadmium-based QDs, these materials exhibit a very high stokes shift, which reduces reabsorption losses.[58] In addition, the emission of these particles is very broad for QDs, often as large as 100 nm. Capturing a large part of visible spectrum is important for creating authentic white light, as this will more authentically reproduce the solar spectrum.[59]

Taken alongside the ease of device processability of nanoparticles, these attributes suggest $CuInS_2$ QDs are particularly useful as downconverters for solid-state lighting (SSL) applications. SSL is an increasingly popular alternative to traditional general lighting that

[53] J. Kolny-Olesiak and H. Weller, *ACS Appl. Mater. Interfaces,* 2013, 5, 12221 - 12237
[54] B. Chen, H. Zhong, M. Wang, R. Liu, B. Zou, *Nanoscale,* 2013, 5, 3514 - 3519
[55] S. D. Perera, H. Zhang, X. Ding, A. Nelson, and R. D. Robinson
[56] Id.
[57] W.-S. Song, J.-H. Lee, H.-S. Lee, Y. R. Do, and H. Yang, *J. Mater. Chem.*, 2012, 22, 21901 - 21908
[58] L. Li, A. Pandey, D.J. Werder, B.P. Khanal, J.M. Pietryga, V.I. Klimov, *J. Am. Chem. Soc.,* 2011, 133, 1176 - 1179
[59] W.-S. Song and H. Yang, *Chem. Mater.*, 2012, 24, 1961-1967

generates light by exciting a material, known as a downconverter, with a blue light LED. Downconverters absorb this light and reemit other wavelengths of visible light for the purposes of illumination. As lighting makes up 20% of global energy consumption, this is a very active area of academic and commercial work. The low scattering, color tenability, and high rendering of $CuInS_2$ QDs are highly appealing for such SSL applications.[60]

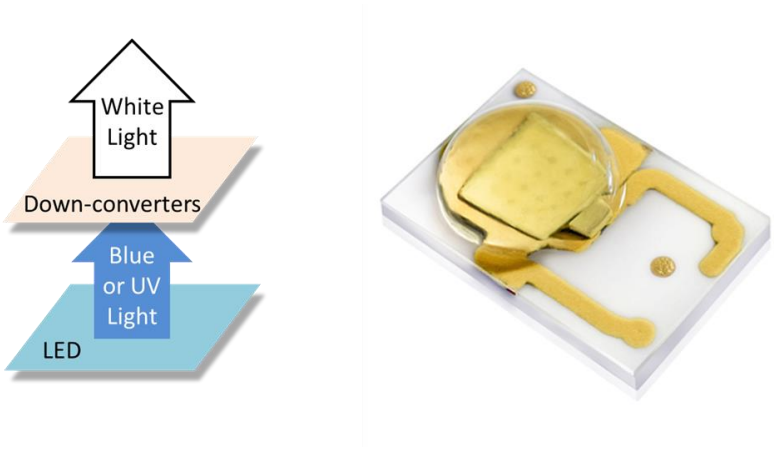

Figure 1. (Left) In a solid-state lighting device, blue light from an LED is converted into lower energy wavelengths of light. A mix of converters would be necessary to create the white light as shown. (Right) A real solid-state lighting device. The down-converters are dispensed in a globule of resin, beneath which are several blue LED chips.

The material most widely employed as a white light phosphor material is cerium doped yttrium aluminum oxide ($Y_3Al_5O_{12}:Ce^{3+}$ or YAG:Ce).[61] However, this material suffers from several drawbacks. As a bulk material, YAG:Ce causes a high degree of reflection and scattering when excited, causing efficiency loss. Furthermore, the device processing of this material is difficult when compared to the solution processing made possible by QD materials. Finally, the color

[60] U.S. Department of Energy, Manufacturing Roadmap: Solid-State Lighting Research and Development, August 2014. Prepared by Bardsley Consulting, Navigant Consulting, SB Consulting, and SSLS, Inc.
[61] A. Alboulaich, M. Michalska, R. Schneider, A. Potdevin, J. Deschamps, R. Deloncle, G. Chadeyron, and R. Mahiou, *ACS Appl. Mater. Interfaces,* 2014, 6, 252-258

created by YAG:Ce is widely known to be deficient in red, the result of which is a undesirable blue/yellow hue in white light devices.[62]

Overall, however, cadmium selenide (CdSe) and indium phosphide (InP_3) QDs have been the subject of more academic investigation than $CuInS_2$ QDs. They not only enjoy many of the same nanoscale advantages as $CuInS_2$ QDs, but have traditionally higher efficiencies of absorbed and emitted light.[63] However $CuInS_2$ QDs do have several important advantages. Unlike $CuInS_2$,, the emission and absorption curves of CdSe overlap to a significant degree. Therefore, when excited, energy is lost to reabsorption.[64] As a phosphide, InP_3 is less stable than a chalcogenide, such as $CuInS_2$ and therefore will have a short lifetime in a device.[65] Both CdSe and InP_3 are also at a disadvantage as environmental hazards. Cadmium is a carcinogen and one of six substances banned in the European Union by Directive 2011/65/EU, while InP_3 syntheses rely on the use of tris(trimethylsilyl)phosphine. Tris(trimethylsilyl)phosphine is not only toxic, but also expensive and highly pyrophoric.[66] $CuInS_2$, by comparison, is environmentally benign.

The exact origin of the unique emission properties of $CuInS_2$ are attributed to a defect related carrier recombination pathway known as donor-acceptor pair (DAP) recombination.[67,68,69] The broad emission and large stokes shift are characteristic of this pathway, which occurs between in intra-gap defect states. In DAP recombination, the carriers become

[62] Id.
[63] M. J. Anc, N.L. Pickett, N.C. Gresty, J.A. Harris, K.C. Mishra, *ECS Journal of Solid State Science and Technology.* 2013, 2 (2), R3071-R3082
[64] I. T. Kraatz, M. Booth, B.J. Whitaker, M. G. D. Nix, and K. Critchley, *J. Phys. Chem. C,* 2014, 118, 24102-24109
[65] R. Xie, M. Rrutherford, X. Peng, *J. Am. Chem. Soc.,* 2009 131, 5691-5697
[66] Id.
[67] I. T. Kraatz, M. Booth, B.J. Whitaker, M. G. D. Nix, and K. Critchley, *J. Phys. Chem. C,* 2014, 118, 24102-24109.
[68] D.-E. Nam, W.-S. Song, and H. Yang, *Journal of Colloid and Interface Science*, 2011, 361, 491-496.
[69] J. Hofhuls, J. Schoonman, and A. Goossens, *J. Phys. Chem. C,* 2008, 112, 15052-15059.

localized to shallow traps states associated with defects within the crystal. Therefore, the energy of emitted light upon recombination is related to the physical distance between the donor and acceptor-like defect sites according to[70]

$$hv = E_g - (E_e + E_h) + \frac{q^2}{4\pi\varepsilon\varepsilon_0 R}$$

where E_g is the bandgap, E_e and E_h are the ionization energies of the donor and acceptor, respectively, ε is the dielectric constant, and R is the distance between the donor and acceptor defects. This in part explains the broad emission, as the broad peak reflects the Gaussian distribution of R within a particle. However a single recombination event also has a wide emission. When a carrier becomes trapped in a recombination site with strong electron-phonon coupling, as in $CuInS_2$, it induces a local lattice distortion. The phonon interaction varies the location of the emission in k-space. Further, the emission takes place over the variation in k-space, leading to a Gaussian shaped emission profile like that shown in the inset of **Fig. 2**.[71]

[70] H. Koyama, T. Ozaki, N. Koshida, *Phys. Rev. B,* 1995, 52, R11 561-564
[71] K. Murayama, S. Miyazaki, and M Hirose, *Jpn. J. Appl. Phys*, 1992, 31, L1358-1361.

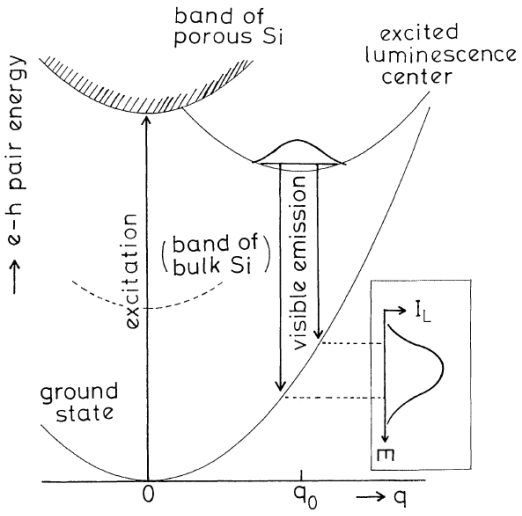

Figure 2. This configurational coordinate diagram shows how a single donor-acceptor pair recombination pathway can lead to a wide, Gaussian shaped PL emission profile in porous silicon. Porous silicon is the most widely studied material which exhibits recombination related to electron-phonon coupling. It serves as a good example for the $CuInS_2$ system, though in $CuInS_2$ theory suggests the donor and acceptor-states are defects and both susceptible to electron-phonon coupling.

This phenomena also helps explain the large stokes shift of the material, as described in an equation devised by Omata *et al.*[72]

$$E_{peak} = E_{ZPL} - S\hbar\omega$$

E_{peak} is the peak energy of the emission, E_{ZPL} is the energy of the zero phonon line, ω is the frequency of the coupled phonon, and *S* is the Huang-Rhys factor, which describes the strength of the electron-phonon coupling.

A large body of work has shown a strong relationship between copper deficiency and high emission efficiencies[73,74,75], further suggesting the radiative recombination pathway is defect

[72] T. Omata, K. Nose, K. Kurimoto, and M. Kita, *J. Mater. Chem. C.* 2014, 2, 6867-6872.
[73] I. T. Kraatz, M. Booth, B.J. Whitaker, M. G. D. Nix, and K. Critchley, *J. Phys. Chem. C,* 2014, 118, 24102-24109.
[74] D.-E. Nam, W.-S. Song, and H. Yang, *Journal of Colloid and Interface Science,* 2011, 361, 491-496.
[75] S.-C. Shei, W.-J. and S.-J. Chang, *Nanoscale Research Letters,* 2015, 10:122.

related. What's more, The $CuInS_2$ system, like many I-III-VI materials, can tolerate a wide degree of off stoichiometry.[76] As copper deficiencies are introduced into the system, the PL becomes more intense, as well as blue-shifted. The increase in PL is associated with the increase in the defect states that facilitate DAP, however the blue shift is attributed to weakened repulsion between Cu d-orbitals and S p-orbitals.[77] It is also not uncommon to observe a shoulder to the red side of the PL emission, which is attributed to next nearest-neighbor donor-acceptor sites.[78] These more distant and less accessible alternatives to the nearest-neighbor recombination produce a less intense lower energy peak, which also contributes to the wide PL emission.

Several important challenges exist for $CuInS_2$ in SSL applications. Copper is more reactive than indium, and therefore measures must be taken to prevent the preferential formation of copper sulfides. In literature, ligands and ions that inhibit the reactivity of copper are often employed.[79] Here we will explore the role of temperature control in producing the correct product. A second challenge relates to the phase of the product. $CuInS_2$ is particularly sensitive to the thermodynamics and kinetics of the system. In a thermodynamically controlled reaction, chalcopryite is the preferred phase, while in kinetically controlled conditions produce the wurtzite phase.[80] This work finds that the choice of reagent, an indium chloride salt or acetate salt, is the main factor in determining the phase of the product. We suspect this relates to how the presence of acetate ions affect the relative speeds of nucleation and growth.

[76] B. Chen, H. Zhong, W. Zhang, Z. Tan, Y. Li, C. Yu, T. Zhai, Y. Bando, S. Yang, B. Zou, *Adv. Funct. Mater.,* 2012, 22, 2081-2088.
[77] Id.
[78] J. Hofhuls, J. Schoonman, and A. Goossens, *J. Phys. Chem. C,* 2008, 112, 15052-15059.
[79] J. Kolny-Olesiak and H. Weller, *ACS Appl. Mater. Interfaces,* 2013, 5, 12221 - 12237
[80] K. Nose, Y. Soma, T. Omata, and S. Otsuka-Yao-Matsuo, *Chem. Mater.,* 2009, 21, 2607-2613

This paper aims to explore challenges related to producing high efficiency dots at a commercially meaningful cost and scale. Like all nanocrystal synthesis methods, the sensitivity of the $CuInS_2$ QD reaction makes it difficult and often expensive to create good quality product on a large scale. For example Nanoco, a manufacturer of QDs, sold 1 kg of CdSe QDs for 2 million dollars in 2012.[81] This does not compare favorably with the $500/kg price of YAG:Ce.[82] The cost of manufacturing these materials at scale must come down in order to be cost competitive with incumbent materials, such as YAG:Ce, in solid-state lighting devices. Our lab pioneers QD synthesis techniques aimed at solving these challenges, and the unique optical properties and commercial applications of $CuInS_2$ make it an ideal candidate for such processes. The work contained here outlines some preliminary attempts to understand how such a system may be adapted to these methods, which involve high concentration regimes, oleylamine solvent, and the use of elemental sulfur or ammonium sulfide as a sulfur source. Several experiments were also conducted to understand the effect of shelling of CIS particles with ZnS. Please refer to chapter 1 for more information on shelling. In short, a large bang-gap material upon the surface of the $CuInS_2$ "core." This shell acts as a potential barrier to the wavefunctions of the carriers, and prevents them from recombining non-radiatively at surface defects.[83]

4.3 Experimental

Chemicals

[81]

[82] Marty Byrne, Associate Director, New York State Center for Future Energy Systems. Personal communication, July, 2014.

[83] C.B. Murray, C.R. Kagan, and M.G. Bawendi, *Annu. Rev. Mater. Sci*, 200, 30, 545-610

All syntheses were carried out in a dry, oxygen-free, nitrogen gas atmosphere by employing standard Schlenk line and glove box techniques, excluding post synthesis washes. Acetone (≥ 99.5%), hexanes (≥ 98.5%), ethanol (≥ 99.5%), oleylamine (70%), oleylamine (≥ 98%), 1-Octadecene (90%), copper (I) chloride (99.995%), indium (III) acetate, indium(III) chloride (99.999%), gallium(III) chloride (99.999%), zinc(II) chloride (99.999%), sulfur (reagent grade, -100 mesh), tetrachloroethylene (≥ 99.5%), and ammonium sulfide (40-48 wt% solution in water) were purchased from Sigma-Aldrich. Molecular sieves (UOP type 3 Å) were purchased from Sigma-Aldrich and activated at 300 °C under dynamic vacuum for 3 hours before use.

$CuInS_2$ with elemental sulfur

In a typical synthesis of $CuInS_2$, a mixture of copper (I) chloride (125 mg, 1.25 mmol), indium (III) acetate (1,460 mg, 5 mmol) and 20 mL 7:3 oleylamine:octadecene was heated to 130 °C until a pale, opaque yellow (~2 hrs). Separately a mixture of elemental sulfur (1,600 mg, 5 mmol) and 20 mL 7:3 oleylamine:octadecene was heated to 80 °C until it turned a deep red color. Both vessels were purged and backfilled three times with N_2 before heating. The vessels were lowered to ~60 °C. 2 mL of the sulfur solution was injected into the metal solution and heated at 12 °C/min to 210 °C. The reaction was kept for 5 – 60 minutes before cooling in a water bath. If an aliquot study was performed with a glass syringe and metal needle, care was taken not to introduce outside atmosphere. In air, the QDs were precipitated with EtOH, separated by centrifugation, and washed one more time with hexanes/ethanol. The purified QDs were dissolved and stored in hexanes.

$CuInS_2$, $CuInZnS_2$, $CuInGaS_2$, and Zn-$CuInGaS_2$ with $(NH_4)_2S$ from nanoclusters

The syntheses of these materials was followed exactly from literature, and will not be reproduced here.[84] The only major difference is that nanocrystal growth phase of some were allowed to age at their reaction temperature in order to perform an aliquot study.

General shelling method

In either core growth method discussed above, the following shell growth procedure can be performed either after separating and washing the cores or directly in the core growth reaction vessel. Below is a typical approach for shell growth after separating and cleaning the cores. The stoichiometry determined as the amount of material needed to grow a 1 nm shell on 100 mg of 4 nm $CuInS_2$ cores. The amount of shelling material should be independently determined according to the size of the cores, the amount of cores, and shell thickness desired.

A mixture a of zinc (II) chloride (280 mg, 2.1 mmol) in 7:3 oleylamine:octadecene is heated to 110 °C until it becomes a faint clear pink. Separately a mixture of elemental sulfur (66 mg, 2.1 mmol) and 20 mL 7:3 oleylamine:octadecene was heated to 80 °C until deep red in appearance. The $CuInS_2$ cores were heated to 210 °C in 30 mL of 7:3 oleylamine:octadecene. All vessels were purged and backfilled three times with N_2 before heating. The S and $ZnCl_2$ vessels were cooled to 60 °C. 5 mL of $ZnCl_2$ solution were added to the cores over 5 min followed by 5 mL of S solution over 5 min. Shells were allowed to grow for 90 minutes before quenching the vessel in water. If an aliquot study was performed with a glass syringe and metal needle, care was taken not to introduce outside atmosphere. The core-shells were precipitated in air with

[84] S. D. Perera, H. Zhang, X. Ding, A. Nelson, and R. D. Robinson

EtOH, separated by centrifugation, and washed one more time with hexanes/ethanol. The purified core-shells were dissolved and stored in hexanes.

Surface treatment

In some cases the particles underwent surface treatment in order to improve PL by surface passivation. 6 drops of OLA or DDT from a glass pipette were added to QDs in 3 mL of tetrachloroethylene (TCE). The QD/TCE mixture is normalized to an optical density 0.2 at 450 nm before the addition. After the addition the solution was sonicated for 1 minute before taking PL.

Characterization

TEM images of the nanoparticle samples were obtained using a FEI Tecnai F12 microscope operating at 120 keV. XRD (X-ray diffraction) spectra were collected using a Scintag theta-theta x-ray diffractometer (Cu Kα radiation). UV-vis absorption data were collected on an Ocean Optics USB2000+VIS-NIR, using a halogen lamp (210–400 nm). Photoluminescence data were recorded on a Horiba Fluoromax-4 spectrometer. Relative quantum yields were determined using a rhodamine 6G standard (PLQY = 0.95) excited at 455 nm with slit widths of 1.5 nm and a 465 – 800 nm emissive range. The photoluminescent Quantum Yield (PLQY) was determined by the linear fit method.[85]

4.4 Results and Discussion

[85] Jobin Yvon, Horiba, A Guide to Fluorescence Quantum Yields, www.horiba.com

	Indium Source	Sulfur Source	Solvent*	Max Temp. (°C)	PL (nm)	Impurities	Resulting Phase
Reaction 1	$InCl_3$	Elemental S	70% OLA	100	None	None	Unclear, likely wurtzite
Reaction 2	$InCl_3$	Elemental S	70% OLA	80	None	None	Amorphous
Reaction 3	$In(Ac)_3$	Elemental S	70% OLA	100	None	In_2O_3	None
Reaction 4	$In(Ac)_3$	Elemental S	70% OLA	200	550 - 700	In_2O_3, $In(OH)_3$	Chalcopyrite
Reaction 5	$InCl_3$	Elemental S	70% OLA	200	None	None	Wurtzite
Reaction 6	$In(Ac)_3$	Elemental S	70% OLA	200	500 - 800	In_2O_3	Chalcopyrite
Reaction 7	$In(Ac)_3$	Elemental S	7:3 OLA:ODE	200	600 - 850	In_2O_3	Chalcopyrite
Reaction 8	$In(Ac)_3$	Elemental S	7:3 OLA:ODE	200	600 - 850	In_2O_3	
Reaction 9‡	$InCl_3$	$(NH_4)_2S$	DDT	145	550 - 700		
Reaction 10‡	$InCl_3$	$(NH_4)_2S$	DDT	145	650 - 850		

* "70% OLA" refers to as received 70% oleylamine while "7:3 OLA:ODE" refers to a mixture of 99% oleylamine and 90% octadecene.

‡ These reactions are doped with Zn, as described in the experimental section.

Comments	
Reaction 4	Cores were grown in one step, washed, and a ZnS shell grown in a second reaction
Reaction 6	Shell material was injected directly into the reaction vessel of cores after growth
Reactions 7 and 8	A slow stir speed was used after an unreported reaction of high stir speed gave undesirable results
Reaction 9	$CuInS_2$ clusters, cores, and shell were executed in distinct steps with washes in between
Reaction 10	CuInS2 clusters, cores, and shell were executed in a "single pot" without washing between

A common problem for $CuInS_2$ NP syntheses is the formation of $Cu_{2-x}S$ side products. According to Hard Soft Lewis Acid Base Theory (HSAB), the reactivity of elemental sulfur, a soft base, is much higher for Cu^+ than In^{3+}, a soft acid and hard acid, respectively.[86] Commonly, a soft Lewis base stabilizer, such as a thiol, is introduced to mitigate Cu^+ reactivity towards S.[87] Another strategy is to use a precursor containing both Cu and In, for example $(Ph_3)CuIn(SEt)_4$, which releases a known ratio of the two cations upon dissolution.[88] Here, our work highlights the

[86] R. Xie, M. Rrutherford, X. Peng, *J. Am. Chem. Soc.,* 2009 131, 5691-5697

[87] W. Zhang and X. Zhong, *Inorg. Chem.*, 2011, 50, 4065-4072

[88] J. Kolny-Olesiak and H. Weller, *ACS Appl. Mater. Interfaces,* 2013, 5, 12221 - 12237

significance of temperature and aging time of particle growth on the type of product produced. We further suggest a growth mechanism for $CuInS_2$ QD formation.

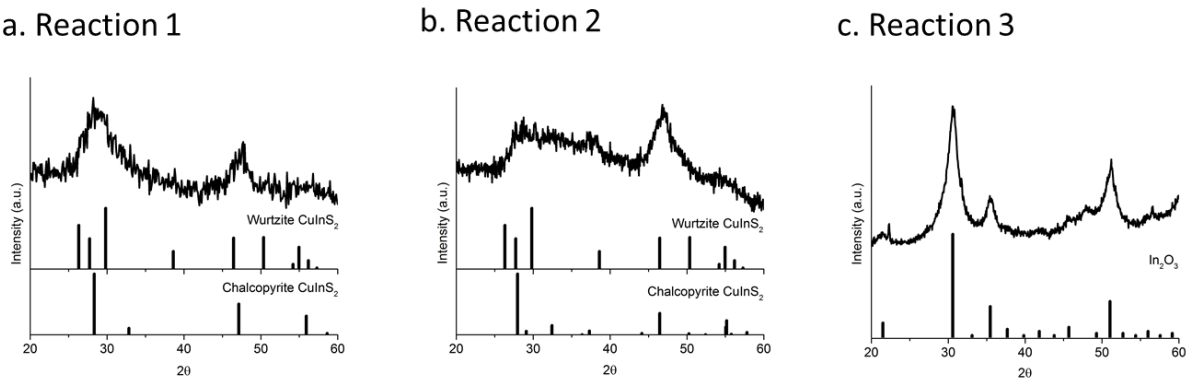

Figure 3. The XRD results of Reaction 1, 2, and 3. Reactions 1 and 2 used $InCl_3$ as the indium source, while Reaction 3 used $In(Ac)_3$. Reactions 1, 2, and 3 were heated to 100, 80, and 100 °C respectively. Reaction 1 can be identified as crystalline $CuInS_2$, though the phase is ambiguous. Reaction 2 suffers from the same ambiguity, though also appears to be amorphous. Reaction 3 may be unambiguously assigned to In_2O_3.

As shown in **Fig. 3c, 4, S6, S7 and S8,** the common side-products of our process were not $Cu_{2-x}S$ phases, but In_2O_3 and $In(OH)_3$. This is ascribed to unreacted In that was oxidized upon exposure to air, post-reaction. This is the result of the condition of 1:4 Cu:In stoichiometric ratio, which served to promote $CuInS_2$ formation as well as produce the more efficient copper-deficient phase.[89] What our results suggest, though, is that when an excess of In precursor is used, both increased growth time and temperature can serve to improve $CuInS_2$ formation. **Fig. 3a** shows that when $InCl_3$, CuCl, and elemental S are allowed to react at 100 °C for 20 min, a $CuInS_2$ phase is produced (be it tetragonal or hexagonal). However when the same reaction is carried out at 80 °C (**Fig. 3b**), a half-formed amorphous product is obtained. Furthermore, XRD of Reaction 5 (**Fig. 4b)**, an aliquot study of the same reaction conditions heated quickly to 200 °C, showed no $CuInS_2$

[89] Y.-K. Kim, S.-H. Ahn, K. Chung, Y.S. Cho, and C.-J. Choi, *J. Mater. Chem.,* 2012, 22, 1516-1520

formation as high as 160 °C. Therefore both the temperature and growth time (100 °C, 20 min) of Reaction 1 were important reaction parameters.

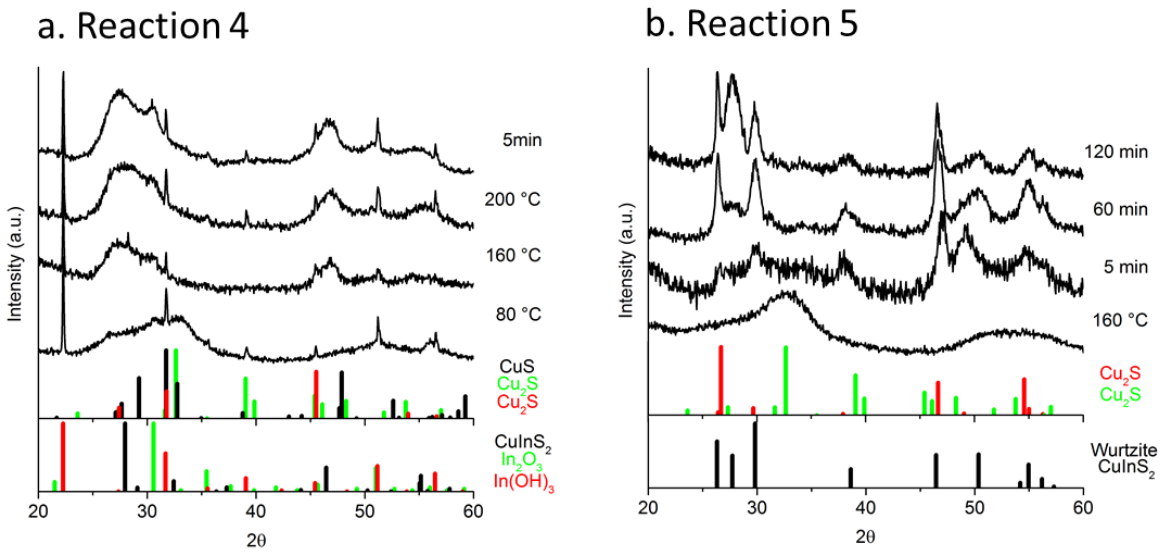

Figure 4. Reactions 4 and 5 were run under identical conditions with the exception of the indium source. $In(Ac)_3$ was used in Reaction 4, while $InCl_3$ served as the indium source in Reaction 5. These XRDs aliquot studies track the progress of the reactions as they are heated to 200 °C and aged for various times. Both gradually evolve from amorphous $Cu_xIn_yO_z$ phases into either the chalcopyrite (Reaction 4) or wurtzite (Reaction 5) phases. The oxides are presumed to have formed after the reaction, upon air exposure.

To explore the significance of heating and growth times, the aliquot studies of **Fig. 4** characterize particle phase at different temperatures and aging times in the reactions. As **Fig. 4** shows, there is a clear evolution from $Cu_{2-x}S$ phases at lower temperatures to $CuInS_2$ phases at longer temperatures and times. Furthermore, the peaks associated with the $In(OH)_3$, particularly those at 22 and 31 2θ, shrink with heat and time. This result implies that the mechanism of $CuInS_2$ formation is to first create Cu_xS (or $Cu_xIn_yS_2$ with $x >> y$) before converting into $CuInS_2$. Time and heat allow In or In_2S_3 to overcome low reaction kinetics to form $CuInS_2$, either through diffusion or cation exchange, into the Cu_xS phase. This result squares well with the very recent, 2015 work

of Tang *et al.*[90], who carried out a very similar set of experiments on $CuInS_2$ QD growth, but instead with DDT as the sulfur source. Their work suggests that commonly in $CuInS_2$ NP growth, $Cu_{1.94}S$ growth is the critical first step, followed by the growth of $Cu_{1.94}S$-$CuInS_2$ heterostructures particles, and finally cation diffusion (facilitated by high Cu^+ mobility) produces heterostructured $CuInS_2$ QD.

Therefore, in order to attain $CuInS_2$, our work suggests the use of longer times and higher temperatures to facilitate the evolution of $Cu_{2-x}S$ into $CuInS_2$. However the drawback of this approach is reduced control over the size and quality of the product, which is critical for controlling emission for SSL applications. With these factors in mind, we suggest there is a temperature and time sweet spot may be discovered between 100 and 200 °C and 5 – 20 minutes.

It was also found that the composition of the solvent used played an important role in side-product formation. When OLA (70%) of ambiguous composition was used, as in Reaction 4 (**Fig 4a**), the presence and identity of In side-product varied considerably. However, when 70% OLA was created through the combination of oleylamine (≥ 98%) and 1-octadecene (90%), as in Reactions 6 and 7 (**Fig. S6 and S7**), the result was unambiguously the formation of large amounts of In_2O_3. We suggest two possible reasons for this result. OLA is a hard acid. In our 7:3 solvent mixture, the OLA concentration may be higher. If so, it would stabilize the In^{3+}, a hard acid, slowing its reactions kinetics. A lower concentration of OLA may serve to address this concern. A second possibility has to do with the growth mechanism. If In^{3+} is indeed diffusing into a $Cu_{2-x}S$ template, as our results suggest, only so much In^{3+} can intercalate into the particle before

[90] A. Tang, Z. Hu, Z. Yin, H. Ye, C. Yang, and F. Teng, *Dalton Trans.,* 2015, Advance Article

saturation occurs. Perhaps an excess of sulfur would allow more material for $CuInS_2$ growth to occur.

A second important problem is the possibility of forming either the tetragonal chalcopyrite or hexagonal wurtzite phases of $CuInS_2$, a problem well documented by Nose *et al.*[91] According to this work, the thermodynamically stabilized growth of the chalcopyrite phase is the result of fast nucleation and slow growth, while the kinetically stable wurtzite growth is the product of show nucleation and fast growth. Other researchers argue the key to making the wurtzite phase is to first grow crystalline $Cu_{2-x}S$ before In^{+3} intercalation[92]. Good lattice match between $Cu_{2-x}S$ and wurtize $CuInS_2$ facilitates this growth. The method for creating chalcopyrite, then, is to either start growing $CuInS_2$ while the $Cu_{2-x}S$ is amorphous or nucleate chalcopyrite $CuInS_2$ phase directly. Our results will suggest the Teng group's hypothesis for phase control in the $CuInS_2$ system.

Information on the preferred phase of $CuInS_2$ for optical applications is scant in literature; however the results of this research (**Table 1**) show that the wurtize phase did not emit in the range studied (300 – 900 nm), while all optically active products were of the chalcopryte phase. Furthermore, all literature results of $CuInS_2$ are assigned to the tetragonal chalcopyrite phase, though not always unambiguously. For the purposes of this work however, we conclude then that the chalcopyrite phase is the preferred phase for optically active product.

In the studies performed, when $In(Ac)_3$ was used as the In source, the result was always the desired chalcopyrite phase. In the cases where $InCl_3$ was chosen as the precursor, the

[91] K. Nose, Y. Soma, T. Omata, and S. Otsuka-Yao-Matsuo, *Chem. Mater.,* 2009, 21, 2607-2613
[92] A. Tang, Z. Hu, Z. Yin, H. Ye, C. Yang, and F. Teng, *Dalton Trans.*, 2015,

optically inactive wurtzite phase resulted. We may say with confidence, then, that in the conditions used, $In(Ac)_3$ is the preferred indium source. However the reason for this is less clear. The theory put forward by Teng *et al.*[93], described above, best matches our results. In the case of Reaction 4 ($In(Ac)_3$, **Fig. 4a**), chalcopyrite $CuInS_2$ formation can be observed as low as 80 °C, and is the dominant phase by 160 °C. In the case of Reaction 5 ($InCl_3$, **Fig. 4b**), $Cu_{2-x}S$ is the dominant phase at 160 °C, and $CuInS_2$ does not appear until five minutes of aging at 200 °C. This suggests that when $CuInS_2$ begins to nucleate at low temperatures, either directly or within the still amorphous $Cu_{2-x}S$ NP, the chalcopyrite phase can grow. However, if nucleation begins at higher temperatures, the wurtizite phase forms, either by templating upon the well lattice-matched $Cu_{2-x}S$ phases, or due to more randomized cation distribution that occurs at higher temperatures, as is characteristic of the wurtzite phase.[94]

This phenomena may also be explained by HSAB theory. The key difference between the two reactions described here is the choice of In precursor. When $In(Ac)_3$ was chosen, the reactivity of In was higher, ultimately leading to the formation of chalcopyrite $CuInS_2$. When $InCl_3$ was chosen, In reactivity was slowed significantly, leading to wurtize phase growth. The attribute the difference to the anions present in solution. As a larger anion with delocalized electrons, acetate is a softer base than chloride. Therefore, it interferes with the kinetics of indium reactivity and diffusion to a less significant degree, explaining the results described. Anion choice is therefore an important factor to consider when growing $CuInS_2$ NPs, and perhaps the elimination of the chloride anion in favor of even softer bases may serve to facilitate chalcopyrite growth.

[93] Id.
[94] M. Kruszynska, H. Borchert, J. Parisi, and J. Kolny-Olesiak, *J. Am. Chem. Soc.,* 2010, 132, 15976 – 15986.

I would like to make a quick note on the role of stir speed in this reaction. Though it could not be explored in depth, it was found that relative stir speed did play a significant role in product formation. In an unreported reaction, a high speed of stirring was employed, such that a definite and large vortex was observed. In the Reaction 7 and 8, a very slow speed was used for otherwise identical reactions. It was found that in the high-speed stir case the product produced no PL and furthermore the XRD could not be convincingly assigned to any Cu or In phase, sulfide or oxide. In both slow stir-speed cases, a significant PL was observed in both cases as well as characterization for chalcopyrite $CuInS_2$.

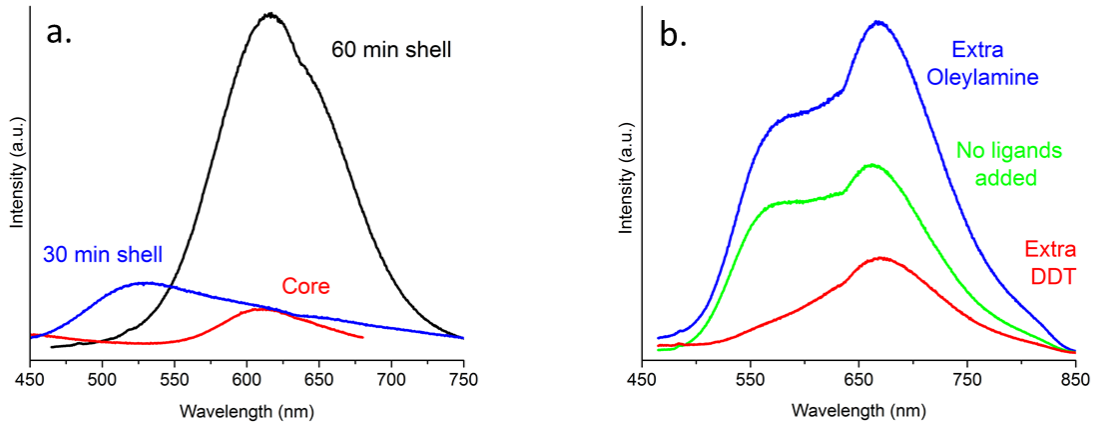

Figure 5. Figure 4a compares the PL of $CuInS_2$ Reaction 4 (made from elemental sulfur) for shelling at various lengths time. 60 min of shelling significantly increases the PL of the core. The source of the blue shifted peak at 30 min of shell growth is unknown, though it may be fluorescence from an indium complex, as described in Figure S14. Figure 4b compares the PL of Reaction 5 $CuInS_2$ core-shells after various post-synthesis surfaces treatments. This figure highlights the importance of normalizing the surface treatment with the appropriate ligands before taking PL.

Finally, two methods were explored to improve the quantum efficiency of the as synthesized $CuInS_2$ cores: shelling with ZnS and improved surface passivation through ligand coverage. However, the effectiveness of this approach varied, depending on the sulfur source

used to growth the cores. The shelling method was found to be effective in the case of the elemental sulfur grown cores (**Fig. 5a and S6**), increasing efficiency significantly. In the case of the ammonium sulfide based reactions, however, the shelling proved to be ineffective. While successful shelling was suggested by the blue shift of the emission evident in **Fig 6c**, the efficiency of the emission was about one third of the core efficiency. The most likely cause is the introduction surface defects as a result of shelling, as might be the case if the created ZnS shell was both defect ridden and too thin to prevent confinement of carrier wavefuctions. This could be the result of complications introduced by the presence of DDT, which is absent on the elemental sulfur reactions, and could possible inhibit shell growth by stabilizing the surface. A second reason may be the instability of the cores formed from ammonium sulfide. If these cores are smaller or defect ridden, they may be instable at the temperatures required for shell growth (230 °C), and fuse into the bulk state as a result. If true, less aggressive conditions may be necessary to grow the shell. More thorough XRD or TEM studies may reveal this to be the case, however, the PL of both Reaction 4 and 9 (**Fig. 5a** and **6**, respectively) are located at similar wavelengths, suggesting the particles are similar in size.

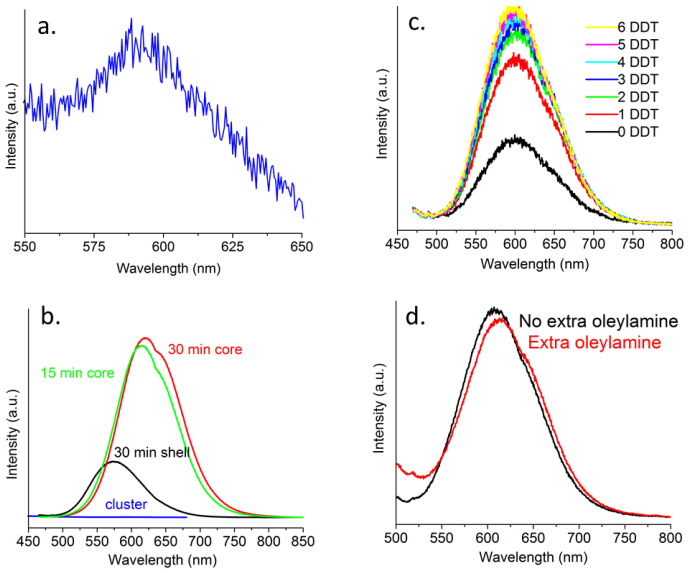

Figure 6. This figure shows the emission results of Reaction 9, Zn-doped $CuInS_2$. The emission of the $CuInS_2$ clusters are shown in Figure 10a. Then Zn was added and the clusters were grown into full NPs at 145 °C for 15 and 30 minutes. Figure 10b compare the PL results of these particles before and after shelling with ZnS. Interestingly, the shell did not improve PL. Figures 10c and 10d compare PL after surface treatment of the core-shell structure with either DDT or OLA. The addition of DDT ligands drastically improves PL, while the addition of OLA did not affect the PL significantly.

Finally, surface passivation through ligand coverage was found to play an important role in emission efficiency of the particles. **Fig. 5b** shows that post-synthesis addition of OLA to dots grown in OLA (the elemental S case) significantly increased PL, while adding DDT post-synthesis decreases the PL. **Fig. 6c,d** show a different trend for particles grown in DDT (the $(NH_4)_2S$ case). In such cases, adding DDT post-synthesis increases PL, while adding OLA leaves the PL unchanged. The fact the PL is unchanged in this case suggests that DDT is the more stable ligand for this particle, as it was not displaced in favor of OLA. For particles grown on OLA, then, it is likely that OLA is displaced in favor of DDT ligands. The departing ligands may then take surface cations

along, introducing defects and reducing PL.[95] Increases in PL can be simply explained by better coverage with a ligand that is already present and is not significantly displaced.

These results are important, as they imply that in order to compare PL data between samples, it is imperative that the sample not only be exposed to the same washing procedures (to remove the same amount of ligands), but that they also be exposed to the same amount of new ligands of the proper type. Only in this way can a complete of passivation as possible be achieved, and PL data between different phases and compositions be rigorously compared.

4.5 Conclusion

Members of the Robinson group at Cornell University will be preforming a design of experiment on the $CuInS_2$ QD system at the WANDA instrument at Berkeley National Labs. This high-throughput nanoparticle synthesis device will allow these researchers to quickly and efficiently explore the variable space of this synthesis with respect to their novel, high-concentration synthetic approach. It has been the purpose of this work to begin exploring the variable space for this process, and identify the key difficulties and significant design choices. We have found that two key challenges are avoiding $Cu_{2-x}S$ formation, as well as producing the desired phase. In the former case, we found that aging time, aging temperature, and solvent choice are important elements of producing $CuInS_2$, rather than unwanted side product. Results suggest an ideal temperature and time exist in the 100 - 200 °C and 5 – 30 min ranges. Furthermore, in order to produce the desired phase our work suggests that the choice of salt

[95] N. Anderson, M. Hendricks, J. Choi, J. Owen, *J. Am. Chem. Soc.,* 2013, 135, 18536-18548

anion plays a key role. The anions present in solution influence the reactivity of the cations significantly, and affect the kinetics and thermodynamics of the reaction.

Time was also spent exploring the shelling of the $CuInS_2$ cores in an attempt to increase emission efficiency. For reactions involving an elemental sulfur source, this method of shelling described here proved effective, increasing the emission efficiency significantly. However in the case of QDs made from $(NH_4)_2S$, the same shelling procedure causes a significant decrease in efficiency. The exact reason for this decrease is currently unknown; however, the presence of DDT or smaller particles size of these reactions offer a possible answer.

Finally this work highlights the important of normalizing surface treatment between samples before taking PL data. Unsurprisingly surface treatment plays an important part in emission efficiency. In order to rigorously compare the emission of different samples, care must be taken to ensure the surface treatment is as identical as possible. This can be achieved by using the same washing procedures for samples and passivating the surface with more ligand than is strictly necessary, as excessive ligand addition does not seem to affect the optical properties of the material.

4.6 Supplemental Part 1: Extended Reaction Results

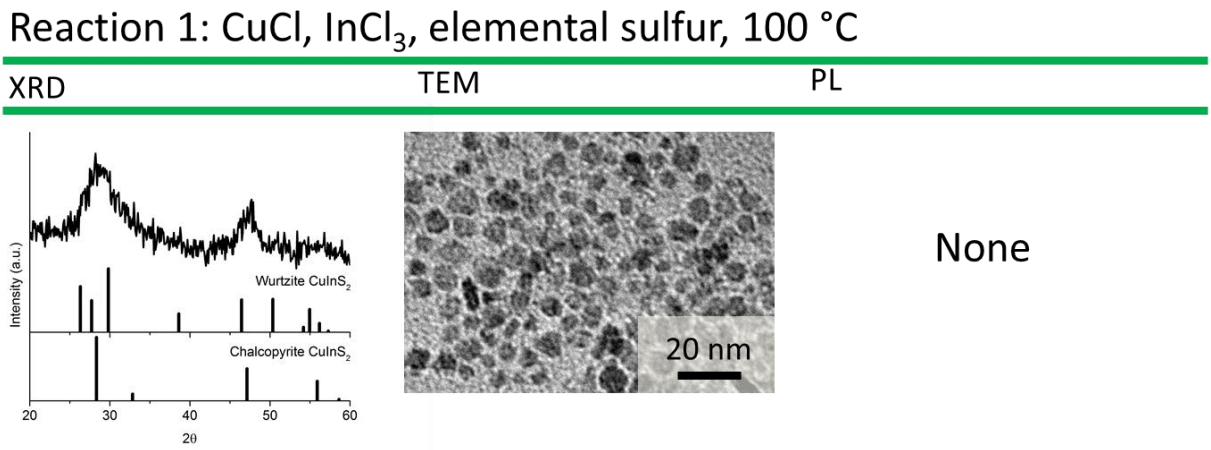

Figure S1. The XRD of this product suggest that $CuInS_2$, either chalcopyrite or wurtzite, was successfully produced, however the shape of the product is highly irregular. Given that this product is not photoluminescent and that the TEM shows likely thin, plate-like particles, we suggest this product is of the wurtzite phase. This PL and TEM results match those of later reactions whose phases are more rigorously determined to be wurtzite.

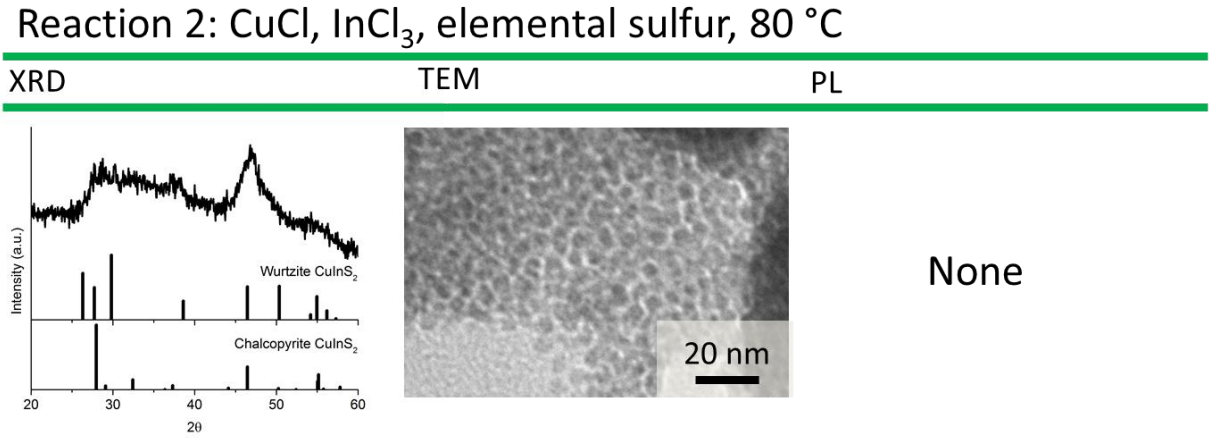

Figure S2. Though the XRD results are amorphous and ambiguous, several peaks are well-matched for both the wurtzite and chalcopyrite phases of $CuInS_2$.

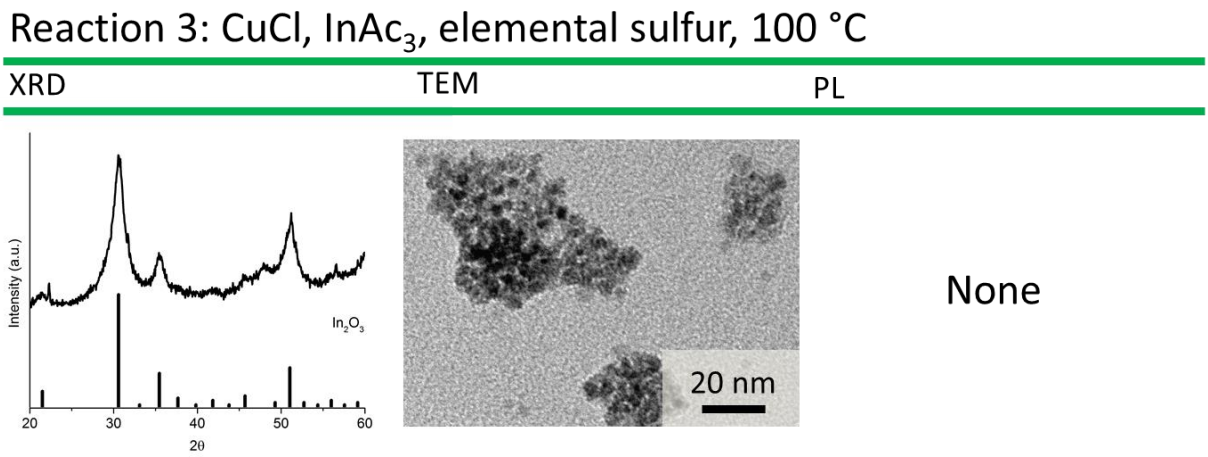

Figure S3. The result of reaction 3 is unambiguously In_2O_3, suggesting that the indium did not react with the sulfur. The lack of a copper peak is explained by the relatively small amount (1/4, stoichiometric) of copper to indium.

Reaction 4: CuCl, $In(Ac)_3$, elemental sulfur, 200 °C

XRD

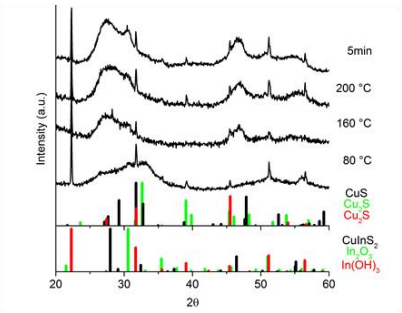

TEM

80 °C

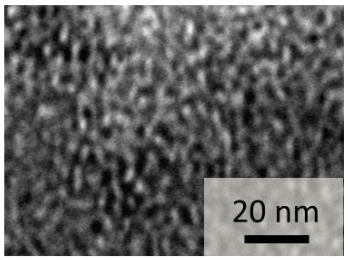

200 °C, 5 min age

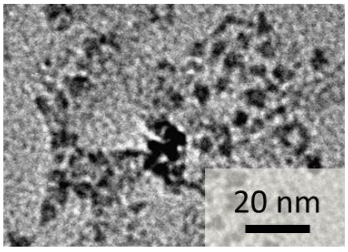

60 minute shell growth

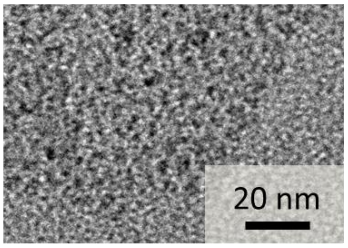

PL

No age vs 5 min age

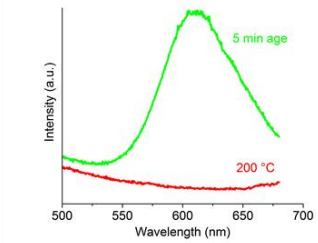

Fresh cores vs air-exposed cores

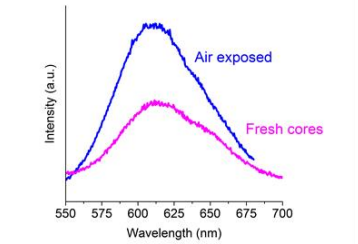

Fresh core vs 30 and 60 min shell

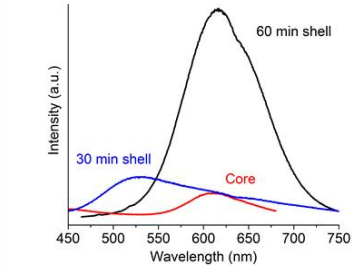

Figure S4. Reaction 4 involved taking aliquots at 80 and 160 °C as the reaction was heating to its 200 °C growth temperature. Aliquots were then taken at 200 °C as well after 5 minutes of aging. The XRD show a clear progression from copper sulfide phases to chalcopyrite $CuInS_2$. Indium impurities are present throughout. The emission data shows an expected red PL peak for the 5 min aged sample. As shown in the "air exposed" emission data, after the material was left in a non-inert atmosphere for 2 weeks, the PL increased and blue-shifted. This suggests light oxidation of the surface acted as a shell, slightly reducing the effective diameter of the core and passivating surface defects. The PL showed a drastic increase after shelling with ZnS. The higher PLs at longer aging times suggest the better passivation of surface defects at longer times.

Reaction 5: CuCl, $InCl_3$, elemental sulfur, 200 °C

XRD	TEM	PL
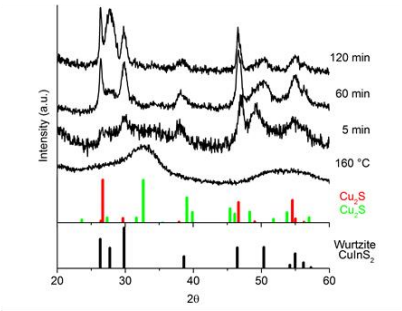	**200 °C, 5 min age** 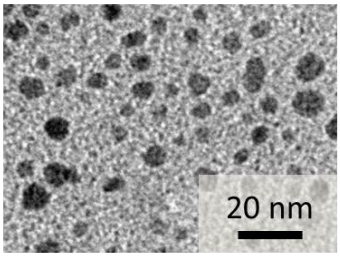 **200 °C, 120 min age** 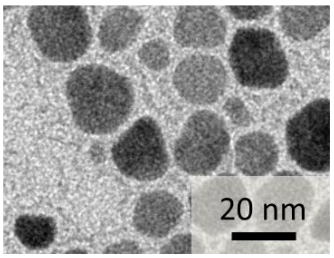	None

Figure S5. The XRD aliquot study characterizes the reaction at 160 °C, and after aging at 200 °C for 5, 60, and 120 minutes. It shows a transformation from Indium and or $CuInO_2$ phases to the wurtzite $CuInS_2$ phase. Both TEM and XRD show in increase in size and crystallization at higher times and temperatures.

Reaction 6: CuCl, $In(Ac)_3$, elemental sulfur, 200 °C

XRD

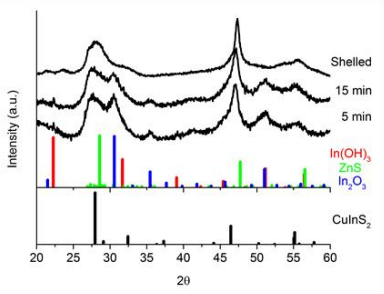

TEM

200 °C, 5 min age

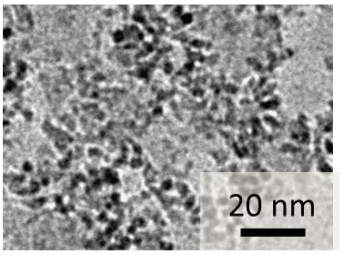

200 °C, 15 min age

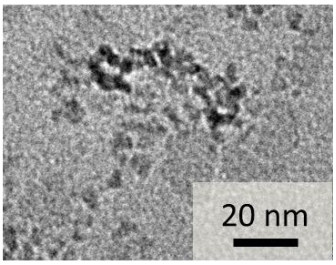

60 min shell growth

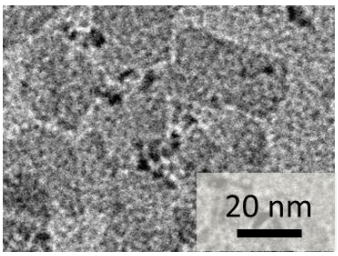

PL

No age vs 5 and 15 min age

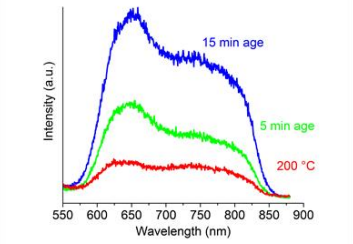

Core vs 30, 60 and 90 min shell

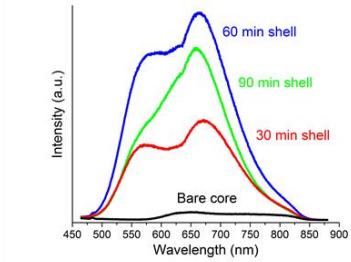

Figure S6. The XRD can be unambiguously assigned to chalcopyrite $CuInS_2$ phases and In_2O_3 phases. Shelling the product lead to the elimination of the indium impurity. The TEM and PL are less clear however. Most of the TEM are polluted with a large, unknown plate-like phase about 20 nm in width. The emission peaks also show two distinct maxima. The reason for this are unknown. Given the presence of In_2O_3 and the fact that many In complexes are photoluminecent, the presence of an indium based compound may be the culprit. The plate like phase offers a second possibility. Shelling with ZnS drastically increases the PL.

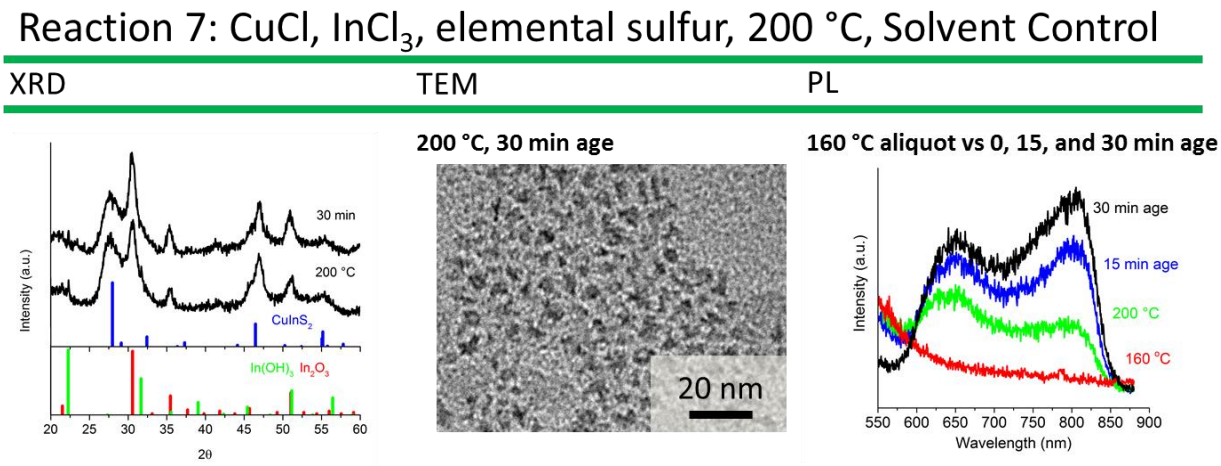

Figure S7. Reaction 6, similar to reaction 7, shows distinct indium oxide and hydroxide impurities, as well as two distinct PL peaks. Solvent control refers to the fact that 7:3 OLA (99%):ODE (90%) was used, rather than as bottled OLA (70)%. As in Reaction 6, two distinct peaks are present in the PL.

Reaction 8: CuCl, $In(Ac)_3$, elemental sulfur, 200 °C, Solvent Control

XRD

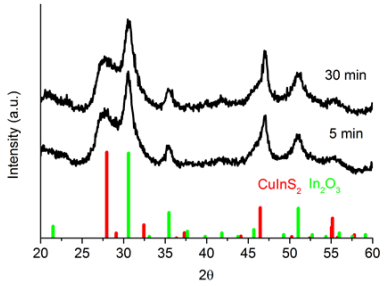

TEM

200 °C, 30 min age

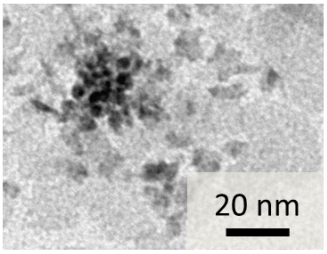

PL

5, 15, and 30 min age

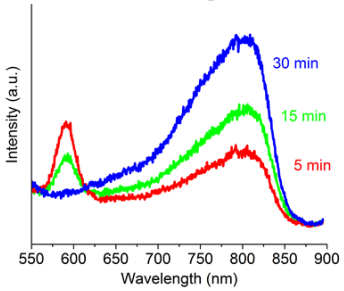

Separated cores vs supernatant*

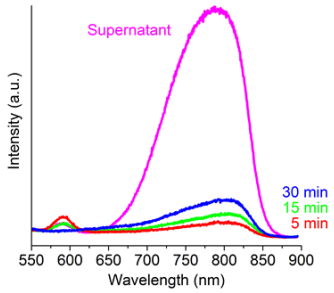

* During wash step solid material is separated from the wash supernatant.

Figure S8. Solvent control refers to the fact that 7:3 OLA (99%):ODE (90%) was used, rather than as bottled OLA (70)%. This XRD shows the familiar In_2O_3 impurity. The PL results, however, are highly unusual. Though there are two peaks, as the particles are allowed to age at 200 °C, one peaks disappears as the other grows. This trend is present and reactions 6 and 7, however they are much less pronounced. What's more, this is not reflected in the XRD, possibly suggesting both peaks are of the same phase. It seems possible then, that there are two distinct sizes of $CuInS_2$ particle, and as the reaction is allowed to proceed, the material of the smaller particles (and lower wavelengths) becomes part of larger particles, perhaps by Oswalt ripening.

4.7 Supplemental Part 2: Supernatant Analysis

Commonly a side product was found in the supernatant of the $CuInS_2$ reactions that used elemental sulfur as a sulfur source. This emission of this material, when excited by near UV light was a very intense cyan color. However the energy of the emission was related, non-linearly, to the energy of the excitation, as described by **Fig S1**. If the source of this emission was pure scattering, then the difference between excitation and emission should not vary as drastically when the excitation energy is changed. If the source of the emission is true photoluminescence, the energy of the emission should not change at all, according to Kasia's rule. Only one other report of such a phenomena was found,[96] a work that attributes the effect to photo-isomerization of *fac*-$Re(CO)_3$-bisthiazoleunder different excitations. It is possible that the same effect may result in this bizarre optical result reported in the current work. Other work has shown the possibility of photo-isomerization in thio-amino acids, analogs of which may exist in our system.[97] Below we summarize our attempts to identify this unknown, strongly emissive supernatant material.

It should be noted that the material was incredibly difficult to separate from solution, requiring at least five separations with methanol and hexanes. This suggests that the material either contains hydrocarbons directly, such as complexes of sulfur and oleylamine, or indirectly, such as very small NPs (< 3 nm), which are mostly hydrocarbon by weight due to an extremely high surface to volume ratio. ICP also suggests this result. Though no metal was found in any

[96] K. E. Henry, R.G. Balasingham, A.R. Vortherms, J.A. Platts, J.F. Valliant, M.P. Coogan, J. Zubieta, and R.P. Doyle, *Chem. Sci.,* 2013, 4, 2490-2495

[97] J. Halbing, H. Bregy, J. Bredenbeck, R. Pfister, P. Hamm, R. Huber, J. Wachtveitl, L. De Vico, and M. Olivucci, *J. Am. Chem. Soc.,* 2004, 126, 8823-8834

significant mass percentage[98], the standard background analysis did suggest a higher than average carbon content, though it cannot be quantified by this method.

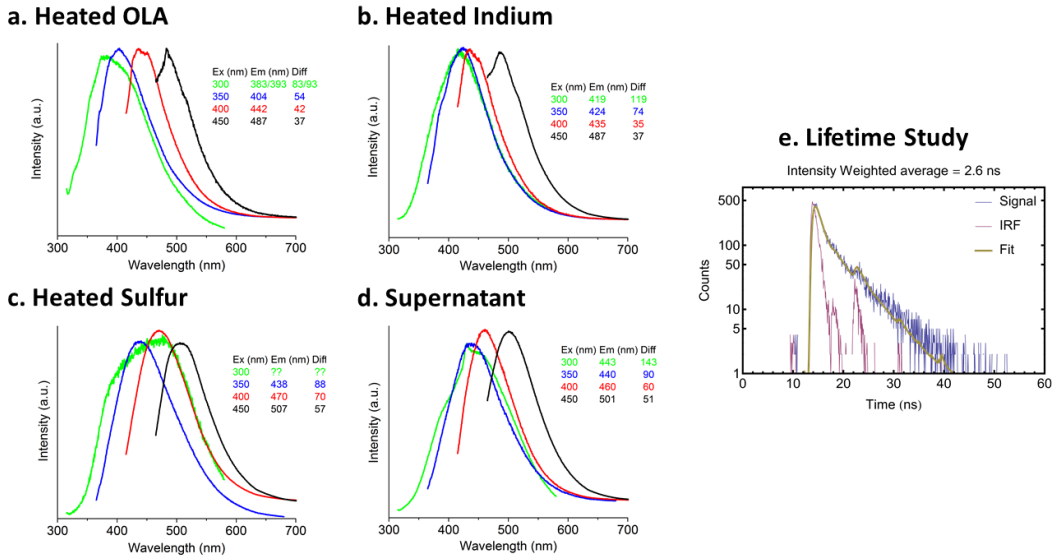

Figure S11. Figures a - d shows the results of reactions which duplicated the conditional of the $CuInS_2$ reaction with individual reagents (e.g. heating elemental sulfur dissolved in OLA to 200 °C for 2 hours). This was done to see if any single reagent was responsible for the bizarre optical results. The emissions at various excitation energies are shown. Interestingly, the In appears to have reacted to become some kind of fluorescing complex, as suggested by a stable emission peak independent of the excitation energy. The emission profile of the heated sulfur matches that of the supernatant most closely, suggesting a S-OLA complex may be responsible for the peculiar emission behavior. Figure e is a standard lifetime study, revealing an average lifetime of 2.6 ns. This value is too large to suggest reflection (usually < 1 ns), yet too small to suggest fluorescence (usually > 10 ns).

[98] Li, B, Na, Mg, Al, Si, S, P, K, Ca, V, Mn, Fe, Co, Ni, Cu, Zn, Sr, Mo, and Ba were tested for.

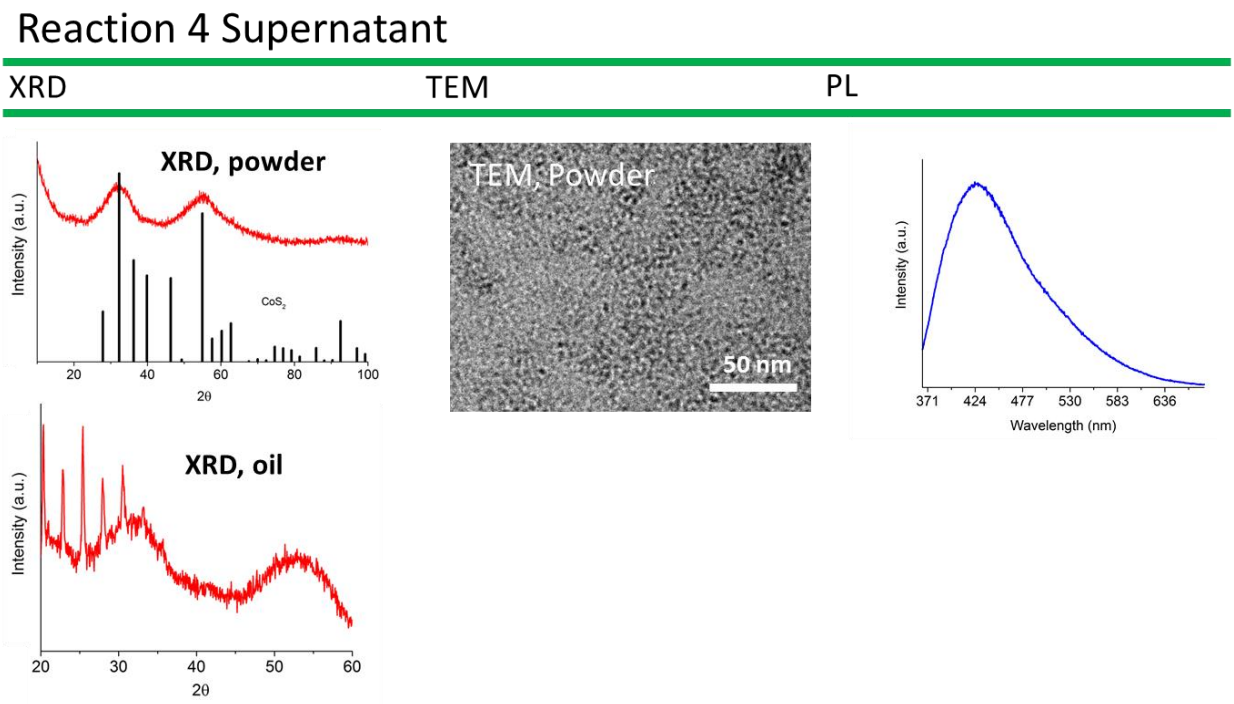

Figure S12. This figure details some of the steps taken to characterize the photo active supernatant of the $CuInS_2$ reactions. The XRD could not be reliably matched, however the spacings do suggest a pyrite structure. The peaks for CoS_2 are shown in figure a., a powder diffraction analysis, though FeS_2 and $Cu_{0.4}Fe_{0.6}S_2$ (Fukuchilite) also fit well. Figure b. shows XRD for an oily (that is, not well cleaned of organics) sample. The sharp regular peaks that are likely part of a regular lamellar spacing. The spacing here corresponds to 3.5 nm. Interestingly, two oleylamine ligands may be approximated to 2.7 – 4.2 nm in length. Papers from Buhro *et al.* and Kotoc *et al.* suggest it may be the result of nanobelts or layers of material coordinated into layers by organics. The TEM offers little insight, while the emission data shown the unusual properties which brought this material to our attention. *Bai, Y; Yeom, J; Yang, M; Cha, S; Sun, K; Kotoc, N J Phys Chem C* ***2013****, 117, 2567-2573. Liu, Y; Wang, F; Wang, Y; Gibbons, P; Buhro, W J. Am Chem. Soc.* ***2011****, 133, 17005-17013.*

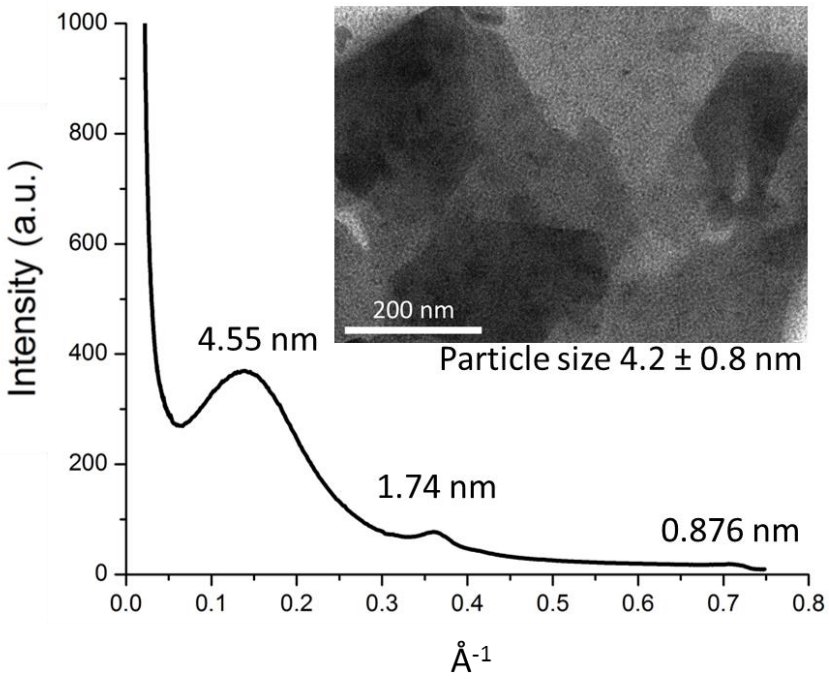

Figure S13. This SAXS data offered little insight into the identity of the material. Shown are the spacings which the peaks correspond to. Our best conjecture is that there are aggregates of 4.55 nm in size, made up of lamellae with a 1.74 regular spacing.

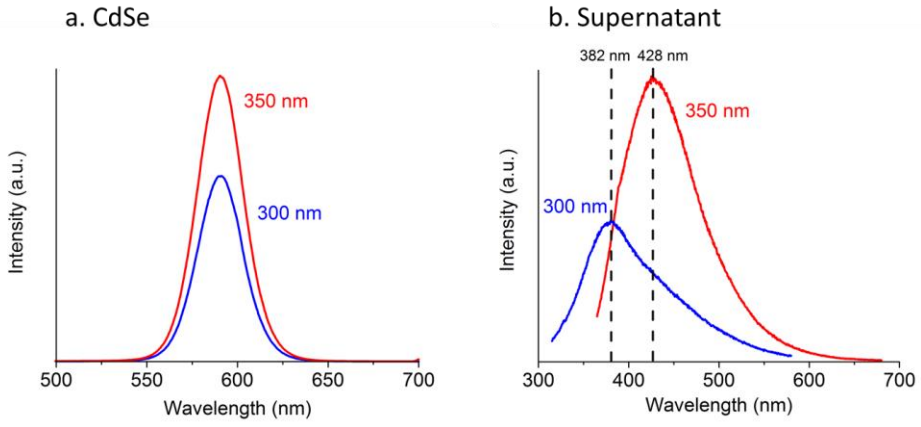

Figure S14. Here two materials, CdSe and the unknown supernatant are excited with different wavelengths of light, 300 nm and 350 nm. The emission energy of a photoluminecent material should not change with excitation energy, as shown in a. However, for the supernatant material the energy of the emission peak does change, suggesting the emission is not a result of photoluminescence. However, the magnitude of the shift in emission (40 nm) does not match that of the difference in excitation (50 nm), as would be expected of light from pure scattering. Therefore, the origin of the emission is unclear.

Chapter 5: Conclusions and Future Outlook

5.1 Summary

This work has attempted to address many issues surrounding the advancement and commercialization of quantum dots. In order to understand how research commonly intersects with the commercial sphere, a significant amount of time was spent exploring how ideas developed in the lab become an integral part of a successful business. Devising such ideas has been a driving force behind the two projects discussed here: an easy high throughput process for making additive-free nanoparticle battery electrons and a large-scale batch process for environmentally benign quantum dots. The motivation for the battery project is to create a process for battery making that can easily make high-efficiency batteries and fewer processing steps. The $CuInS_2$ project was motivated by a commercial need for a large-scale, low-cost dots for energy saving applications. There is much potential for further work in both cases.

5.2 Next Steps for PureQuantum

The following explains the immediate next steps for PureQuantum, the startup based on the work of Chapter 4.

- Finish developing the core technology at Cornell University. This includes refining the process to produce $CuInS_2$ with a quantum efficiency of in excess of 80%. The number was determined through conversations with industry contacts.

- Help Cornell Center for Technology Licensing develop adequate protection for core technology. Negotiate terms of licensing agreement and license from Cornell University.
- Refine understanding of core customer segment as well as entry to market approach. Verify product meets third party and customer validation standards. Acquire partners in this way.
- Raise $2 MM to establish pilot plant.

These are a few high level next goals for PureQuantum. If successful in these endeavors, the company could go on to produce quantum dots, sell them to customers, and expand operations.

5.3 Future Work for Additive-free Nanoparticle Electrodes Processed by EPD

- The Ge NP electrodes did not compare favorably to those of literature (containing additive). Further investigation should be performed to investigate the cause, which is likely related to pulverization.[99] One possible solution is to EPD binder along with the nanoparticles, creating a dense binder network and helping to accommodate stain associated with pulverization.
- EPD has strong potential as a high volume processing approach. There are interesting chemical engineering questions surrounding the process, such as making it more robust and reliable. A more rigorous approach to this method should be developed and scaled up, perhaps in a continuous reactor approach.

[99] M.-H. Park, Y.H. Cho, K. Kim, J. Kim, M. Liu, and J. Cho, *Angew. Chem.,* 123, 9821-9824

5.4 Future Work for Large-scale Copper Indium Sulfide Synthesis

- $CuInS_2$ is a prime candidate of a design of experiment procedure. There are many open questions surrounding what concentrations, shear speeds, heating schemes, and compositions produce the most optically efficient material.
- The solvent chosen for this reaction clearly has a strong influence on the thermodynamics, kinetics, and ultimately quality of the product. Investigations should be conducted into the exact nature by which different ratios of oleylamine, dodecanethiol, and octadecene affect the reactions. One method to gain deeper insight into this is to perform IR and NMR spectroscopy on the reaction at different points to understand what intermediates are formed in different solvent conditions.
- Ultimately this project should be adapted for the scalable high-concentration approach employed by other members of the Robinson Lab. Having conducted significant work with this process on the $Cu_{2-x}S$ system, adapting this approach for $CuInS_2$ is a logical next step. In fact the work of Chapter 4 represents a primary investigation into this challenge.
- The high temperature required for the shelling procedure may have adverse effects on the $CuInS_2$ shell when elemental sulfur is used. $(NH_4)_2S$, as a sulfur source which reacts at much lower temperatures, may shell the material in more gentle conditions and grow the shell without compromising the core material.

Appendix A: PureQuantum Business Plan

The following is a business plan for the business “PureQuantum,” a startup founded by Richard Robinson, Joseph Caron, Douglas Nevers, and Curtis Williamson. It is intended as reference for business plan structure and content only, and should not be distributed without the permission of the founders. This business plan is redacted from its original form.

PureQuantum

Business Plan

January 2015

PureQuantum

110 Stewart Ave, Unit 2

Ithaca, NY 14850

(203) 615-1241

jmcaron91@gmail.com

Executive Summary

Product: PureQuantum is developing a new manufacturing process for making high quality quantum dots (QDs) in large scale with low production cost. Our approach is environmentally friendly due to the lack of toxic material, the low energy usage, the small reaction volume, and the minimal waste generation. By functioning as electricity-to-lighting converter with superior efficiency and precise wavelength, the resulting QDs can be easily used to replace conventional phosphor in solid-state lighting products. The use of our QDs will allow the creation of specialized premium lighting devices that can generate light at any color point efficiently for fulfilling specific needs in various business sectors.

Market: It is estimated that the global market for QD solid nanoparticles in LED applications can reach at least $50M by 2017 with projected cost of $400,000/kilogram and volume of 125 kilogram. We project our QDs will be initially adopted by solid-state lighting companies that specialize in producing LED lighting devices. As we continue improving our manufacturing process, the resulting QDs will be indispensable for the production of specialized solid-state lighting products and the technology behind PureQuantum will be attractive for licensing by companies from the lighting sector.

Investment Cost: PureQuantum anticipates requiring $600,000 seed funding to reach the operational pilot plant phase because this milestone will require product validation, capital expenditures, legal expenses, and cultivating champions in potential partnering companies. We intend to seek further funding from venture capitalists and/or corporate partners to develop our manufacturing capability and reach the necessary milestones. An investment of $2.5M is required for improving production capacity, continuing product development, setting up company infrastructure, acquiring customer, and running the sales and marketing team.

Projected Payoff: PureQuantum is projected to achieve break-even in 3 years and cash flow positive in 2 years after the first round of investment. Our revenue stream will originate from selling high quality QDs, which are produced with our manufacturing process, to companies specializing in manufacturing solid-state lighting devices. Within 4-5 years, PureQuantum anticipates collaboration with a strategic partner in the form of licensing our technology, entering into a joint development agreement (JDA), or getting acquired. This step will provide PureQuantum with resources to accelerate company growth and offer liquidity to investors.

Management Team: The management team will consist of Cornell-educated engineers: Joseph Caron (Chief Executive Officer), Curtis Williamson (Chief Technology Officer), and Douglas Nevers (Lead Researcher). The core team members will be accompanied by experienced advisors: Richard Robinson (Assistant Professor at Cornell University), Clayton Poppe (Chief Technology Officer at e2e material), and Michael Castro (Technology, Operations and Strategy Consultant for Early Stage Energy Companies). We are currently recruiting a Chief Operations Officer to assist with the pilot plant stage. We are also planning to recruit more people to assist in other areas of business as well.

Market Research

Market Opportunity and Size

Solid-state lighting mainly refers to the use of light-emitting diodes (LED) or semiconductor devices that can generate light in response to a passing electric current. In comparison to the conventional incandescent and fluorescent illuminating devices, the use of LED is becoming increasingly popular due to its numerous advantages: reduced power consumption requirement, high efficiency, and long product life. But LED-

based lighting technology still faces numerous technical challenges before it can be adopted by the mass market, primarily due to the use of YAG phosphor for converting electricity to light in conventional LED devices. While YAG phosphor can provide LED lamps with decent luminance efficiency, such approach results in numerous disadvantages: low color-rendering index of less than 70%, short service lifetime of just 25,000 hours, reduced power efficiency due to light emission in the non-visible spectrum, and high manufacturing cost because of inconsistent fabrication and use of rare metals. This situation necessitates a replacement for YAG phosphor such that solid-state lighting devices can be produced with superior luminance efficiency, better color-rendering index, longer service lifetime, cheaper manufacturing process and more flexibility in design/application. The resulting high quality products will allow not only the production of LED devices that can compete with incandescent and fluorescent illuminating devices, but also the creation of premium specialty lighting products with superior performance and design flexibility for fulfilling the needs of various business areas (i.e. car dealership, casino, and surgical room).

Since Quantum Dot (QD) can emit light of different color in a size-dependent manner when excited by UV light, QDs can be used to replace YAG phosphor in LED for solid-state lighting applications. The use of QDs will allow for efficient energy consumption, precise color generation, narrow wavelength spread, flexible form factor, and easy color adjustment. According to a market report by BCC Research, the overall market for QD has been estimated to be as large as $121M in 2014 and projected to grow into $3,058M in 2018 (CAGR of 90.8%), with the specialty lighting portion getting 17 times as large. The report also adds that the global market for QD solid nanoparticles in LED applications can reach at least $50M by 2017 with projected cost of $400,000/kilogram and volume of 125 kilogram. While current manufacturing process is still hampered with numerous challenges, a better manufacturing process for making good quality QD will provide access to this big and growing market.

Macroeconomic Trends

As of now, QD-based solid-state lighting product is still yet to be launched. But the increasing interest in QD can be illustrated by the use of QD-based display technology in recently launched and announced premium television products. Sony launched its Triluminos TV back in 2013 with the claim that the use of QD technology allows for natural color to be reproduced accurately and vividly. LG has recently announced its upcoming QD-equipped TV in December 2014 with claimed 4K resolutions, improved color reproduction, and increased overall brightness. Samsung has also been planning to announce its line of QD-based LCD TV in January 2015. Based on a report by Frost and Sullivan, this trend can also be observed in the intellectual property (IP) landscape with the increasing number of patents being filed for QD-based technologies with only 7 patent filings (4 by companies) in 2003 and 108 patent filings (21 by companies) in 2010. The patents have been developing from initially focusing on the development of colloidal QD to the various approaches for using QD in display- and lighting-based technologies. This point is further made evident by the increased number of patents from the private sector, suggesting improved emphasis on using QD to improve existing electronic devices and/or make better ones. The current regulatory landscape for QD solid nanoparticle production is still at its early stage and does not represent any barrier to us for entering the market. The latter point is especially true for PureQuantum due to the lack of toxic material and/or heavy metal in our manufacturing process. Because many chemicals that are often used in QD production (i.e. cadmium and lead) have been designated as hazardous and toxic, OSHA requires the Chemical Hygiene Plan (CHP) to contain Permissible Exposure Limits (PELs) and monitoring procedures for each of those chemicals. European Directive has also phased out cadmium. This situation is currently advantageous for PureQuantum because the use of toxic material and/or heavy metal has hampered the commercialization of QD-based products. For nanoparticle-related work, OSHA has only produced Prudent Practice Standards for Nanoparticles that essentially acts as a list of suggested procedures and

considerations. As the core team members are familiar with the appropriate procedures, our QD production process can be initiated immediately and developed without complicated regulatory pathway.

Competition

We have identified four major competitors in the QD-based lighting technology: Nanoco, QD Vision, Nanosys, and Quantum Materials Corporation (QMC). In general, the main advantage of our competitors is their existing partnership with major players in the market with established supply chain network. Nanoco and Quantum Materials Corporation (QMC) are our main competitors due to their focus on high-volume QD manufacturing. Nanoco is a UK-based company with a patented manufacturing process for QD production without heavy metal with the capacity reaching 40 kilogram/year. Despite its collaboration with Sigma Aldrich to market QD crystals globally under the name Lumidots, the produced QD still costs $2,000,000/kilogram and uses a dangerous material called tris(trimethylsilyl) phospide. Quantum Materials Corporation has recently entered into a business partnership involving several other companies for improving QD manufacturing and this company has also started a large scale manufacturing of QD. In the meantime, the other companies are currently limited to providing QD films for improving electronic display. Nanosys already formed partnership with Samsung to develop QD-based optical films that will be integrated into the LCD display of Samsung products. Nanosys has also signed an agreement with 3M to replace its LCD diffuser with the one based on QD optical film technology. But its QD production still utilizes a toxic heavy metal called Cadmium. QD Vision is a company that produces commercial QD optical films using a technology developed at MIT. QD Vision has collaborated with Nexxus Lighting to commercialize QD-based lighting devices and signed an agreement with LG for technology development and integration into various electronic products from LG. Our research suggests that QD Vision has received $1.3M from DARPA and approximately $50M from several venture capital firms. While this company has spent more than $75M, its yearly production is still very low with less than 10 kilogram/year, unknown production cost, and reliance on Cadmium. Based on precedents, these competing companies may

respond to our decision to enter the market by attacking our patents. Since we anticipate PureQuantum's patents to come under scrutiny in such scenario, we have taken several precautionary measures from the beginning. Both Cornell's tech transfer office and the PureQuantum co-founders have conducted a preliminary prior art search. Furthermore, a team of IP law students has thoroughly explored the IP landscape for a semester-long project and the resulting report indicates no potential problem with the IP protection moving forward.

Table 1. Competitors' Profile

Company	Partner	Production Cost	Money Spent	Toxicity
Nanoco	Sigma Aldrich	$2,000,000	$4M	Tris(trimethylsilyl) phospide
QMC	Solterra (owned)	Unknown	Unknown	Unknown
Nanosys	Samsung, 3M	Unknown	Unknown	Cadmium
QD Vision	Nexxus Lighting, LG	Unknown	Unknown	Cadmium

Intellectual Property

The work that will make up PureQuantum's IP has been conducted at Cornell University as the graduate work of the company co-founders, therefore making the relevant IP is therefore wholly owned by Cornell University. These IP must be licensed from Cornell University before PureQuantum may begin to make and sell product. While there exists one patent that may be required to move forward, a more comprehensive disclosure has been made to Cornell's tech transfer office and it was submitted as a patent application in the fall of 2014. (SENTENCE REDACTED) Looking ahead, PureQuantum plans to expand its patent portfolio by adapting the patented QD synthesis process for a variety of reaction conditions, QD materials, nanoparticle sizes, and emission wavelengths.

Company and Products

Overview

PureQuantum is a privately held company focusing on the development of efficient manufacturing process to produce high quality QD that can be used in various solid-state lighting applications. Founded by a group of Cornell University graduate students in material science and chemical engineering, we have developed a novel QD production process and also reached out to various people from academia and industry for assessing our technology and business model. PureQuantum has raised $50,000 in support from NYSERDA through the Nexus-NY program.

Business Model

Our value proposition is to provide a novel QD manufacturing process that allows for cheaper production of QDs for a specific market with higher quality, larger scale, and better environmental impact. We will be generating profit in two ways. First, sell QDs that can be readily used as raw materials in the production of solid-state lighting device. This approach will provide us with a revenue stream as we further optimize the production method and bring attention to the competitively priced high quality QD made with our technology. Second, collaborate with a strategic partner (i.e. manufacturing company) by licensing our technology, entering into a joint development agreement (JDA), or getting acquired. While we anticipate such collaboration to be profitable, we will be the source of expertise in large-scale QD manufacturing and we therefore perceive a substantial opportunity in obtaining collaboration in each of the specific markets (i.e. lighting, display, solar energy, and medical imaging).

The Product

Our technology consists of a chemical process to produce high quality non-toxic quantum dots (QDs) at large scale with low cost in an environmentally sustainable manner. The approach used here is based on heat-up colloidal synthesis, in which case QD crystalline is formed by dissolving precursor compounds in the solvent solution, heating the mixture to a specific temperature, and then cooling it down rapidly to initiate crystal growth. Unlike most quantum dots, this novel manufacturing technique avoids the use of toxic component (i.e. Cadmium) or other dangerous and/or imported materials. (SENTENCE REDATED. The synthesis method can also be easily tuned to obtain QD phosphor for generating difficult-to-obtain color points. The offered QD production process will create values for customers in several ways. From the manufacturing point of view, QD production can be performed far more efficiently with better material, low cost, large scale, and environmentally friendly procedure. Using QD synthesized with our technology, manufacturing companies can now produce solid-state lighting devices with narrow emission spectrum, superior color quality, improved energy efficiency, and competitive price. This will accelerate the customer adoption of solid-state lighting product.

Competitive Advantages

Low Cost: While QDs are currently sold on the order of $2,000/gram, our process will allow QDs to be produced at less than $0.80/gram. Such cost reduction is made possible because the reaction only requires an anhydrous organic solvent without the need for water and the primary solvent can be purified for re-use in producing another batch of QD. The estimated energy use is quite low at around 70 kWh/kg due to the low reaction temperature.

Large Scale: The large QD production scale results from the synergistic combination of high reaction yield and low dispersity in the resulting QD nanocrystals. (SENTENCE REDACTED)

QD with High Quality Color: QDs with tunable color point will allow solid-state lighting device to produce light at any wavelength including those that are currently difficult to obtain using existing technology. The capability of providing light at any wavelength with narrow emission spectrum will facilitate solid-state lighting device to solve various problems (i.e. creating authentic light and/or killing airborne bacteria). Our process will provide the flexibility of tailoring the process to produce phosphors for creating certain color points. Such quality is further ensured by the production of QD in large batch that guarantees particle uniformity.

QD with High Quantum Efficiency: While QD-based LED lamps are known for their capability to produce more lumen per watt with superior PLQY in comparison to that of conventional LED lamps, our process builds upon this advantage even further. Our process can be further optimized for producing QDs with high quantum efficiency or photoluminescence quantum yield (PLQY) that ranges from 80 to 95%, which represents a big leap even in the QD space itself.

Adaptability to Existing Manufacturing Process: When the QDs produced by our method are used as phosphors, they can be simply integrated into existing manufacturing process for solid-state lighting devices. In contrast to bulk phosphors, QDs are far easier to apply as they can be deposited with low impact techniques (i.e. electrophoretic deposition).

Environmentally Friendly Process: Unlike other common QD synthesis methods, PureQuantum's synthesis technique does not rely on any hazardous materials to efficiently produce QDs. This is the result of the materials that comprise the QDs and the solvent. (PORTION REDACTED) efficient use of solvent will

generate much less waste. The ability of our solvent to be purified for another batch further reduces the waste generation.

Figure 1. Implementation Schedule

Segments	**Year**			
	2015	2016	2017	2018
Product Development	Achieve 80% PLQY Reach 0.04 kg/week Product validation	Achieve 90% PLQY Reach 0.14 kg/week	Reach 0.29 kg/week	Reach 0.77 kg/week
Marketing	Identify and approach earlyvangelist	Cultivate earlyvangelist	Do customer validation Acquire X customers	Acquire 2X customers
Legal	Acquire IP from Cornell	Create further IP		
Financing	Formalize business plan Prepare business pitch Raise $600,000	Raise $2,500,000		
Operations	Obtain space Hire COO Recruit R&D personnel Buy equipment	Recruit S&M personnel	Hire HR Hire office manager Buy more equipment	Buy more equipment Recruit R&D personnel

Development Plan

Development Status

This novel QD production process is still under development. We have validated the approach to create batches of copper sulfide (CuS) QD at large scale and low cost. While CuS was used as a cheap model system for our QD manufacturing technology, we need to make QD with the desired specifications. Our initial feedback stage has led us to pursue the production of copper indium sulfide (CIS) QD as this particular material can be used in solid-state lighting and numerous other applications. We are currently in the process of adapting this method to refine CIS QD as this particular material has potential for use in the solid-state lighting device. Work is currently focused on optimizing the experiment parameters: ratio of elements, ratio of solvent to material, mixture concentration, heating temperatures, and mixing process. This basic research will serve to further solidify our IP on the technology. In parallel, we are also testing the produced QD both internally and externally through academic laboratories specializing in QD. Once we optimize the method for producing QD with 80% PLQY and validate this particular metric, we plan on moving the manufacturing location from the laboratory to the pilot plant.

Difficulties and Approaches

Experimental Parameters

Work on identifying experimental parameters is challenging because it requires an advanced understanding of the entire process and the materials. Changing ratio of elements and/or solvents will also alter the optimal concentration, heating temperature, and mixing process. But the process is fairly easy to execute once the parameters have been worked out. We are currently working to identify which parameter is important for the process. The selection will be done based on several quantitative metrics that cover cost, quantum efficiency, and color quality.

Material Identification

Due to the general nature of PureQuantum's approach to QD synthesis, the core process can be adapted to a variety of materials. The materials may include copper (II) sulfide type nanoparticles, of which there are many, and different similar variations on this particle, including copper indium sulfide, copper zinc indium sulfide, and gallium doped copper indium sulfide. Since each of these materials has different optical and electronic properties, material control is an important parameter for controlling such properties in the resulting QD.

Manufacturing Plan

Current Process

The method that formed the basis of our technology is based on heat-up colloidal synthesis of nanoparticles that involves the formation of QD crystals by dissolving raw materials in the chemical solvent, heating up the mixture to a precise temperature, and cooling it down rapidly. The production is currently performed in a laboratory at Cornell University using a prototype reactor that was built in-house using commercially available equipment: 4L vessel, Schlenk line (vacuum gas manifold), stirring motor, and stir bar. The prototype reactor will function exactly as the full-scale reactor except that it is running at 1/4 capacity at the moment to demonstrate the process and material development. QD synthesis will require the use of reactor, raw materials, and energy input. This synthesis step will take 4 hours. The resulting sample will be purified using a centrifuge and energy input. This purification stage will only take 2 hours. We have successfully demonstrated that this method can be used to produce a QD batch weighing 80 grams every 3 days. Raw materials can be obtained with a maximum lead time of 2 weeks. Quality control will be performed using a spectrometer that can precisely verify the wavelength of QD batch produced. The current product cost today is close to $151,000/kg due to costs associated to raw material ($1,442/kg), labor

($129,600/kg), and energy ($105/kg). We expect QD distribution to utilize normal shipping with $10 per kilogram of QD delivered.

Pilot Plant Production Strategy

Once we have completed the adaptation of our manufacturing process into the production of CuS QD, work will begin on constructing the pilot plant to initiate large scale QD production. The main goal of establishing the pilot plant is to accelerate the production capacity. Another goal is to independently develop future IP with our own equipment for strengthening the patent portfolio and ensuring competitiveness in the market. The production plant will be located in Ithaca (NY) with more reactors running in parallel and each reactor running at increased capacity. The location was strategically selected to ensure easy access by our core team members and advisors. Due to the environmentally safe nature of our process, this facility will only require a laboratory bench and a fume hood. Given our experience with the regulatory environment for chemical-based products and QD, we do not anticipate any delay in the preparation of standard workplace practices. We are expecting lead-time of 6 months from funding to having an operational pilot plant. Such time constraint is not uncommon, as we will be obtaining the production space, buying equipment, ordering raw materials, and hiring employees. Phase 1 (pilot) is geared toward refining MVP with the aim of making QD at 0.04 kg/week, requiring $600,000 initial investment. This step is estimated to go for 2 years from 2015 to 2017. We plan on optimizing the production cost to go down into $48,454/kg with the same combination of costs: raw material ($591/kg), labor ($40,000/kg), and energy ($29/kg). Phase 2 (manufacturing) is aimed at generating advanced MVP with the goal of producing QD at 1.54 kg/week, requiring $2.5M investment.

Sales and Marketing Plan

We believe that there is an attractive market in the solid-state lighting industry for inexpensive high quality QD phosphor produced in large scale with environmentally safe process that only utilizes non-toxic materials. The marketing strategy is to make QD with our proposed process and position the resulting QD as (1) competitively priced, (2) high quality, and (3) ready integration into the existing manufacturing process. We plan on directly selling our QD priced at $200,000/kilogram to manufacturing companies that specialize in solid-state lighting devices. From industry contacts, we know that people in solid-state lighting companies are interested in getting such QD as they have spent time working with such material. But the work is still in its preliminary phase, such that there is no commercial QD-based lighting product is available yet. This approach will allow us to generate a revenue stream from early on, build relationship with companies, bring attention to our product, and obtain sufficient interest in our technology for a possible partnership with a company. Obtaining even a small slice in this rapidly growing market will provide us with the resources needed to sustain the business, continue product development, and branch out to different markets. Examples of potential areas of interest include solid-state lighting, electronic display, solar energy, and medical imaging. The pricing strategy is based on competition because QD produced by the competitor is priced around $2,000,000/kilogram, thus making our price of $200,000/kilogram to be a very compelling advantage for cost conscious customer. Customer acquisition cost is currently projected at $100-200K for each $1M of revenue. This cost will cover the fee for marketing materials, attending workshops, compensating the sales force, and maintaining a strong web presence.

We intend to reach customers by attending solid-state lighting trade shows and scientific conferences. This will allow us to meet R&D senior scientists and have them buy our QD product. Alternatively, we may be introduced to science staff through business development contacts. In either case, we will rely on such a scientist as a "champion" within his or her company to advocate a partnership with PureQuantum. This is standard procedure for a materials company, and cultivating relationships with our "champions: will be an important part of our market plan. From attending two trade shows, we have contacted 50+ interested

individuals representing nearly as many companies. Identified champions have stated that they are waiting for us to develop the MVP. In addition to establishing a strong network of contacts, we have also made at least one contact with nearly every major (and many small) solid-state lighting device manufacturing companies. Based on these successes, we plan on continuing this strategy to reach customers and expand the marketing. We are also looking to work together with the academia as a way to build credibility as we enter the market. For example we have already taken the first steps towards collaboration with Bob Karlick, head of the Smart Lighting Center at Rensselaer Polytechnic Institute.

While direct selling comprises our initial marketing strategy, we intend on initiating collaboration with a strategic partner at any point in time. We primarily anticipate licensing our technology, although we are open to entering into a joint development agreement (JDA) or getting acquired. Building on existing relationship with manufacturing companies through direct selling of high quality QD, we hope to bring attraction into the production method for generating the QD. We plan on sub-licensing of our QD manufacturing process to a company that makes QD for implementation into end-user product in a specific market with solid-state lighting being the primary focus. Sub-licensing will be done via the exclusive route, where the technology will be licensed to one large company in each market and the agreement will be tailored to a specific field of use. Our preliminary assessment suggests that royalties will be based on net sales with the amount that varies depending on the area of application (i.e. 3.9-4.9% for general hardware and 3.9-5.4% for medical equipment).

We will initiate demands on our manufactured QD by having a strong Internet presence through website and various social media sites. We will also be aggressively advertising our product through industry publications, newsletters, press releases, and print articles (i.e. academic journals and major newspapers). In order to achieve these goals, we plan on creating a sales and marketing team after the first year of

operation. The team will consist of a VP of sales and business development ($110,000/year), a marketing manager ($85,000/year), a sales engineer ($60,000/year), and a sales staff ($60,000/year) with a possible plan for further recruitment once all milestones have been achieved. This team will be assisting us on preparing marketing materials, direct selling, building contacts, traveling to trade shows, and reaching out to customers. Once we have obtained collaboration in a specific industry, we will continue to seek out opportunities in another market by customizing our manufacturing process to generate QD with specifications tailored for that market. We currently know that we can reach the electronic display market with practically no change in the product, while medical imaging market may require further validation in a few more areas in accordance to the available regulations.

We further intend to handle customer retention by offering personal assistance to our customers who may require extra input or expertise on the use of quantum dots. This will be possible due to the manageable number of customers (3-5) within our first few years of operation. We will therefore concentrate on not only cultivating good relationships with our customers after the first sale, but also following up regularly to understand and address their changing needs.

Financial Projection

We have developed this financial projection to estimate the financial performance of PureQuantum for the next 5 years, consisting of: income statement and cash flow. Below we have summarized the important parts of the financial projection. With our gross profit margin of 20%, we predict that PureQuantum will reach breakeven within the first 3 years of operation (2017) and become cash flow positive 2 years after second investment (2018). In order to achieve these goals, we will require $600,000 in seed funding and $2.5M in first round of investment.

Figure 2. Income Statement

Income Statement	**Pilot**		**Manufacturing**					
	Year 0		Year 1		Year 2		Year 3		Year 4	
	2015		2016		2017		2018		2019	
Revenue										
Amount sold (kg)	0.4		3		9		27.5		70	
Sales Price ($/kg)	$200,000		$200,000		$200,000		$200,000		$200,000	
Production Cost ($/kg)	$128,137		$86,288		$67,316		$51,643		$48,454	
Total Revenue	**$80,000**	100%	**$600,000**	100%	**$1,800,000**	100 %	**$5,500,000**	100 %	**$14,000,000**	100 %
COGS	$51,254.99	64%	$258,865	43%	$605,848	34%	$1,420,193	26%	$3,391,801	24%
Gross Profit	$28,745	36%	$341,135	57%	$1,194,152	66%	$4,079,807	74%	$10,608,199	76%
Expenses										
R&D	$240,000	300%	$280,000	47%	$500,000	28%	$1,000,000	18%	$2,800,000	20%
S&M	$40,000	50%	$435,000	73%	$440,500	24%	$686,525	12%	$1,353,351	10%
G&A	$302,600	378%	$461,500	77%	$551,575	31%	$732,004	13%	$1,345,454	10%
Operating Expenses	**$582,600**	728%	**$1,176,500**	196%	**$1,492,075**	83%	**$2,418,529**	44%	**$5,498,805**	39%
Operating Profit	**$553,855**	-692%	**$835,365**	-139%	**$297,923**	-17%	**$1,661,279**	30%	**$5,109,394**	36%

Figure 3. Adoption Curve

DOE Adoption Curve	**Pilot**	**Manufacturing**			
	Year 0	Year 1	Year 2	Year 3	Year 4
Data	2015	2016	2017	2018	2019

Amount of Light Bulbs Produced	4.00E+08	6.00E+08	9.00E+08	1.10E+09	1.40E+09
Amount Required per Bulb (kg)	4000	6000	9000	11000	14000
Market Penetration Rate	0.01%	0.05%	0.10%	0.25%	1%
Amount Sold (kg)	0.4	3	9	27.5	70

Figure 4. Cash Flow Statement

Cash Flow	**Pilot**	**Manufacturing**			
	Year 0	Year 1	Year 2	Year 3	Year 4
	2015	2016	2017	2018	2019
Beginning Cash	**$0**	**$32,728**	**$1,566,462**	**$1,103,675**	**$2,599,987**
Gross Profit	$28,745	$341,135	$1,194,152	$4,079,807	$10,608,199
Expenses	$582,600	$1,176,500	$1,492,075	$2,418,529	$5,498,805
Investment	$600,000	$2,500,000			
Capital Expense	$10,000	$17,000	$34,000	$78,000	$156,000
Inventories	$3,417	$113,901	$130,863	$86,967	$31,786
Change in Cash	$32,728	$1,533,734	$462,787	$1,496,311	$4,921,608
Ending Balance	**$32,728**	**$1,566,462**	**$1,103,675**	**$2,599,987**	**$7,521,594**

Figure 5. Capital Expenditure

CAPEX	**Pilot**	**Manufacturing**			
	Year 0	Year 1	Year 2	Year 3	Year 4
	2015	2016	2017	2018	2019
Item 1: Reactor	$0	$6,000	$8,000	$4,000	$16,000
Item 2: Centrifuge	$0	$12,000	$16,000	$8,000	$32,000

Item 3: Vacuum Pump	$0	$9,000	$12,000	$6,000	$24,000
Item 4: Others	$0	$24,000	$32,000	$16,000	$64,000
Total CAPEX	$0	$51,000	$68,000	$34,000	$136,000
Cumulative CAPEX	$0	$51,000	$119,000	$153,000	$289,000

Management Team

PureQuantum was founded by a group of Cornell University graduate students in engineering: Joseph Caron, Douglas Nevers, and Curtis Williamson. They have worked together as a team in developing the chemical process that forms the basis of PureQuantum, thus making them particularly skilled in the relevant areas: chemical synthesis, reactor design, process scale-up, and nanomaterials. These skills are particularly relevant since our development milestones will involve the development of a high performance MVP and optimization of core chemical processes. The team has also participated in two NSF Innovation Corps (I-Corps) programs and raised $50,000 in support from NYSERDA through the Nexus-NY program. PureQuantum also has several dedicated advisors that are experienced in research, product development, business plan writing, and entrepreneurship. PureQuantum is in the process of recruiting people to assist with sales, marketing, manufacturing, operations, business development, technology licensing, and dealing with the lighting industry. PureQuantum is also actively seeking a full-time COO to move forward with the pilot plant development.

Core Team Members

Joseph Caron will serve as Chief Executive Officer. He is currently a candidate for the Masters of Science degree in Materials Science and Engineering. His responsibilities will include the overall direction of the company, attracting investments, communicating with the board, communicating with important customers, and organizing meeting. He bring strong leadership and organizational skills to the company, as well as experience representing PureQuantum. Joseph is experienced in founding a variety of projects that range from volunteer organizations in Baltimore to a biofuels engineering project team in Ithaca. He is currently a candidate for the Masters of Science degree in Materials Science and Engineering.

Curtis Williamson will serve as Chief Technological Officer. Curtis has been instrumental in developing the core technology. Building on three years QD synthesis at Evident Technologies, a competing QD synthesis company he was able to develop the techniques that allow PureQuantum to make a competitive product, and will continue to refine the technology to create more efficient products with a wider scope of material. He is currently a PhD candidate in Chemical Engineering at Cornell University.

Douglas Nevers will serve as Lead Researcher. He has worked alongside Curtis to develop the large-scale reactor technology, employing his formidable knowledge of reactors and nanoparticle growth modeling. His knowledge will be critical in optimizing the performance of the reactor, as well as controlling key parameters to create particles of a particular size. Douglas brings five years of industry experience understanding and building reactors. He is currently a PhD candidate in Chemical Engineering at Cornell University.

Advisors

Richard Robinson is an Assistant Professor in Materials Science and Engineering at Cornell University. The inventor of our technology, Professor Robinson's research focuses on nanostructured materials for alternative energy applications. He earned his MS in Mechanical Engineering from Tufts, and a PhD in

Applied Physics from Colombia University. He has been awarded $1.5 MM in basic research grant from the NSF to study the large-scale synthesis of nanoparticles.

Clayton Poppe is the Chief Technology Officer at e2e material and manages strategic customer relationships. His experience includes product development for Aksys Ltd., maker of the first kidney hemodialysis machine for home use. Clayton has a BSE in Mechanical Engineering and Material Science from Duke University, and an MS/MBA from MIT's through the Leaders for Global Operations program.

Michael Castro is a technology, operations and strategy consultant for early stage energy companies. He has 10+ years experience in manufacturing, with strong experience in technology roadmaps, evaluation, integration, transfer, ramp up and modeling as well as significant experience forming strategic technology partnerships in Europe and Asia.